Hydro Structural Coupling of a Composite Propeller

Auteur : Ali, Kashan
Promoteur(s) : Rigo, Philippe
Faculté : Faculté des Sciences appliquées
Diplôme : Master : ingénieur civil mécanicien, à finalité spécialisée en "Advanced Ship Design"
Année académique : 2023-2024
URI/URL : http://hdl.handle.net/2268.2/22251

Hydro Structural Coupling of a Composite Propeller

submitted on 02 August 2024

by

ALI Kashan | 3 Rue De Gaillac | 44800 Saint-Herblain | kashan.ali@uni-rostock.de

Student ID No.: 223202133

First Reviewer:

Prof. Patrick Kaeding

Chair of Ship Structures

University of Rostock

Albert-Einstein-Str.2, 18059 - Rostock

Germany

Second Reviewer:

Dipl.-Ing. Gunnar Kistner

Chair of Ship Structures

University of Rostock

Albert-Einstein-Str.2, 18059 - Rostock

Germany

EMship+
Advanced Design

Master Thesis

CONTENTS

LIST OF FIGURES

LIST OF TABLES

ABSTRACT

Composite propellers are emerging as a promising alternative to the traditional metallic propellers in the maritime industry, offering potential cost savings through increased efficiency and reduced maintenance requirements. The industry is increasingly focusing on the feasibility of using composite materials for propellers and developing robust design evaluation tools for their certification. CoPropel Project is one similar effort by the industry where the objective is to present a holistic approach that realizes the practical application of composite propellers and to increase the Technology Readiness Level (TRL) of composite propellers.

This report presents the work done as part of CoPropel Project with the objective of validating the design of composite propeller, which is modeled after an already existing metallic propeller. The design is developed by MECA Group, a CoPropel Project Industrial Partner, which includes hydrodynamic and structural analyses. The results of these hydrodynamical and structural analysis are validated using Fluid Structure Interaction (FSI) simulations in this report. Two FSI coupling schemes were employed: Computational Fluid Dynamics-Finite Element Method (CFD-FEM) and Boundary Element Method-Finite Element Method (BEM-FEM). The CFD-FEM analysis, conducted using STAR CCM+ and FEMAP, utilizes the Reynolds-Averaged Navier-Stokes Equations (RANSE). The BEM-FEM analysis is performed using ComPropApp, a design assessment tool that integrates the BEM software PROCAL with the FE software TRIDENT. The results obtained from the CFD-FEM coupled FSI analysis are also used to validate the BEM-FEM coupled FSI results from ComPropApp.

Keywords: Composite Propellers, Fluid Structure Interaction (FSI), Finite Element Analysis (FEA), Boundary Element Method (FEM), Computational Fluid Dynamics (CFD)

1. INTRODUCTION

Marine propellers have been one of the main sources of propulsion for ships and underwater vehicles for the past few decades, the other prominent modern propulsion source being water jet propulsion. Metals have been the primary material of construction for these propellers since forever, including bronze, brass and stainless steel. But as in every other field, the technological revolution in manufacturing processes and advancement in materials was bound to challenge the status quo of metallic propellers. In recent decades, there has been a growing interest in using composite materials for propeller design, driven by their potential of

- improved hydrodynamic efficiency
- lower weight
- reduced underwater radiated noise
- reduced cavitation
- higher strength to weight ratios
- corrosion resistance
- enhanced performance in varying operational conditions
- tailoring material properties to achieve desired performance characteristics

A lot of research work is being carried out to gauge the feasibility of composite propellers replacing the traditional metallic propellers (Mouritz et al., 2001; Motley et al., 2009). One of the most significant aspects of using composite propellers is the ability of propellers to passively adapt their shape under varying hydrodynamic loads, (Young, 2008; Maljaars et al., 2017).

As interest in the use of composite propellers for marine applications is developing, there is a need to develop robust criteria for design of these propellers. Unlike rigid metallic propellers, where the focus is primarily on hydrodynamic design, composite propellers require concurrent consideration of both structural and hydrodynamic design since composite propellers are less rigid and deform under the application of hydrodynamic loads. This deformation can significantly alter the flow field, which in turn affects the loads on the blade. This interplay between fluid and structure is studied under the framework of Fluid-Structure Interaction (FSI) analysis (Li et al. 2017). Several methods have been developed for FSI analysis of composite propellers. These range from simplified one-way coupling, where fluid loads are computed on the undeformed geometry and then applied to the structural model, to fully coupled two-way methods that iteratively solve the fluid and structural problems until convergence (Mulcahy et al. 2010).

A traditional approach of evaluating the hydrodynamic performance of rigid propellers involves performing experimental tests using scaled models of actual propellers. But these practical setups happen to be time consuming and costly. Alternatively, numerical solvers based on Boundary Element Method (BEM) or Panel Method, Reynolds-Averaged Navier-Stokes Equations (RANSE), and Large Eddy Simulation (LES) are used.

- BEM is computationally efficient and widely used in initial design stages, but it struggles with highly deformed geometries and separated flows (Kerwin and Hadler 2010). BEM assumes the fluid to be inviscid, irrotational and incompressible which is an over-simplification for practical flows (Maljaars et al. 2017).

- Solvers based on RANSE methods can handle viscous effects and moderate to large deformations, but at the cost of requiring more computational resources and time as compared to solvers based on BEM (Taketani et al. 2013).

- Solvers based on LES provide the most detailed flow information for transient phenomena like cavitation, but its high computational cost limits its use in design optimization (Bensow and Bark, 2010; Gaggero et al., 2019).

The anisotropic and orthotropic nature of composites makes their Finite Element (FE) modelling and analysis complex as compared to isotropic materials. Finite Element (FE) modelling is a computational technique used to simulate and analyze the physical behavior of structures and systems. The structure is divided into smaller, manageable finite elements, which are then mathematically solved to predict how the structure will react under external loadings. Different composite FE modelling approaches are available based on the type of element chosen including plate laminate elements, solid volume elements and solid laminate elements. Several researchers have used one or the other in their research work such as Lin et al. used solid laminate elements to study composite propellers (Lin et al. 2016) while Singh et al. implemented the use of plate laminate elements to develop FE model of composite propellers (Singh et al. 2021). Material models must account for the orthotropic properties of composites, potential non-linearities in large deformations, and failure modes like delamination (Chen et al. 2006).

The effort of maturing the Technology Readiness Level (TRL) of the composite propellers comes with its own challenges. These challenges include scaling up laboratory tests to full-scale applications, long-term durability in marine environments, repairability, and the development of design standards and certification processes for composite propellers (Mouritz et al. 2001). Compared to metallic propellers, the cost of manufacturing the composite propellers is significantly higher and as such, practical experiments such as sea trails prove to be very costly, which are used to validate the numerical models in the R&D process. This has

proven to be a hurdle in maturing the technology of composite propellers. On the numerical modelling side, the computational cost of high-fidelity FSI analysis remains a bottleneck, particularly for unsteady problems like maneuvering or operation in waves (Turnock and Wright 2000).

1.1. Objective of Thesis

This thesis work is performed as part of the European research project CoPropel. The objective of CoPropel project is to present a holistic approach that realizes the practical application of marine propellers made out of composite materials. Nine organizations from five different countries are part of this project. Out of these, four are research institutes, four are industrial organizations and one is certification body (CoPropel, 2024)

Research Institutes	
University of Ioannina (UoI)	Coordinator
Brunel University London (BUL)	Associated Partner
TWI Limited	Associated Partner
Bulgarian Ship Hydrodynamics Centre (BSHC)	Partner
Industrial Partners	
Loiretech Ingenierie	Technical Coordinator
MECA Group	Partner
Glafcos Marine Ltd (GME)	Partner
Danaos Shipping Company Ltd	Partner
Certification Body	
Bureau Veritas Marine & Offshore (BV)	Partner

The objective of this thesis work within the scope of CoPropel project is

- To validate the structural and hydrodynamics results produced by MECA. This is achieved by performing fluid structure interaction (FSI) analysis for the propeller using two types of FSI couplings
  - CFD-FEM coupling. Computational Fluid Dynamics (CFD) is a method for analyzing fluid flow domain by numerically solving the governing equations of fluid mechanics; the Navier Stokes Equations. It involves discretizing the flow domain and applying mathematical models to predict fluid behavior and properties. More details on this in section 3.4.1.

- o BEM-FEM coupling. The Boundary Element Method (BEM), also known as the panel method, is numerical tool used for solving the partial differential equations by reformulating them as integral equations on the boundary of the domain. Compared to CFD, BEM has reduced dimensionality of the problem, making it computationally efficient for flow problems, as in the case of propeller. More details on this in section 3.4.2.

- To validate a BV in-house composite propeller design software called **ComPropApp** (short for Composite Propeller Application) using the results obtained during thesis work. **ComPropApp** is developed by CRS (Cooperative Research Ships - https://crships.org/) and is an application mainly developed by MARIN which performs FSI analysis by achieving coupling between a BEM based solver PROCAL and FEA software TRIDENT which uses VAST solver. The loads generated by PROCAL in form of surface pressure are transferred to TRIDENT and used to carry out nonlinear static analysis. The deformed geometry obtained as a result of this nonlinear static analysis is transferred back into PROCAL where new surface pressures are generated using this deformed geometry. This process is iterated until a converged solution is reached.

The geometry of the propeller is based on an already existing metallic propeller which is a five blades fixed-pitch propeller mounted on Le Palais passenger vessel as shown in Figure 1. The diameter of the propeller is 1.095 and the La Palais vessel has two identical propellers.

Figure 1. Le Palais vessel and one of its metallic propellers

1.2. Organization of Thesis

The thesis work is performed in following steps

- First a study is carried out to understand the effects of using three different kinds of Finite Elements (FE) models based on the type of elements used for modelling the propeller. These elements are plate laminate elements, solid elements and solid laminate elements. A very simple rectangular plate was modelled for this study and the structural results were compared for these models. The details are given in section 4. This study is significant since MECA is using plate laminate elements for FE modelling of the propeller blade as compared to solid laminate elements that are used in the FE models used in the thesis work.

- The next step is to create the FE model of the propeller blade based on the scantling details provided by MECA. This step requires starting from raw data, that defines the geometry of the propeller blade, to developing the final FE model ready for FSI analysis. The details are given in section 5. The scanting of the propeller blade provided by MECA is confidential and hence the details about it are not included in this thesis report. Only a general idea of how the layup looks like, and the kind of materials used for the layup is provided in this report.

- The next step is to carry out BEM-FEM and CFD-FEM coupled FSI analysis. The BEM-FEM coupled FSI analysis is carried out using ComPropApp while CFD-FEM coupled FSI analysis is carried out manually through files exchange between CFD software STAR CCM+ and FEA software FEMAP (FEMAP uses NX NASTRAN solver). CFD-FEM is carried out in collaboration with **Bureau Veritas Solutions Marine and Offshore (BVS M&O)** which is an engineering consultancy branch of Bureau Veritas Marine and Offshore. To achieve CFD-FEM coupling, BVS carried out the CFD simulations using STAR CCM+ while the FEA is carried out by the author of this report.

- The final step is validation of results. Two validations are performed under the scope of thesis work:
    - Validation of MECA's results by comparing the results obtained from BEM-FEM and CFD-FEM coupled FSI analysis with MECA's results
    - Validation of ComPropApp by comparing the results obtained from BEM-FEM coupled FSI analysis with the results obtained from CFD-FEM coupled FSI analysis

2. PROPELLER THEORY

To define the geometrical and hydrodynamical characteristics of a marine propeller, a prerequisite is to establish an appropriate reference system. The global reference frame to be used is shown in Figure 2 which is a right-handed rectangular coordinate system. The X-axis is aligned along the shaft of the propeller while the positive Y axis is positive towards the starboard side. The positive Z-axis is oriented vertically downwards. Since propeller is a rotating object, it makes more sense to define a local reference system where the local x-axis is aligned with the global X-axis while allowing the local y and z axis to rotate relative to global Y and Z axis as shown in Figure 2 (Carlton 2018).
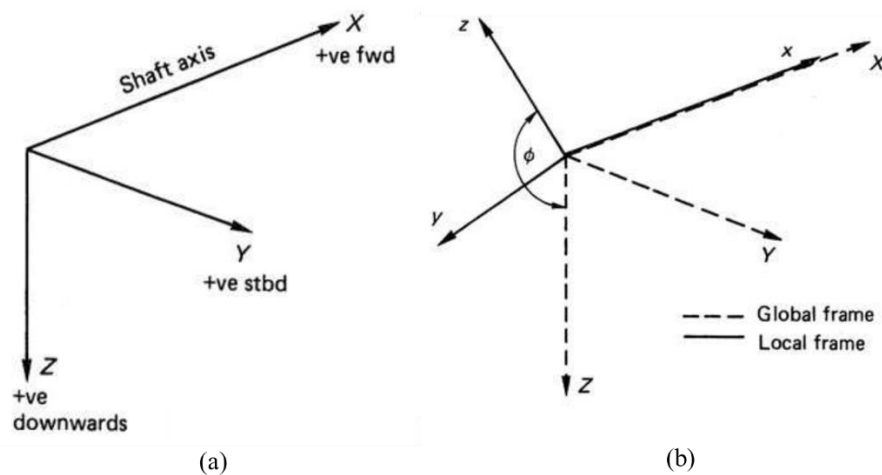
Figure 2 (a) Global reference system, (b) Local reference system (Carlton 2018)

Before going into the details of the geometrical parameters used to define a propeller's geometry, it is important to understand how and where on the propeller blade these parameters are defined. Propeller geometrical characteristics are defined using aerofoil sections at different values of ratios between section radii (r) and the propeller radius (R) given as $r/R = [0.2,0.3,0.4,0.5,0.6,0.7,0.8,0.9,1.0]$. The r/R values presented here are not standard and are changed based on requirements. The aerofoil sections that make up the blades of a propeller are positioned on the surfaces of cylinders whose axes align with the propeller shaft. This configuration is often referred to as "cylindrical sections" in the context of propeller design. As illustrated in Figure 3, these sections are placed at an angle on the surface of the cylinder. The line connecting the leading and trailing edges of each section, known as the nose-to-tail line, creates a helix around the cylinder (Carlton 2018). This can be shown for each individual value of r/R.
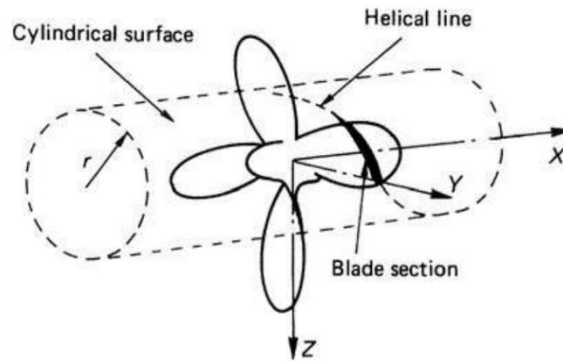
Figure 3 Helix line and cylindrical section (Carlton 2018)

The propeller shape is described using three different types of outlines/areas.

2.1. Projected outline

The projected outline of a propeller blade is the view seen when looking directly along the center line of the shaft, perpendicular to the y–z plane. By convention, this view is considered as looking forward. In this perspective, the helical sections are displayed at their respective pitch angles, and they appear to lie along circular arcs centered on the shaft axis. Left side of Figure 4 illustrates this view along with developed view/outline. The projected area of the propeller is the visible area when viewed from the front along the shaft axis (Carlton 2018).

2.2. Developed Outline

The developed outline of the propeller blade is visible in the left view in Figure 4 with a helical basis view where each section pitch has been reduced to zero, and it is oriented within the thwart-ship plane. This perspective is employed to accurately show the true form of the propeller blade and to outline the distribution of chord lengths. The views that show both the developed and projected outlines of the propeller blade are the most employed representations in propeller drawings (left side view in Figure 4), showing their relationship to the actual expanded outline (right side view in Figure 4) (Carlton 2018).

For the purpose of calculating the developed area, it is essential to numerically integrate the area beneath the developed profile curve if an exact value is desired. Nevertheless, for most applications, approximating the developed area A_D, using the expanded area of the blade A_E, is sufficient and can be expressed as

$$A_D \approx A_E \tag{1}$$

Historically, several empirical relationships have been proposed for estimating the developed area A_D. A notable formula provided by Burrill (Carlton 2018) is one such relationship, which calculates A_D as:

$$A_D \approx \frac{A_P}{\left(1.067 - 0.229\frac{P}{D}\right)} \tag{2}$$

where A_P is the project area, P represents pitch, and D denotes diameter. This formula is presented to offer a practical and less detailed alternative to precise numerical integration.
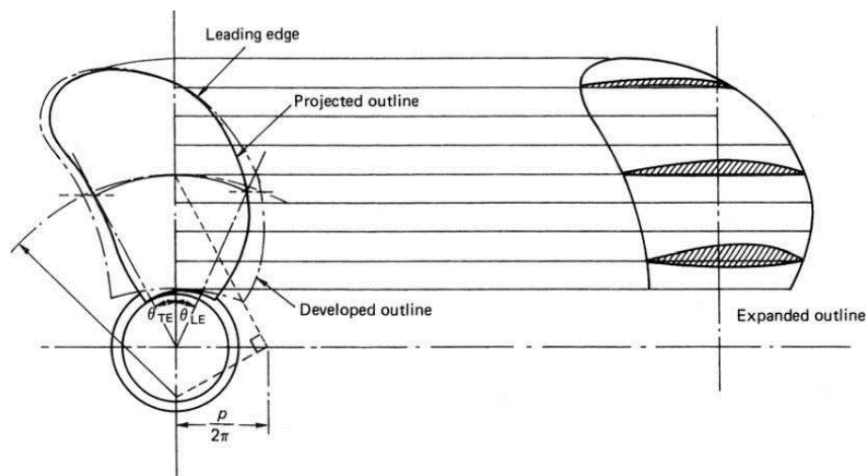
Figure 4 Different outlines of a propeller (Carlton 2018)

2.3. Expanded Outline

The term "expanded outline" might be somewhat misleading as it does not conform to traditional geometric outlines in literature. More accurately, it could be described as a mapping of the chord lengths positioned correctly around the directrix (In propeller theory, the directrix line is a fixed reference line that is perpendicular to the axis of rotation. It serves as a guide for generating the helical surface of the propeller blade, defining the path along which the generating curve moves to form the blade's shape through rotational and translational movements). This mapping does not attempt to illustrate the helical structure of the blades; instead, it simplifies the representation by reducing the pitch angle of each section to zero. Despite this simplification, this perspective is valuable as it shows the shapes of blade sections. These sections are typically illustrated over the chord lengths, as shown in Figure 4. This depiction aids in visualizing how the blade sections are configured and formulate the geometrical shape of the propeller blade.

Expanded outline can also be understood with the help of "cylindrical sections". The imaginary cylinder in Figure 3 can be unwrapped in the XY plane, converting it into a 2D plane. The blade sections are then defined in this XY plane. Through this view, one gets a clear idea of actual distribution of the chord lengths throughout the propeller blade (Carlton 2018).

2.4. Pitch

The pitch of the propeller is defined as the distance that the propeller covers along the X-axis during one complete rotation of the propeller blade. The idea behind the term pitch is similar to the pitch of a screw in a nut, where the distance that the screw advances inside the nut is termed as pitch. This idea can be applied to propellers where a propeller is like the screw and the surrounding fluid is similar to the nut. However, it is important to differentiate between the geometric pitch and the effective pitch.

- Geometric Pitch: The distance that a propeller covers if it was screwed into a nut
- Effective Pitch: While rotating inside a fluid, a propeller doesn't cover the same distance as it would do when screwed into a nut, rather it would keep rotating even if there was no distance travelled. This actual distance that the propeller travels inside the fluid is called effective pitch

Figure 5 demonstrates the idea of geometric pitch of a propeller using the concept of "cylindrical sections". The cylinder is unwrapped in the XZ – plane here as the circumference gets rolled along the z-axis and the pitch of the propeller blade gets laid out along the x-axis. The equation used for obtaining the pitch angle is also shown in the same figure (Carlton 2018).
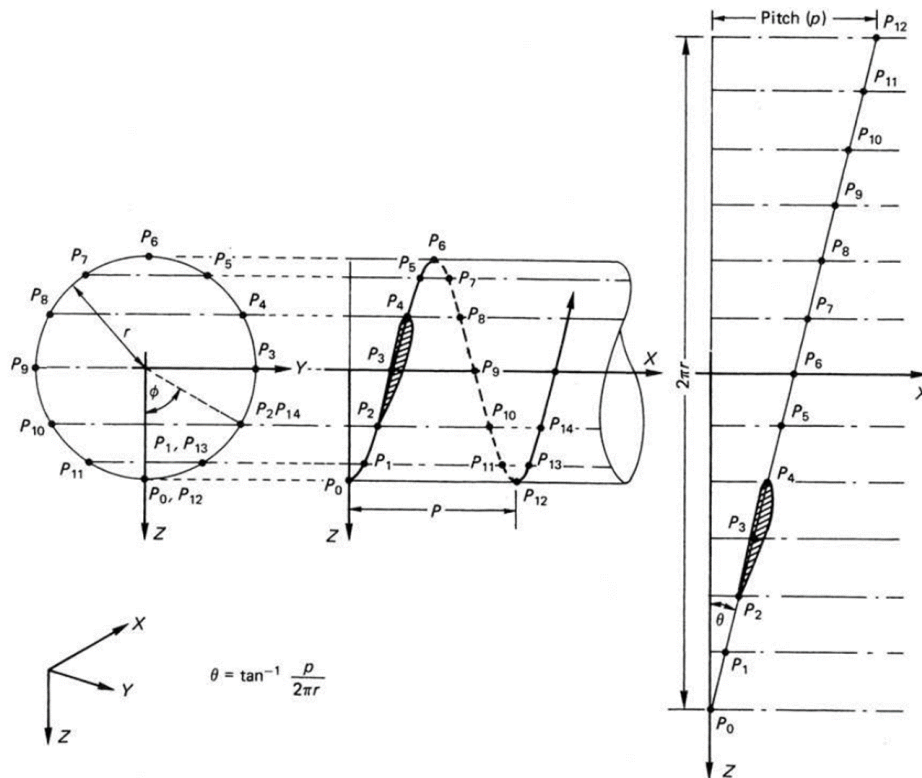
Figure 5 Geometrical pitch representation (Carlton 2018)

2.5. Rake and Skew

Rake and skew are coupled parameters for propeller's geometry although each of them defines the propeller in a sperate plane. Normally, skew in a propeller induces rake which is termed as skew induced rake. Rake can be defined as the axial displacement of the blade sections relative to a radial line perpendicular to the shaft centerline. It can also be understood as the angle of the propeller blade relative to hub's axial plane. This angle is measured between the chord line of the blade section and a plane perpendicular to the propeller shaft. The rake angle θ_R is mathematically expressed as:

$$\theta_R = \tan^{-1}\left(\frac{z}{r}\right) \tag{3}$$

Where z is the axial displacement of the blade tip from the root and r is the radial distance from the hub centerline to the blade tip. Rake can be positive or negative depending on the direction. Positive rake is when the propeller blade tip is angled towards the stern while negative rake is when the propeller blade tip is angled towards the bow. Visual representation of rake is given in . Geometrical parameters of a propeller

Skew, on the other hand, is defined as the tangential displacement of blade sections relative to a radial line from the shaft centerline. Similar to rake, it can be measured as an angle as well, where the angle is measured between the blade reference line and the line through the maximum chord length. Skew angle is given mathematically as

$$\theta_S = \frac{\Delta r}{R} \cdot \tan^{-1}\left(\frac{\Delta y}{r}\right) \tag{4}$$

Where Δr is the incremental radial distance, Δy is the circumferential displacement of the blade section, R is the radius of the propeller and r is the radial distance from the hub centerline to the specific point on the blade where the skew is being measured.

In addition to pitch, rake and skew, other important parameters used to define propeller geometry are

- Propeller Diameter (D)
- Number of blades (N)
- Leading Edge: The edge of the propeller blade that faces the inflow of water
- Trailing Edge: The edge of the propeller blade from which the water exists the blade.
- Chord Length (c): The distance between the trailing edge and the leading edge.
- Pressure Side: The face of the propeller blade that pushes the water during forward motion of the vessel. It is the side of the blade that faces upstream of the flow.
- Suction Side: Face of the propeller blade that faces downstream of the flow.
- Camber: Camber is defined as the asymmetry between the pressure side and suction side of the blade section. It is the difference in the curvature of the two faces of the blade section.
- Maximum Blade Thickness (t)
- C_LE: Defined as the distance from the leading edge of the profile section to the point on the profile section chord line where the helix line (shown in Figure 3) intersects the plane defined by the x-axis and the directrix.

Some of the stated parameters are visually represented below in Figure 6 (Bertram, 2011).
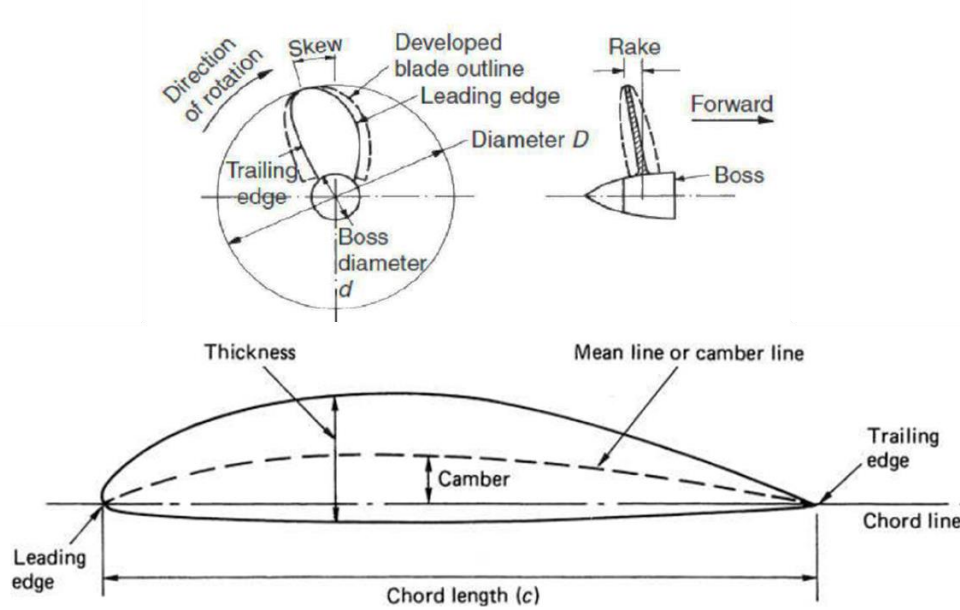
Figure 6. Geometrical parameters of a propeller (Bertram, 2011)

2.6. Hydrodynamic Characteristics of Propellers

The performance of propellers in marine applications can be evaluated through various non-dimensional coefficients that describe different aspects of their operation. These coefficients help in comparing propeller performance across different setups and conditions by normalizing the key physical quantities. The most important parameters are described here

2.6.1. Thrust Coefficient K_T

This parameter quantifies the thrust generated by the propeller relative to its dimensions and operating conditions, calculated using the equation:

$$K_T = \frac{T}{\rho n^2 D^4} \tag{5}$$

Where T is the thrust in Newtons, ρ is the water density in kg/m^3, n denotes the revolutions per second (rps) of the propeller, and D is the diameter of the propeller in meters.

2.6.2. Torque Coefficient K_Q

This coefficient measures the torque applied to the propeller shaft, represented by the formula:

$$K_Q = \frac{Q}{\rho n^2 D^5} \qquad (6)$$

Here, Q is the torque on the propeller shaft in Newton-meters.

2.6.3. Advance Ratio J

This term is used to describe the ratio of the vessel's advance velocity to the circumferential velocity of the propeller's tips, defined as:

$$J = \frac{V_a}{nD} \qquad (7)$$

V_a represents the advance velocity of the vessel. It is important to mention here that the advance velocity is not equal to the vessel velocity. It is basically the velocity of the water that the propeller is experiencing which, practically, is always less than the velocity of the vessel.

2.6.4. Cavitation Number σ

This number indicates the propensity for cavitation, calculated by:

$$\sigma = \frac{p_0 - e}{0.5\rho V^2} \qquad (8)$$

where p_0 is the reference pressure, e is the vapor pressure of water, and V is the representative velocity.

2.6.5. Propeller Efficiency η_p

The efficiency of the propeller is given by:

$$\eta_p = \frac{K_T J}{K_Q 2\pi} \qquad (9)$$

3. FLUID STRUCTURE INTERACTION

Fluid-structure interaction (FSI) is a multidisciplinary field that plays a crucial role in solving complex multi-physics problems. These problems require the application of principles and equations from different physical disciplines to be effectively addressed, namely fluid and structural. FSI presents computational challenges due to its complex geometries and physics; however, the manner in which the interactions between fluid and structures are defined can significantly decrease computational efforts. According to Benra et al. (2011), FSI can be classified based on the solution methods used. These classifications are illustrated in Figure 7.
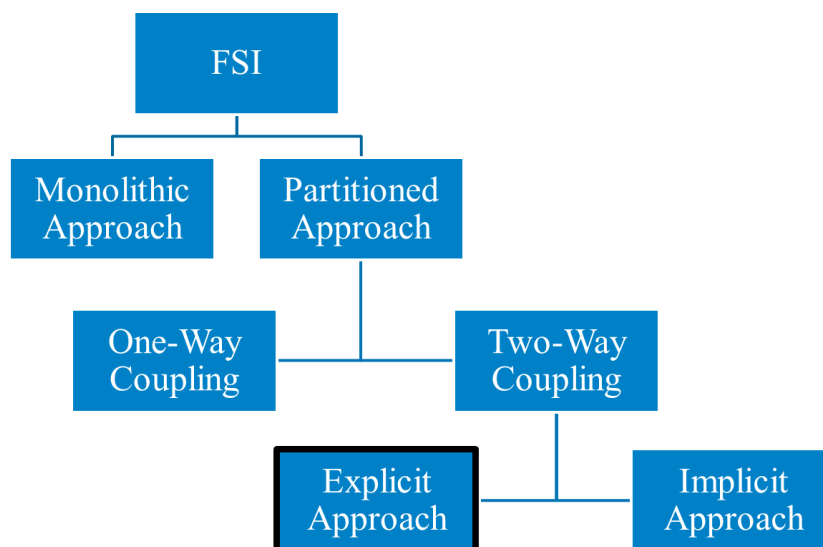
Figure 7. FSI classifications

3.1. Monolithic Approach

Monolithic approach treats both the fluid and the structural model in a single domain. What this means is that the equations for both the fluid and the structural part are combined into one system of equations. FSI solutions using monolithic approach provide the most accurate results, but the computations are of very complex nature so monolithic approach is limited to FSI analysis of structures experiencing small deformations under the action of fluid forces (Heil 2004).

3.2. Partitioned Approach

In partitioned approach, the fluid and structural problems are solved independently by using individual solvers for each domain. These are then coupled using an interface module

responsible for the exchange of boundary conditions. Partitioned methods are attractive because they allow the utilization of well-optimized and mature solvers for both the fluid and structural domains, and they are more modular and flexible when compared to monolithic methods (Heil 2004). Partitioned Approach can further be classified as

- One-Way Coupling
- Two-Way Coupling

In one-way coupling, the fluid solver computes the flow field and the forces acting on the structure. These forces are then transferred to the structural solver, which computes the structural response. However, the structural deformations are not fed back into the fluid solver to influence the fluid flow and calculate modified pressure forces. This approach is computationally efficient and can give reasonable results when the structural deformations are small and do not significantly affect the fluid flow, such as in the analysis of wind loads on stiff buildings.

Two-way coupling methods account for the mutual interaction between the fluid and structure. After the structural solver computes the deformation based on the fluid forces, this deformation is passed back to the fluid solver, which updates the fluid mesh and recalculates the flow field. This process is repeated until convergence within each time step. Two-way coupling is essential for problems where structural deformations significantly influence the fluid flow, such as in the analysis of flexible aircraft wings or composite propellers.

Two-way coupling methods are further divided into explicit (weak) and implicit (strong) schemes:

3.2.1. *Explicit (Weak) Two-Way Coupling*

In explicit two-way coupling, the fluid and structural solvers exchange the load and deformations information between the fluid and structural solvers only once per time step. This coupling approach is adopted to carry out the two-way CFD-FEM coupling in the scope of this thesis work. The fluid forces are computed based on the structure's position at the beginning of the time step, and the deformations obtained as a results of application of these forces on the structural model are used to update the structural position for the next time step. The flowchart of explicit two-way coupling is shown Figure 8. While computationally efficient, explicit coupling can suffer from stability issues, especially for problems with strong added-mass effects (Piperno and Farhat 2001).
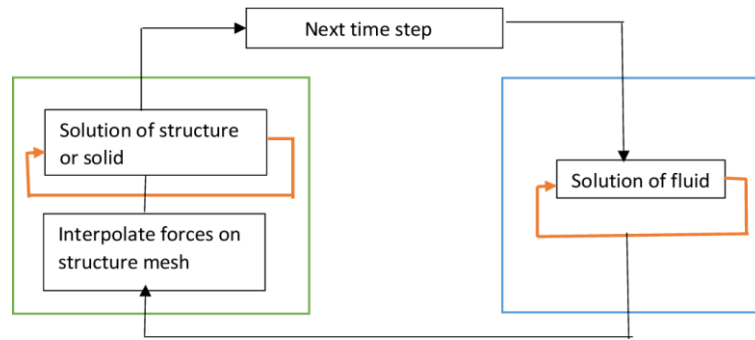
Figure 8. Explicit two-way coupling

3.2.2. *Implicit (Strong) Two Way Coupling*

In implicit two-way coupling, the fluid and structural solvers exchange information multiple times within each time step until convergence is achieved. The parameters of fluid and structural simulations are synchronized with each other. This ensures that the interface conditions are satisfied accurately within every time step. The flowchart of explicit two-way coupling is shown in Figure 9. In terms of approach to solving the FSI problem, implicit two-way coupling is the closest to the monolithic approach. Implicit two-way coupling provides better stability and accuracy, especially for FSI problems with large deformations or strong added-mass effects. But this comes at the cost of increased computational effort (Piperno and Farhat 2001).
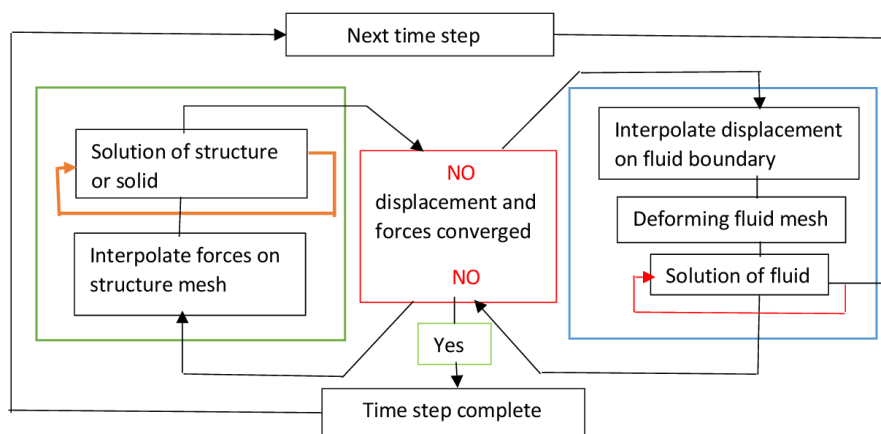
Figure 9. Implicit two-way coupling

The analysis of Fluid-Structure Interaction (FSI) is categorized into different types based on various parameters

- Fluid Structure Interactions can be divided into two categories based on the nature of the fluid – compressible flows and incompressible flows. Compressible flows show variations in density with variating pressures, like air, while incompressible flows

assume constant fluid density. FSI analysis using compressible flows require additional considerations of energy conservation and shock wave propagation (in flows with extremely high velocities). The complexity of these additional considerations can lead to phenomena such as flutter, buffeting, and acoustic resonance, each of which require specialized analysis techniques (Bazilevs et al. 2013).

- Rigid bodies and flexible bodies also demand different approach in terms of setting up the FSI analysis. Rigid bodies show negligible deformations which doesn't have any significant effect on the fluid and pressure fields around that body. Flexible bodies show large deformations under loading and hence affect the pressure and flow fields which in turn changes the loads acting on these flexible bodies. The FSI analysis involving flexible bodies often require advance numerical methods to handle large deformations, such as Arbitrary Langrangian-Eulerian (ALE) formulations or immersed boundary methods (Hou et al. 2012).

3.3. ComPropApp

ComPropApp is a software application developed by MARIN in collaboration with LR Martec for the members of the CRS consortium. The application enables the analysis of fluid-structure interaction (FSI) effects as experienced on flexible marine propellers in behind ship conditions (i.e. operating in a wake flow) as well as in open water (i.e. operating in a uniform flow). More specifically, the software computes the propeller blade loading distribution and subsequent deformed blade shape with internal stress distribution as a function of angular blade position. The user interface of ComPropApp is shown in Figure 10. The application uses CRS boundary element method (BEM) solver PROCAL for the analysis of the hydrodynamic propeller loads in combination with a finite element analysis (FEA) software TRIDENT for the structural analysis. During the analyses, deformed propeller geometry fairing is performed by program P4C (PROPART for ComPropApp) based on the PROPART toolbox of MATLAB routines developed within CRS. ComPropApp's FSI solution method is based on work performed by PhD student Pieter Maljaars (Maljaars 2019).
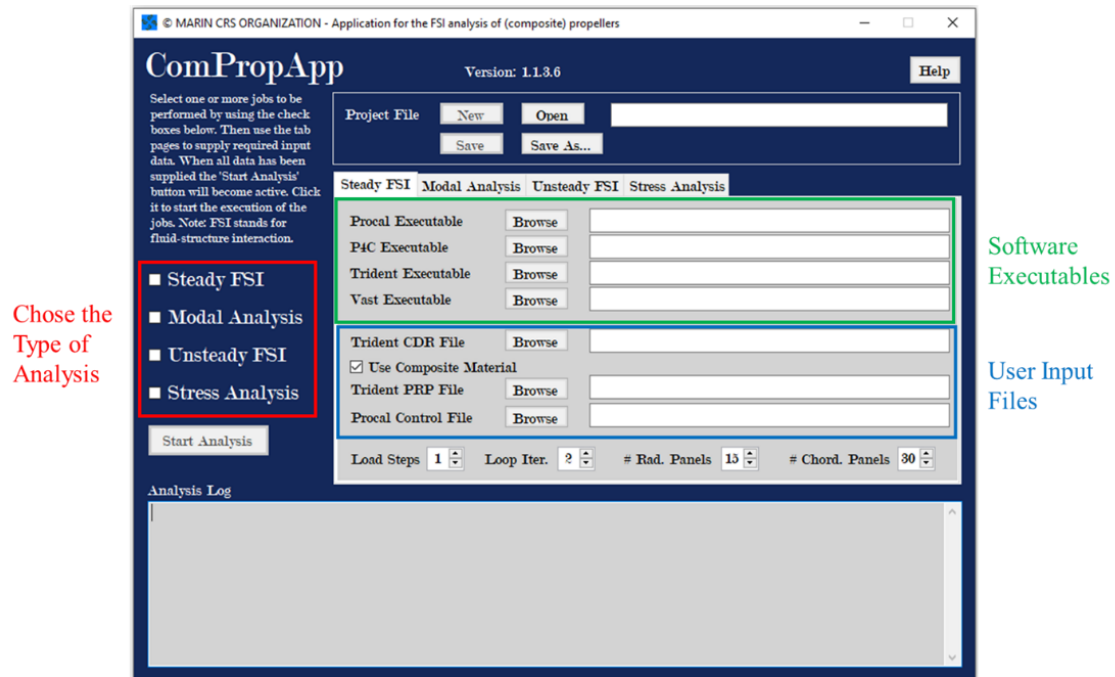
Figure 10. User interface of ComPropApp

Only steady FSI analysis has been performed in the scope of this thesis work. Steady FSI refers to the FSI analysis of the propeller blade loaded by a uniform incident flow. The solution is a time-independent deformed blade shape and internal stresses with corresponding hydrodynamic load. For the steady analysis, a geometrically non-linear finite element procedure is applied. Thus, no limitation with regards to the magnitude of the deformations has to be imposed. To avoid divergence, the load is applied to the structure in increments, called load steps. PROCAL computes the incremental load by reducing the RPM and advance velocity in such a way that a certain percentage of the total load is obtained, whilst keeping the advance coefficient constant. The latter is to maintain the loading distribution while increasing its magnitude. For every load step TRIDENT/PVAST computes the deformed blade shape. On that basis a new propeller panel file is generated by program P4C, which is input to PROCAL for the next load increment. After the full load has been applied in the finite element analysis, one or more iterations at constant maximum load can be performed until the thrust and maximum blade deformation converge. The sum of the load steps and the additional iterations is called loop iterations. The entire workflow is depicted in the flowchart in Figure 11 which is taken from the user manual of ComPropApp.
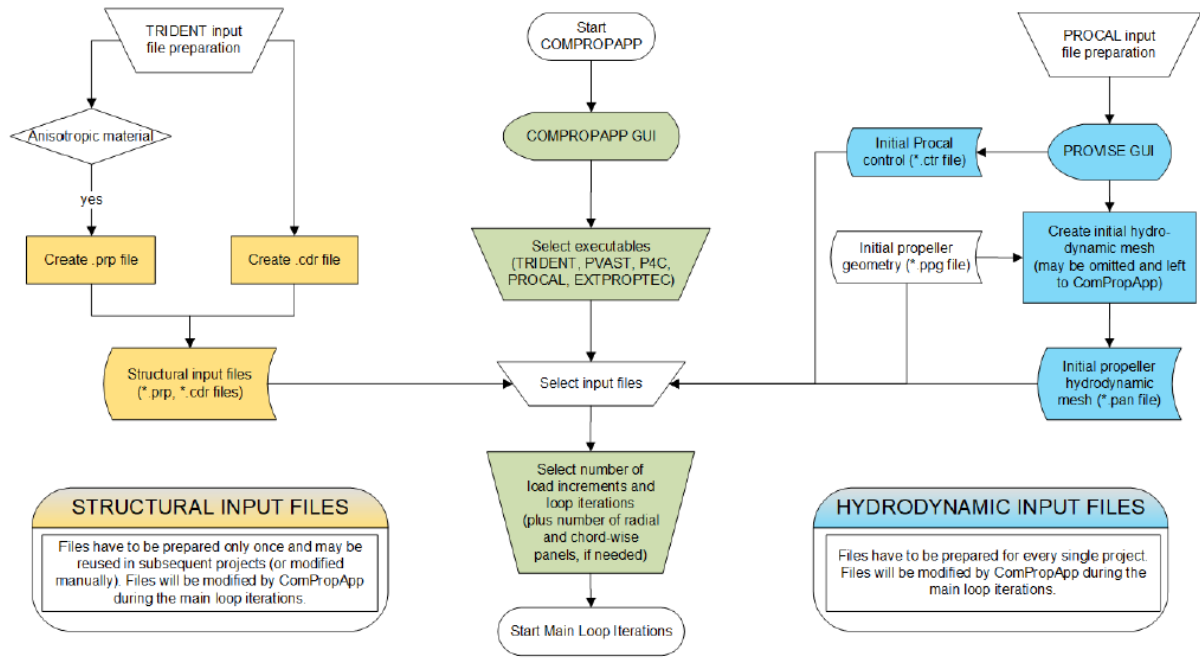
Figure 11 ComPropApp workflow

3.4. Theoretical background

3.4.1. Theoretical basis of RANSE based CFD solvers

Reynolds Averaged Navier Stokes Equations (RANSE) are based on fundamental fluid flow equations, the Navier-Stokes-Equations (NSE), which are derived from the fundamental principles of mass and momentum conservation for fluid flow. The flow is a function of both spectral and temporal variables (White 2006) and is defined in the 3D space as

$$\vec{u} = u(x, y, z, t)\vec{\imath} + v(x, y, z, t)\vec{\jmath} + w(x, y, z, t)\vec{k} \qquad (10)$$

Where u, v, and w represent the velocity components along the x, y, and z axis, respectively, and t represents time. The continuity equation, which expresses the conservation of mass, is given by:

$$\frac{\partial \rho}{\partial t} + \nabla \cdot (\rho \vec{u}) = 0 \qquad (11)$$

Where ρ is the fluid density, and $\nabla \cdot (\rho \vec{u})$ represents the divergence of the mass flux with ∇ being the Laplacian operator. For incompressible flows, $\frac{\partial \rho}{\partial t} = 0$ which implies that the inflow of the fluid into a finite control volume is equal to the outflow of the fluid. In other terms, the divergence of the fluid is zero. This is mathematically expressed as

$$(\rho \vec{u}) = \frac{\partial(\rho u)}{\partial x} + \frac{\partial(\rho v)}{\partial y} + \frac{\partial(\rho w)}{\partial z} = 0 \tag{12}$$

$\nabla \cdot$ Since ρ is constant, it is factored out simplifying the equation

$$\frac{\partial u}{\partial x} + \frac{\partial v}{\partial y} + \frac{\partial w}{\partial z} = div\,\vec{u} = 0 \tag{13}$$

The above equation is the continuity equation for incompressible fluids in a 3D space. Using Newton's second law of motion and considering the non-stationary and viscous effects in fluid flow, we get the three-dimensional Navier-Stokes-Equations which is a representation of conservation of momentum equation

$$\rho \left(\frac{\partial \vec{u}}{\partial t} + \vec{u} \cdot \nabla \vec{u} \right) = -\nabla p + \mu \nabla^2 \vec{u} + \rho \vec{g} \tag{14}$$

Where ∇p is the pressure gradient, $\rho \vec{g}$ represents the external force such as gravity and $\mu \nabla^2 \vec{u}$ represents the internal stress forces because of the viscous effects.

The Navier-Stokes-Equation, in its instantaneous form, describes the complete motion of a fluid flow, including turbulent fluctuations. However, resolving all the turbulent fluctuations requires extremely fine computational grids and high computational resources, which is impractical for practical engineering applications. Instead of using NSE, Reynolds-Averaged Navier-Stokes-Equations (RANSE) approach is used which is a technique to model turbulent flows by decomposing the instantaneous velocity into time-averaged and fluctuating components (Wilcox et al. 1998):

$$u_i = \overline{u_i} + u_i' \tag{15}$$

Where $\overline{u_i}$ is the time-averaged velocity component, and u_i' is the fluctuating velocity component. Substituting this decomposition into NSE and applying a time-averaging operation yields the RANSE equations:

$$\frac{\partial \overline{u_i}}{\partial t} + \overline{u_j} \frac{\partial \overline{u_i}}{\partial x_j} = -\frac{1}{\rho} \frac{\partial \overline{p}}{\partial x_i} + v \frac{\partial^2 \overline{u_i}}{\partial x_j \partial x_j} - \frac{\partial \overline{u_i' u_j'}}{\partial x_j} \tag{16}$$

In this equation, $\overline{u_i}$ represents the mean velocity components, $\overline{p}$ is the mean pressure, v is the kinematic viscosity, and $\overline{u_i' u_j'}$ represents the Reynolds stress tensor, which accounts for the turbulent fluctuations. This Reynolds stress tensor introduces additional unknowns, known as

the closure problem, which requires turbulence modeling to relate the Reynolds stresses to the mean flow variables. Various turbulence models, such as the k-epsilon, k-omega, or Reynolds stress models, are used to close the RANSE equations. The RANSE method with $k - \omega\ SST$ turbulence closure model is used in the scope of this thesis work to achieve CFD-FEM coupling through the use of START CCM+ software.

3.4.2. Theoretical basis of BEM based solvers

The Boundary Element Method (BEM) is a numerical technique based on potential flow theory in which the fluid is assumed to be inviscid, incompressible and irrotational. The BEM theory presented in this section is the specific background of PROCAL BEM solver used in the ComPropApp. Only the formulations that have been implemented are presented. Background information on these and alternative formulations can be found in e.g. Katz and Plotkin (2001). The system of equations that is solved in PROCAL is based on Green's integral theorem in a formulation proposed by Morino et al. (1975). The geometry of the propeller blade is discretized into panels as shown in Figure 12. For every collocation point p (defined as the center of each panel), the following equation is valid for the disturbance potential φ

$$\varphi(p) = -\frac{1}{2\pi} \int_S \left[\mu n \cdot \nabla \left(\frac{1}{|r|} \right) + \sigma \frac{1}{|r|} \right] dS_b - \frac{1}{2\pi} \int_S \left[\Delta\mu_w n \cdot \nabla \left(\frac{1}{|r|} \right) \right] dS_w \tag{17}$$

in which μ corresponds to the dipole strength, σ corresponds to the monopole (or source) strength, n is the normal to the surface and r is the vector connecting a point on the surface and point p. In the right-hand side, a distinction is made between the body surfaces S_b and the wake surfaces S_w
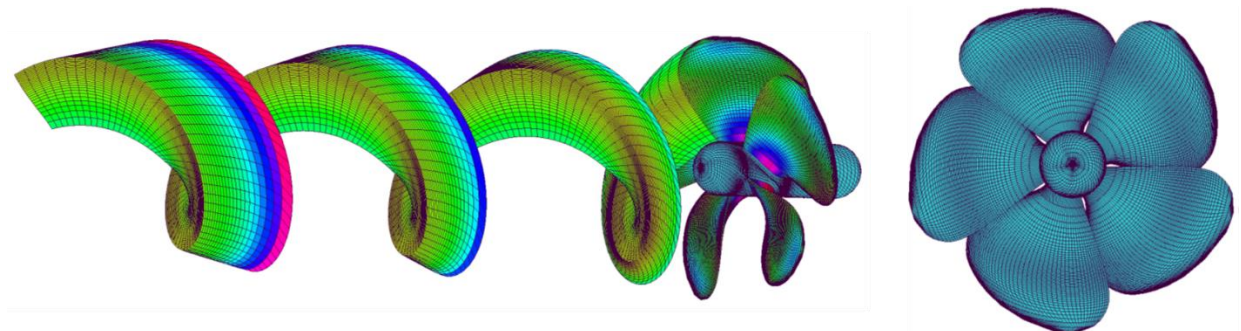
Figure 12. Propeller blade and wake discretization in PROCAL using BEM

The strength of the source panels and dipole panels on the blade and the hub are then defined by the following boundary conditions.

The first boundary condition states that the body surface is impermeable, and thus the normal velocity to the element is equal to zero:

$$n \cdot u = n \cdot \nabla \Phi = n \cdot (\nabla \varphi + U_\infty) = 0 \Leftrightarrow \sigma = n \cdot \nabla \varphi = -n \cdot U_\infty \tag{18}$$

The second boundary condition assumes local 2D flow and states that the velocity component on the upper side u of the trailing edge is equal to the velocity component on the lower side l of the trailing edge which is also termed as the Kutta boundary condition. By specifying that the potential outside the volume V (inside the propeller blade) equals zero, the following boundary condition for the dipole strength is obtained

$$\mu = -\varphi \tag{19}$$

Expressing the velocity as a change in potential leads to the following equation

$$\mu_w = -\Delta \varphi_w = -\Delta \varphi_b = -\left(\varphi_{b,u} - \varphi_{b,l}\right) \tag{20}$$

where subscript b corresponds to the body trailing edge and w corresponds to wake of the. This boundary condition is applied for each wake panel at the trailing edge.

Using the Boundary conditions, equation 17 becomes

$$\varphi(p) - \frac{1}{2\pi} \int_S \left[\varphi n \cdot \nabla \left(\frac{1}{|r|}\right)\right] dS_b - \frac{1}{2\pi} \int_S \left[\Delta \varphi_w n \cdot \nabla \left(\frac{1}{|r|}\right)\right] dS_w = -\frac{1}{2\pi} \int_S \left[\sigma \frac{1}{|r|}\right] dS_b \tag{21}$$

Where all the unknown quantities are arranged on the left side of the equation. The discretized equation for point p then becomes

$$\sum_{isurf=1}^{Nsurf} \sum_{isym=1}^{Z} \sum_{i=1}^{Ni_{isurf}} \sum_{j=1}^{Nj_{isurf}} D_{nij}\varphi_{ij} + \sum_{isurf=1}^{Nsurf} \sum_{isym=1}^{Z} \sum_{i=1}^{Nwi_{isurf}} \sum_{j=1}^{Nwj_{isurf}} W_{nij}\Delta\varphi_{ij}$$
$$= \sum_{isurf=1}^{Nsurf} \sum_{isym=1}^{Z} \sum_{i=1}^{Ni_{isurf}} \sum_{j=1}^{Nj_{isurf}} S_{nij}\sigma_{i,j} \tag{22}$$

In which D, W, and S correspond to the hydrodynamic influence coefficient matrix for a dipole on the body, a dipole on the wake, and for a source on the body respectively. The summation is taken over N_{surf} number of surfaces, each consisting of Z symmetry surfFaces of which each one consists of $Ni_{isurf} \times Nj_{isurf}$ body panels and $Nwi_{isurf} \times Nwj_{isurf}$ wake panels. The

system of equations is closed as the equations are set up for center points on all surfaces. The wake strengths are treated as unknowns and the system of equations is added with equation 20 for each wake strip j. The parameters in equation 22 are shown in Figure 13.
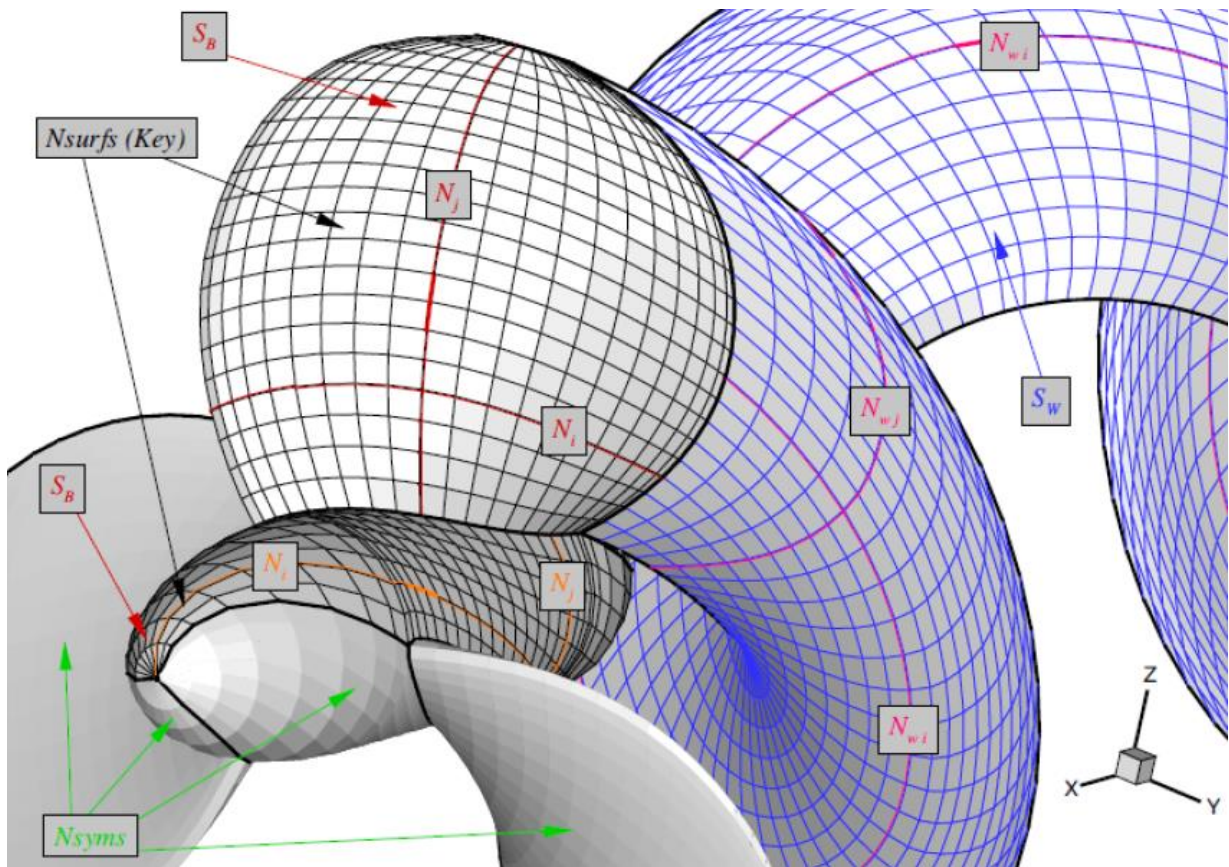
Figure 13. Geometry discretization parameters in PROCAL (Maljaars 2019).

The system of equations for each panel is then solved using Lower Upper (LU) decomposition technique. These systems of equations give potential functions which are then further used to compute pressure forces. Detailed theoretical background on pressure computation using the above equations can be found in the Ph.D. work performed by Maljaars in 2019.

4. BENCHMARK STUDY OF FINITE ELEMENTS

The type of finite elements chosen for creating the FE model significantly impacts the structural results of the composite propeller blade. To understand this impact, a benchmark study was conducted to analyze the static structural response of a composite plate model using three different types of elements

- Plate laminate elements
- Solid volume elements
- Solid laminate elements

The study aims to compare the effect of using these three element types on the structural results of the plate, mainly deformations and stresses. The plate is divided into five zones, as shown in Figure 14, based on the number of plies and the total thickness of each zone. The composition of each zone is given in Table 2. The composite plate is made of unidirectional and twill layers of carbon fiber and epoxy resin with a repeating pattern of stacking as shown in Figure 15.

Table 1 - Layup properties

Properties	Units	Unidirectional (U)	Woven Roving (X)
Fiber Volume Fraction	-	0.30	0.30
Fiber Mass	g/m^2	600	600
Individual Layer Thickness	mm	1.117	1.117
Individual Layer Density	-	1.412	1.412
Longitudinal Stiffness E_1	MPa	73570.18	38855.52
Transverse Stiffness E_2	MPa	3861.83	38855.52
Out of Plane Stiffness E_3	MPa	3861.83	3861.83
Shear Modulus G_{12}	MPa	2413.19	2413.19
Shear Modulus G_{13}	MPa	2413.19	2171.87
Shear Modulus G_{23}	MPa	1689.23	2171.87
Poisson Ratio υ_{12}	-	0.290	0.029
Poisson Ratio υ_{13}	-	0.290	0.256
Poisson Ratio υ_{23}	-	0.223	0.256

The individual layer properties of each of these layers are given in Table 1. The properties are calculated using "**BV NR546 Hull in Composite, Plywood and High Density Polyethylene Materials**" (BV NR546, 2022). Alternatively, the properties can also be obtained from the BV freeware **ComposeIT.** But the use of ComposeIT in itself isn't sufficient to obtain the out-of-

plane properties for each layer since ComposeIT is restricted to providing only in-plane properties. Hence the out of plane properties for each layer (Unidirectional and Woven Roving) would still need to be calculated using BV NR546. An excel sheet was developed to calculate the individual properties of both unidirectional and woven roving layers based on BV NR546

Table 2 - Zone layers and thicknesses

Zone	Number of Plies	Thickness [mm]
1	26	29.05
2	20	22.35
3	14	15.64
4	8	8.94
5	2	2.23
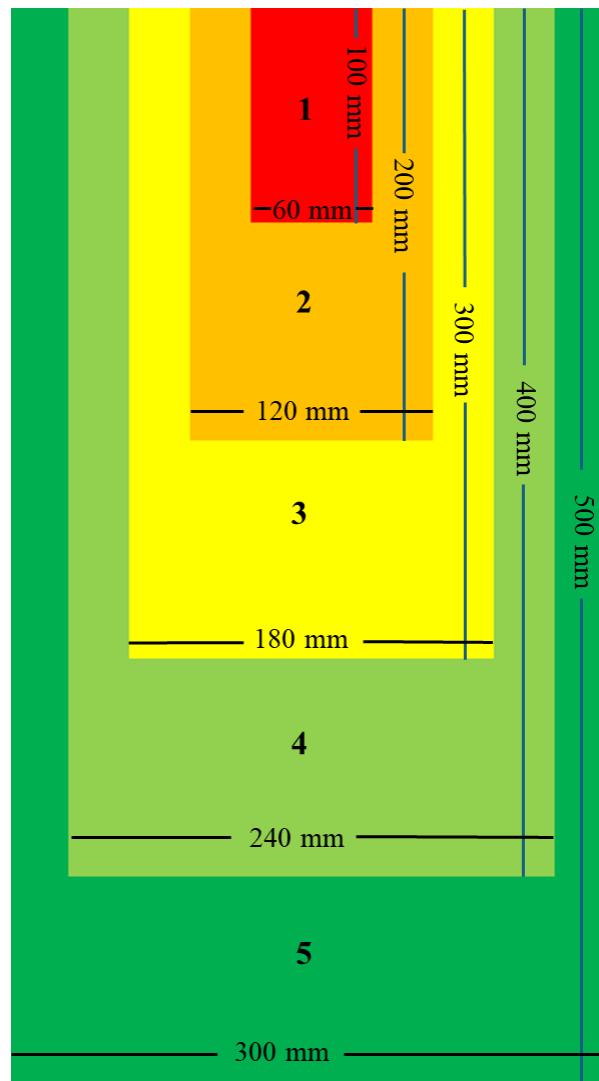
Figure 14 - Division of zones in the blade model

The plies are numbered from bottom to top of the blade and their layup is defined in Figure 15 where "X" implies woven roving and "U" implies unidirectional. This numbering scheme of plies is consistent throughout this chapter and these numbers are used as the identification to locate the plies with the maximum stress within the laminate.

ZONE 1	ZONE 2	ZONE 3	ZONE 4	ZONE 5	
X					Ply 26
U					
U	ZONE 2				
X	X				Ply 20
U	U				
U	U	ZONE 3			
X	X	X			Ply 14
U	U	U			
U	U	U	ZONE 4		
X	X	X	X		Ply 8
U	U	U	U		
U	U	U	U	ZONE 5	
X	X	X	X	X	Ply 2
X	X	X	X	X	Ply 1
U	U	U	U		
U	U	U	U		
X	X	X	X		Ply 1
U	U	U			
U	U	U			
X	X	X			Ply 1
U	U				
U	U				
X	X				Ply 1
U					
U					
X					Ply 1

Figure 15 - Zones layup and numbering scheme

4.1. Modelling

Three different modelling approaches were used for the blade geometry considering the type of elements used for each model of the blade.

4.1.1. Plate Laminate Elements

Plate Laminate elements are an extension of normal shell elements, except that they are composed of one or more layers, each of which can be individually defined. Plate laminate

elements are typically used for slender bodies where out of plane behavior of the element is not important.
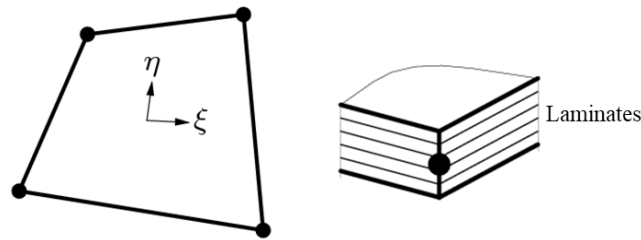
Figure 16. Plate laminate element with four nodes

A 2D mid-surface shell model of the composite blade was created and subsequently divided into zones to assign zone-specific properties to each of the five zones. The shell model is demonstrated in Figure 17.
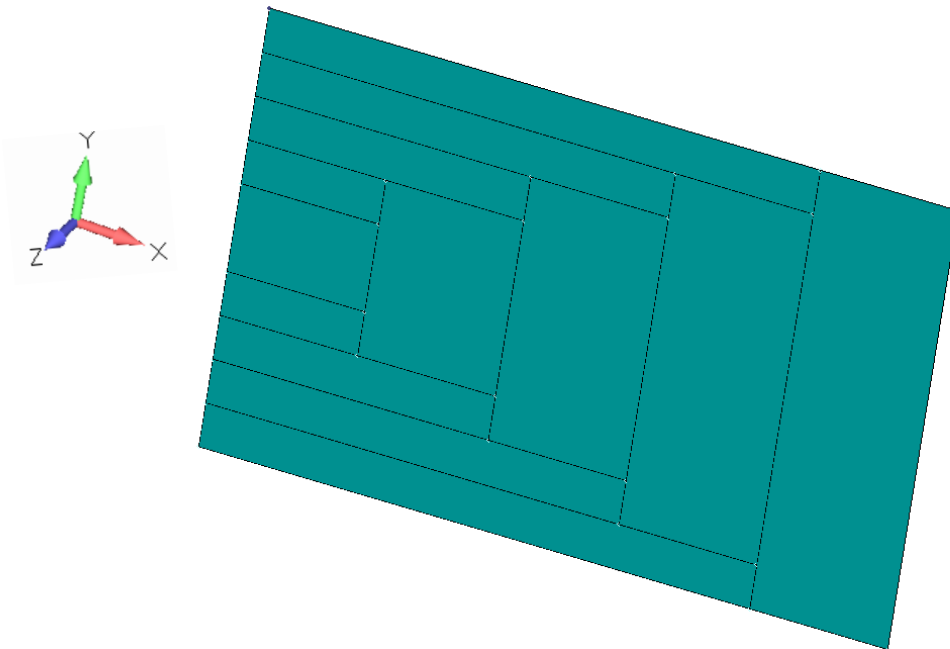
Figure 17. 2D mid-surface shell model created to be meshed using plate laminate elements

4.1.2. Solid Elements

Solid elements are general purpose elements that prove to be handy when dealing with arbitrary geometries as they eliminate the need for creating mid surface models as required for shell elements. As opposed to shell elements, solid elements also account for out of plane behavior and hence become useful where the out of plane results such as bending moments are important. Using solid elements for composite modelling is a risky endeavor as each individual ply inside a layup requires its own element. This means that the FE model requires as many through-

thickness solid elements as the number of plies in the layup. This significantly increases the computational time, even for very simple geometries such as the plate model in current study.
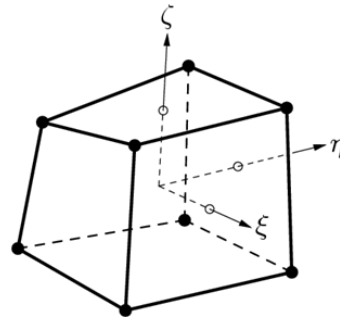
Figure 18. An eight node isoparametric solid brick element

The blade geometry had to be modelled according to the zone-specific thickness for each individual zone as shown in Figure 19 and then material properties relevant to each zone were assigned using eight node solid elements.
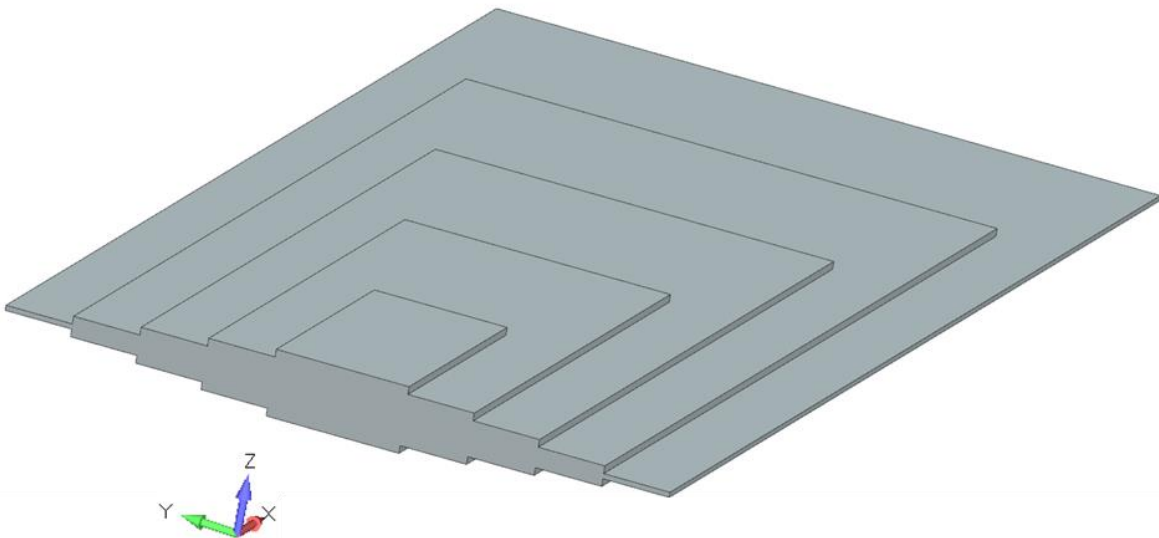
Figure 19. 3D model created to be meshed using solid elements

4.1.3. Solid Laminate Elements

Solid laminate elements behave exactly like solid elements, except that they are made up of one or more plies. This eliminates the requirement of having as many through thickness elements as the number of plies. Rather, only one through thickness element is sufficient to capture the layup properties of the model. This also eliminates the need for creating stepped geometry for meshing as used in the case of solid elements.
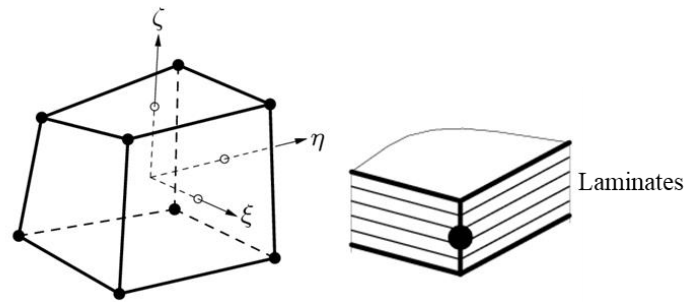
Figure 20. Solid laminate element with eight nodes

The blade geometry was modelled with continuous taper without any need for stepped transition between zones as solid laminate elements have the capability to capture tapered and curved geometry shapes efficiently.
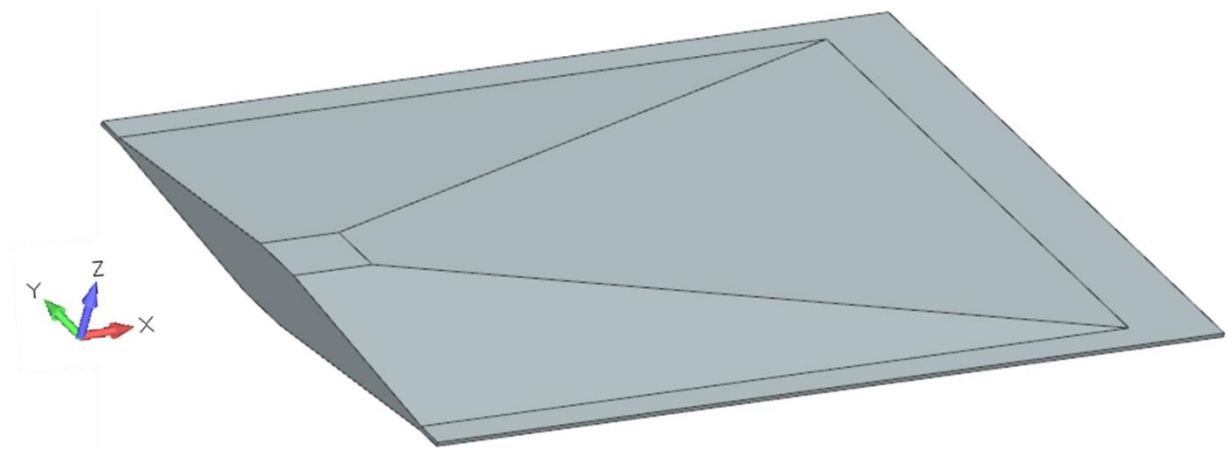
Figure 21. 3D model created to be meshed using solid laminate elements

4.1.4. Loads Application

The plate behavior was analyzed using four separate load cases

- 0.01 MPa surface Pressure in -Z direction
- 1500 N out of plane concentrated load in -Z direction
- 100 kNmm Torque about the +X-axis (longitudinal axis)
- 10 kN in plane distributed load along +X-axis (centrifugal force)

The load application points and their values are shown in Figure 22
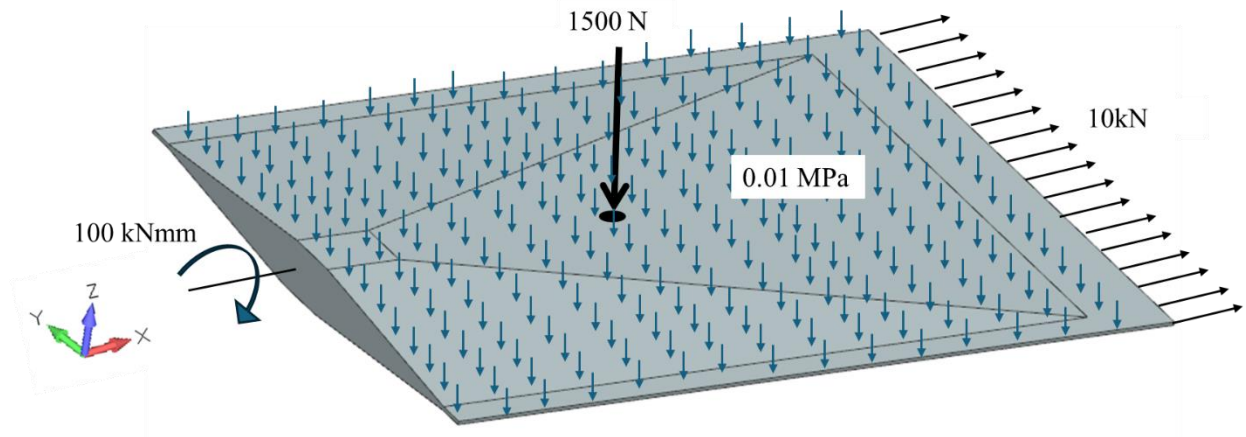
Figure 22. Loads on the plate

4.1.5. Constraints

The plate is clamped at one end marked in Figure 23 where all the degrees of freedom are restricted for all the nodes at the marked edge of the plate.
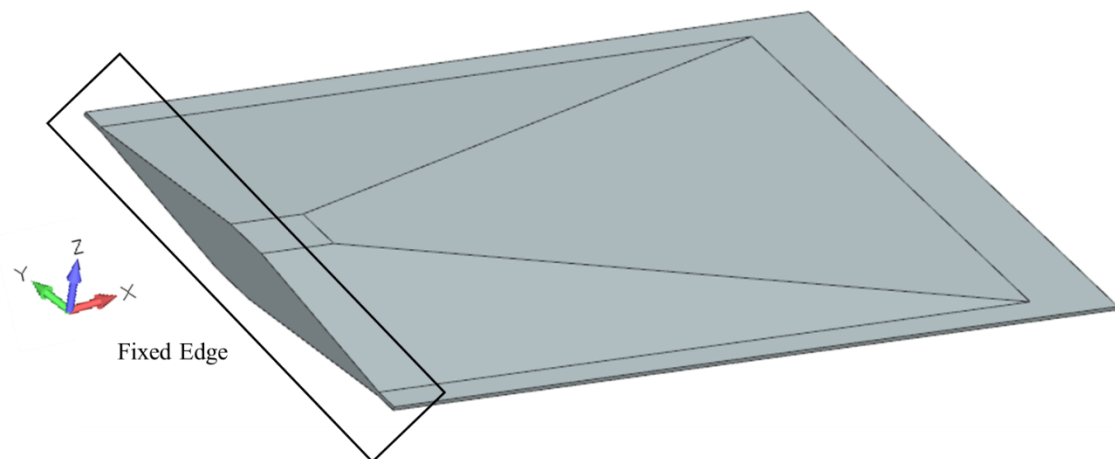
Figure 23. Boundary constraints on the plate

4.2. Results and Discussions

The structural response to the applied loading conditions using different element types shows significant differences in terms of principal stresses and deformations. The results are presented based on individual load cases. The comparison is established for two parameters:

- Maximum deformation in the z-direction – T_3
- Maximum stress along the x-direction - σ_{11}

The directions are based on the coordinate system shown in Figure 23. Only for the load case of centrifugal force, instead of T_3, the maximum deformation in the x-direction – T_1 is studied.

4.2.1. Surface Pressure

As the plate acts like a cantilever beam in bending, the maximum deformation in the z-direction T_3 occurs at the free edge opposite to the clamped edge of the blade (tip of the blade). The plate laminate model and the solid element model with one element per ply thickness show similar results for displacement T_3 but show significant difference in the maximum stress in the fiber direction σ_{11}. While the solid laminate model deviates from the other two models in both displacement T_3 and stress σ_{11} significantly.
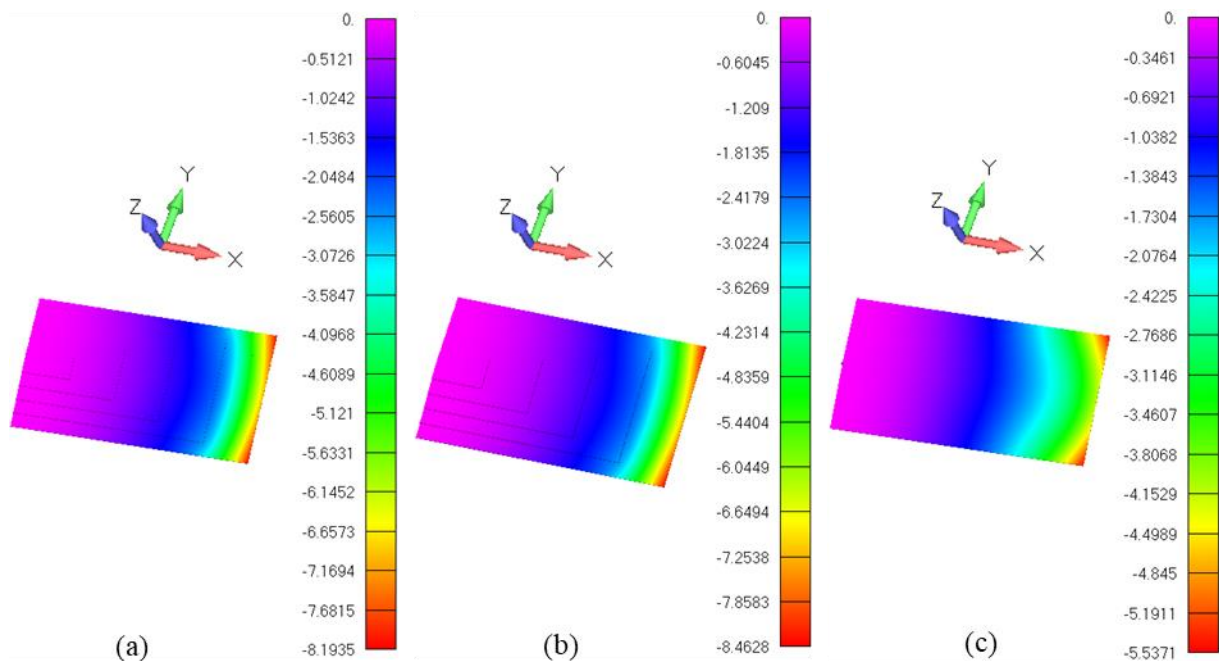
Figure 24. Max deformation T_3 for each model - (a) Plate laminate, (b) Solid , (c) Solid laminate
Load Case – Surface Pressure, All the values are in "mm"

The plate laminate model and the solid element model show excessive amount of maximum stress σ_{11} as compared to the solid laminate model. The reason for this can be attributed to the stepped geometry for both models that results in stress concentration points each time there is a thickness drop (as we move from one zone of the plate to another zone). The maximum of these stress occurs at the transition points between zone 4 and zone 5 as demonstrated in Figure 25 for both models. These values are impractical and based on these values the actual areas of the plate that experience the maximum value for σ_{11} (plies 2 and 25 of zone 1) could be neglected.
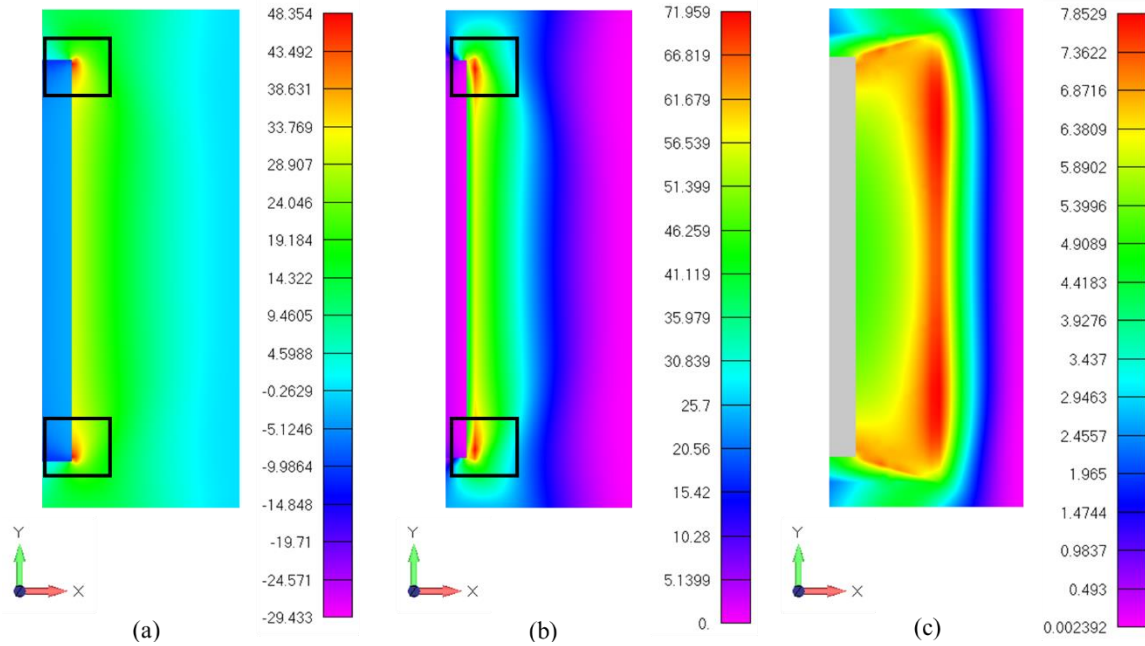
Figure 25. Max stress σ_{11} for each model – (a) Plate laminate, (b) Solid, (c) Solid laminate
Load Case – Surface Pressure, All values are in "MPa"
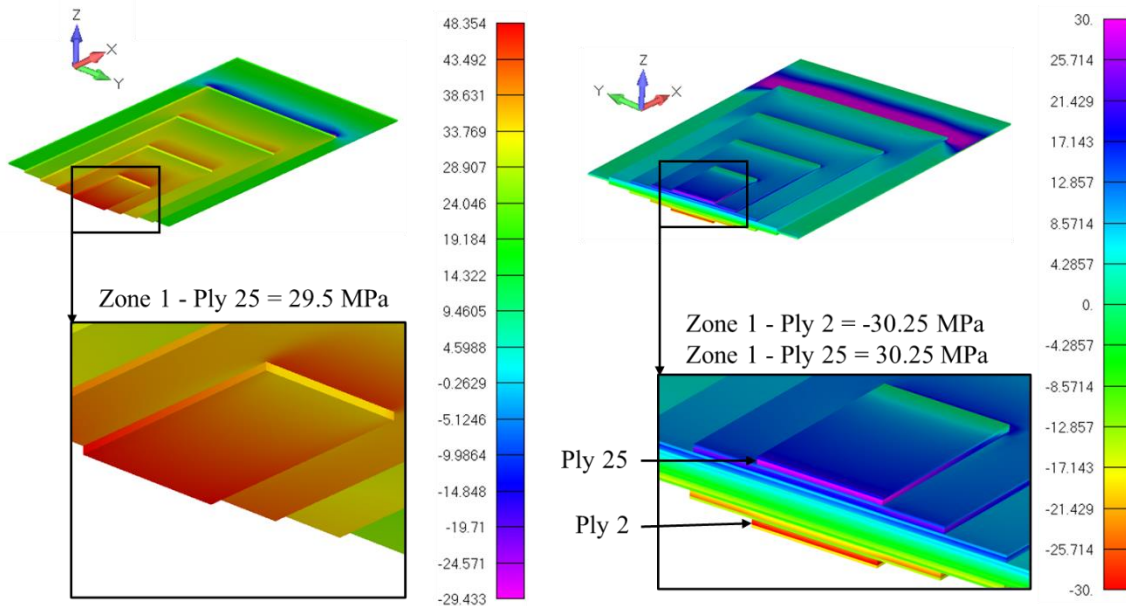
Figure 26. Stress σ_{11} contour for - (Left) Plate laminate model, (Right) Solid element model
Load Case – Surface Pressure, All the values are in "MPa"

The solid laminate element model shows a continuous distribution of stress σ_{11} throughout the blade based on the modelling approach used for this element. The maximum stress σ_{11} occurs in plies 2 and 25 in zone 1 and is around 30 MPa which is validated by the previous two models with plate laminate and solid elements. The results are tabulated below where Table 3 shows the comparison of structural results using linear elements while Table 4 gives the same comparison using quadratic elements. Zone and ply number indicates the location of the

maximum values in the plate model where the stress hotspot areas in plate laminate and solid element models are neglected.
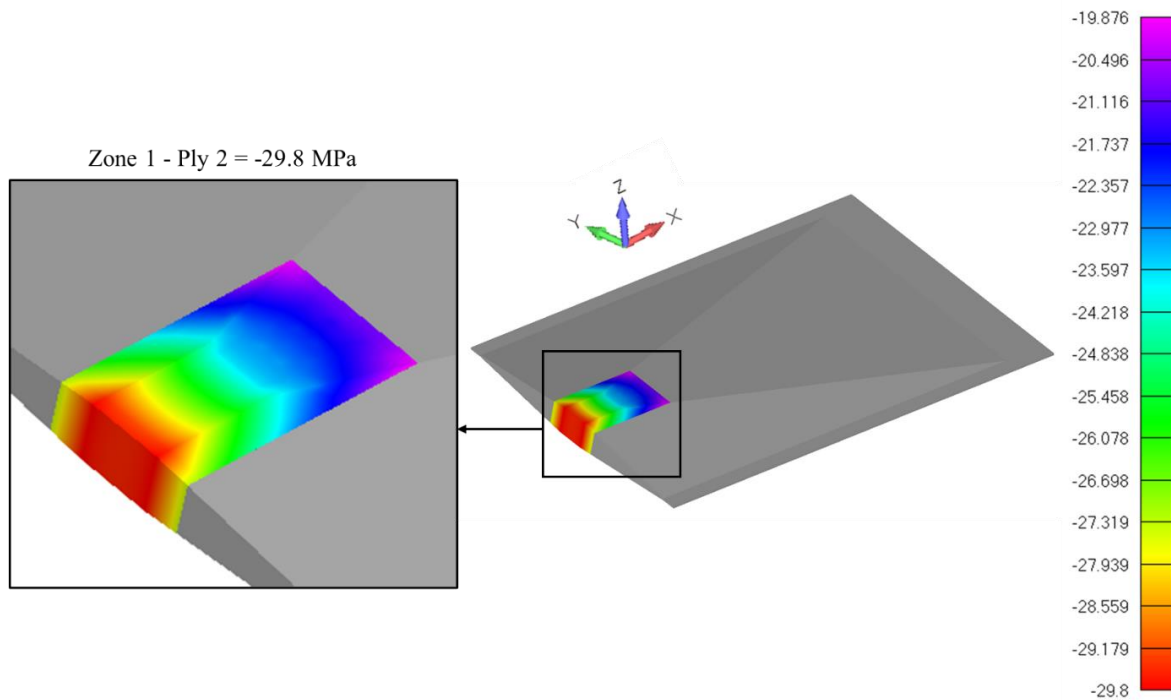
Figure 27. Max stress σ_{11} contour for solid laminate model - Load Case – Surface Pressure
All values are in "MPa"

Table 3. Surface pressure results – Linear elements

Elements Type	Maximum Deflection T₃		Maximum Stress σ₁₁			Zone & Ply #
	mm	*% Difference*	*MPa*		*% Difference*	
Plate Laminate	8.19	48.1	Compression	-29.43	-1.2	Zone 1 Ply 2
			Tension	29.43		Zone 1 Ply 25
Solid	8.46	52.9	Compression	-30.25	1.51	Zone 1 Ply 2
			Tension	30.25		Zone 1 Ply 25
Solid Laminate	5.53	-	Compression	-29.8	-	Zone 1 Ply 2
			Tension	29.8		Zone 1 Ply 25

Table 4. Surface pressure results - Quadratic elements

Elements Type	Maximum Deflection T₃		Maximum Stress σ₁₁			Zone & Ply #
	mm	% Difference	MPa		% Difference	
Plate Laminate	8.21	48.1	Compression	-29.31	-1.3	Zone 1 Ply 2
			Tension	29.31		Zone 1 Ply 25
Solid	8.54	54.1	Compression	-30.09	1.3	Zone 1 Ply 2
			Tension	30.09		Zone 1 Ply 25
Solid Laminate	5.54	-	Compression	-29.70	-	Zone 1 Ply 2
			Tension	29.70		Zone 1 Ply 25

If we ignore the stress concentration areas marked in Figure 25, all three models show similar behavior in terms of maximum stress values and the location of these maximum stress values but there is certain discrepancy in the deformation results. The possible justification for this is provided in section 4.3.

4.2.2. Out of Plane Concentrated Load

The behavior of the blade under the action of concentrated out of plane load mimics the behavior of the blade when subjected to uniform pressure over the surface of the blade, except that the peak values for displacement T₃ are different. The solid element model gives greater value of max deformation T₃ (conservative results) while the solid laminate element gives the least value of max deformation T₃ (non-conservative results). The laminate element model gives intermediate values as shown in Figure 28.
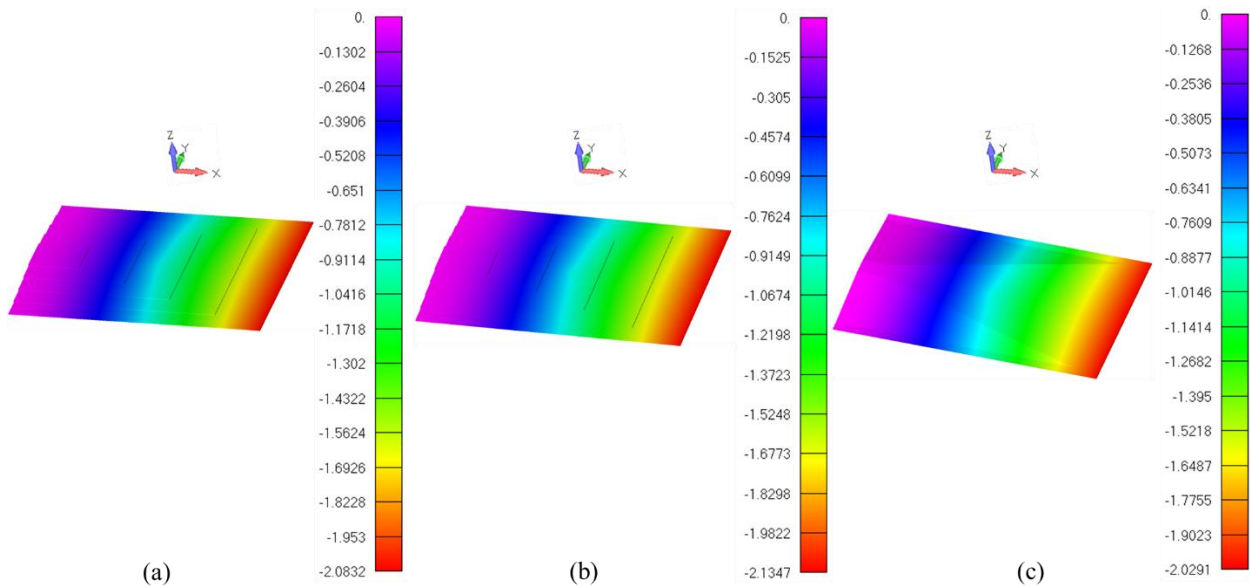
Figure 28. Max deflection T_3 for models - (a) Plate laminate, (b) Solid, (c) Solid laminate
Load Case – Concentrated Load, All the values are in "mm"

The max value for stress σ_{11} shows similar behavior for each of the element model, but the laminate and solid element models exhibit high stress regions around the transition points between two zones in the blade. These results are expected as these areas experience stress concentration due to inherent stepped geometry of the blade in both of these models as shown in Figure 29.

On the other hand, the solid laminate model shows a very smooth distribution of stress σ_{11} all over the blade. Only the point of application of the out of plane concentrated load shows a peak in the stress value when compared to the adjacent elements/nodes, but this is already expected as point loads using a node are not practical, rather there would be some contact area on the plate surface in practical case for any concentrated load which would make the stress more evenly distributed.
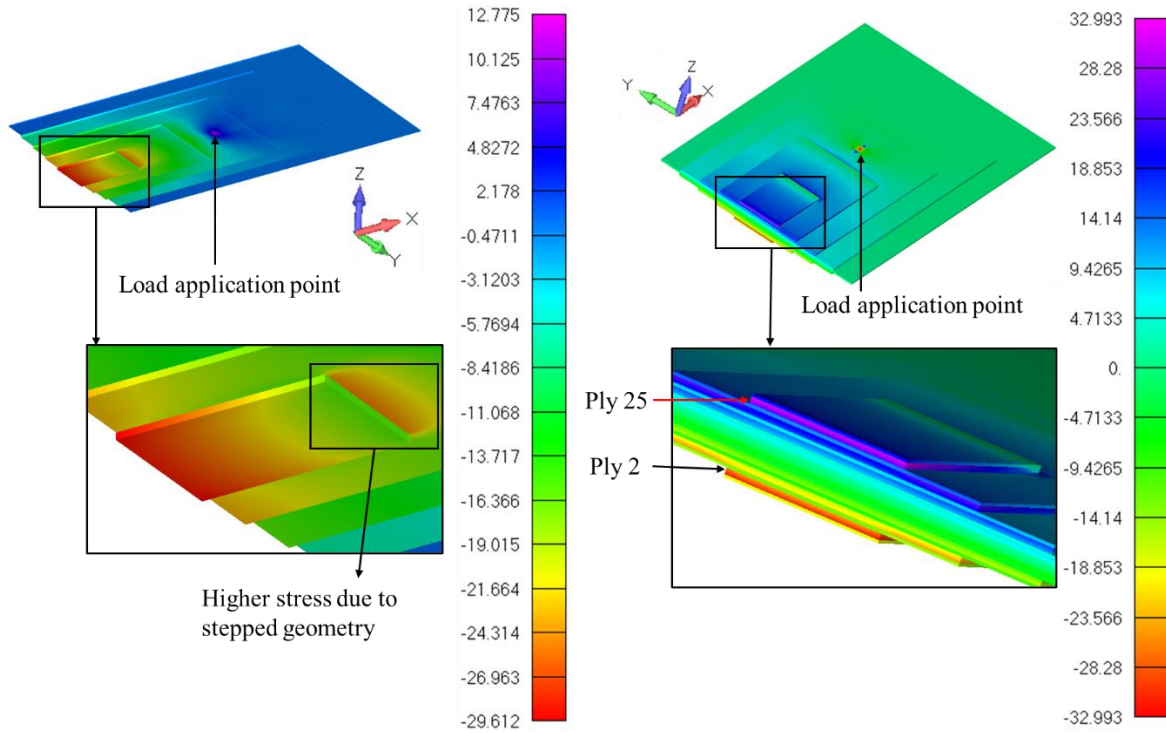
Figure 29. Stress σ_{11} contour for - (Left) Plate laminate model, (Right) Solid element model Load Case – Concentrated Load, All values are in "MPa"
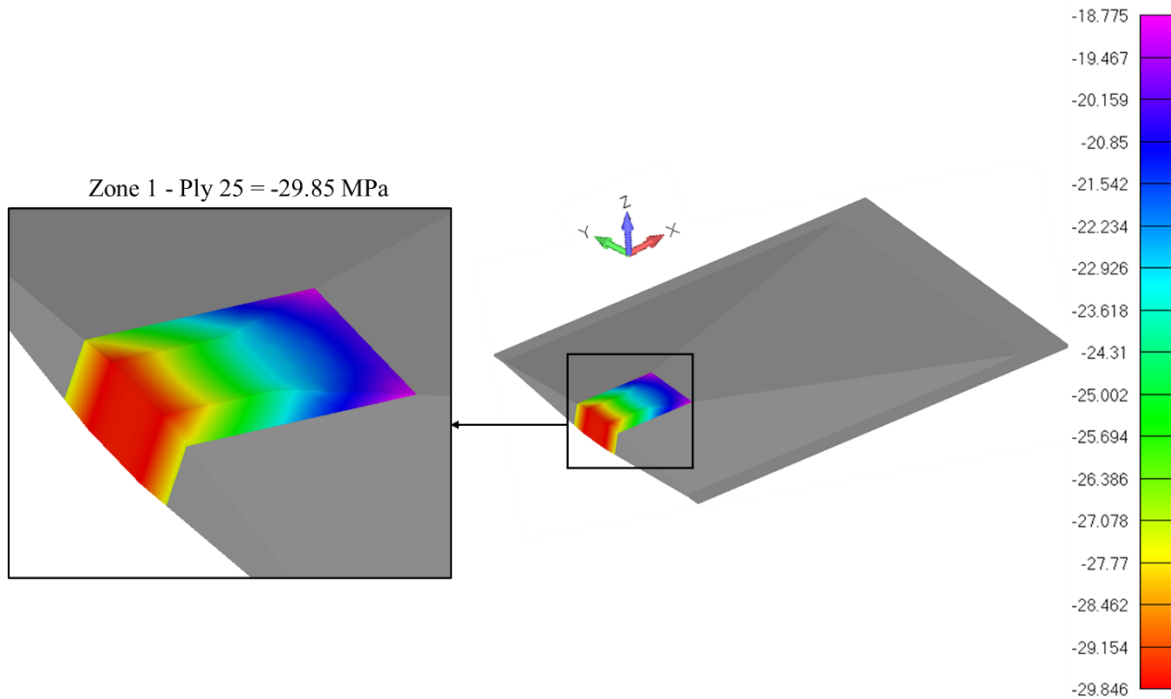
Figure 30. Stress σ_{11} contour for Solid laminate model - Load Case – Concentrated Load, All values are in "MPa"

The results are tabulated below where Table 5 shows the comparison of structural results using linear elements while Table 6 gives the same comparison using quadratic elements. Zone and Ply # indicate the location of the maximum values of stress in the plate model.

Table 5 - Concentrated load results – Linear elements

Elements Type	Maximum Deflection T3		Maximum Stress σ11			Zone & Ply #
	mm	% Difference	MPa		% Difference	
Plate Laminate	2.08	2.9	Compression	-29.61	-0.7%	Zone 1 Ply 2
			Tension	29.61		Zone 1 Ply 25
Solid	2.13	5.4	Compression	-32.99	10.55	Zone 1 Ply 2
			Tension	32.99		Zone 1 Ply 25
Solid Laminate	2.02	-	Compression	-29.84	-	Zone 1 Ply 2
			Tension	29.84		Zone 1 Ply 25

Table 6 - Concentrated force results - Quadratic elements

Elements Type	Maximum Deflection T₃		Maximum Stress σ₁₁			Zone & Ply #
	mm	% Difference	MPa		% Difference	
Plate Laminate	2.09	3.4	Compression	-29.49	-0.9%	Zone 1 Ply 2
			Tension	29.49		Zone 1 Ply 25
Solid	2.13	5.4	Compression	-30.34	1.9	Zone 1 Ply 2
			Tension	30.34		Zone 1 Ply 25
Solid Laminate	2.02	-	Compression	-29.76	-	Zone 1 Ply 2
			Tension	29.76		Zone 1 Ply 25

4.2.3. Torque About the X-axis of the blade

A torque of 100 kN.mm was applied about the longitudinal ais of the blade (X-axis). The three models give similar trends in terms of conservative and non-conservative behavior as of pressure and concentrated forces. The solid element model gives the greater value of maximum tip deformation T_3 while the solid laminate element model gives the minimum value of maximum tip deformation T_3 out of the three models. The results for the plate laminate models are intermediary.
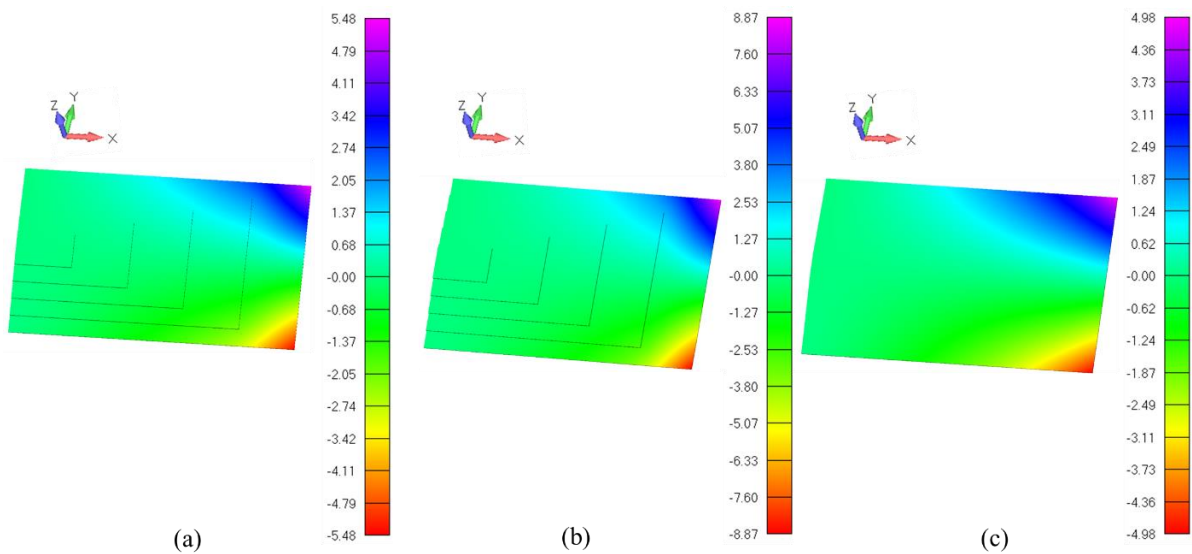
Figure 31. Max deflection T_3 for models - (a) Plate laminate, (b) Solid, (c) Solid laminate
Load Case – Torque, All values are in "mm"

The three models give close results in terms of stress σ_{11}. The stepped geometries for the laminate and the solid element models again create regions of abrupt thickness drop with stress concentration, where the maximum stresses occur in zone 5 as shown in Figure 32. These max σ_{11} values are geometry dependent, as the solid laminate model with a tapered thickness drop gives smooth distribution of stress σ_{11} over the blade without any hotspots due to abrupt thickness change. Figure 33 shows the maximum values of stress for plate laminate and solid element models when the stress hotspot areas due to the stepped geometry are neglected.
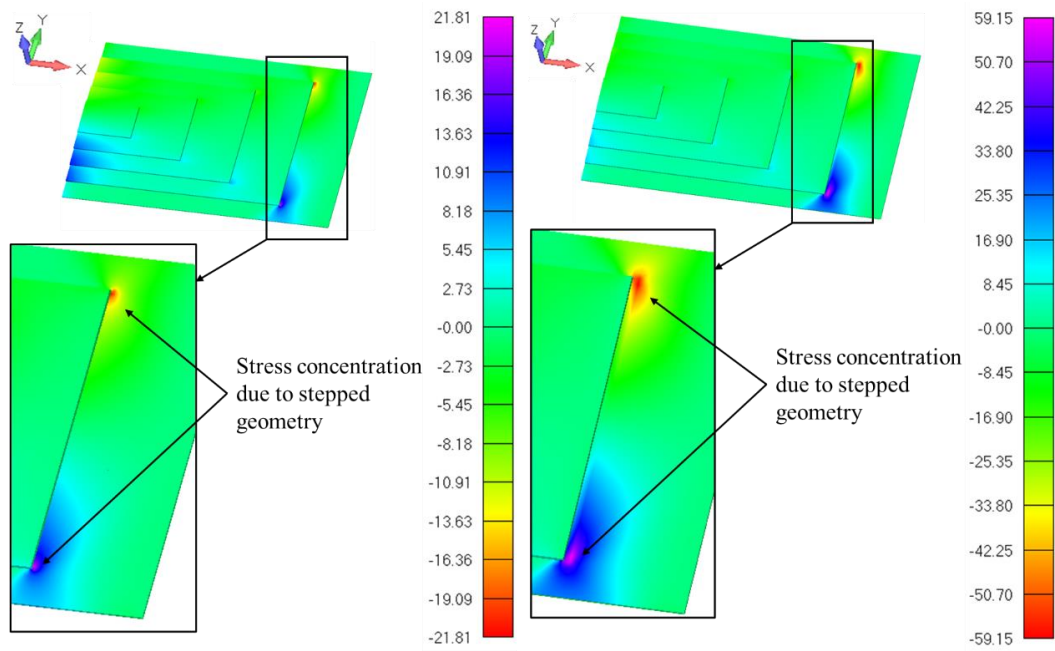
Figure 32 – Stress σ_{11} concentration areas in models - (Left) Plate laminate, (Right) Solid element Load Case – Torque, All values are in "MPa"
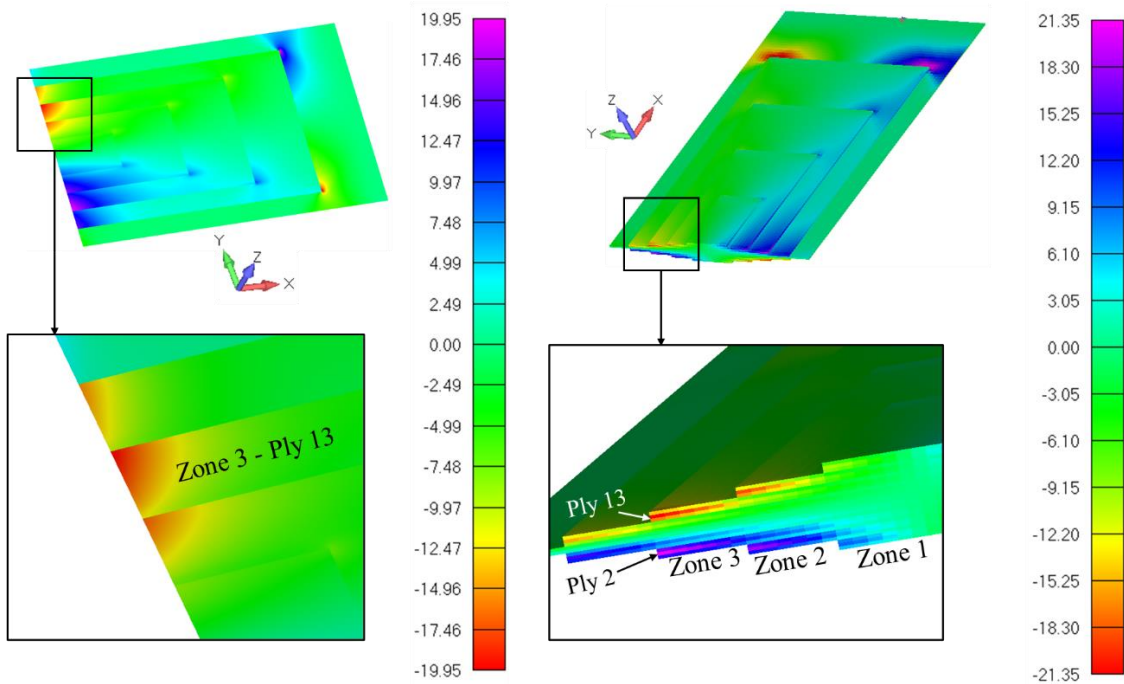
Figure 33 - Stress σ_{11} contour in - (Left) Plate laminate model, (Right) Solid element model Load Case – Torque, All values are in "MPa"
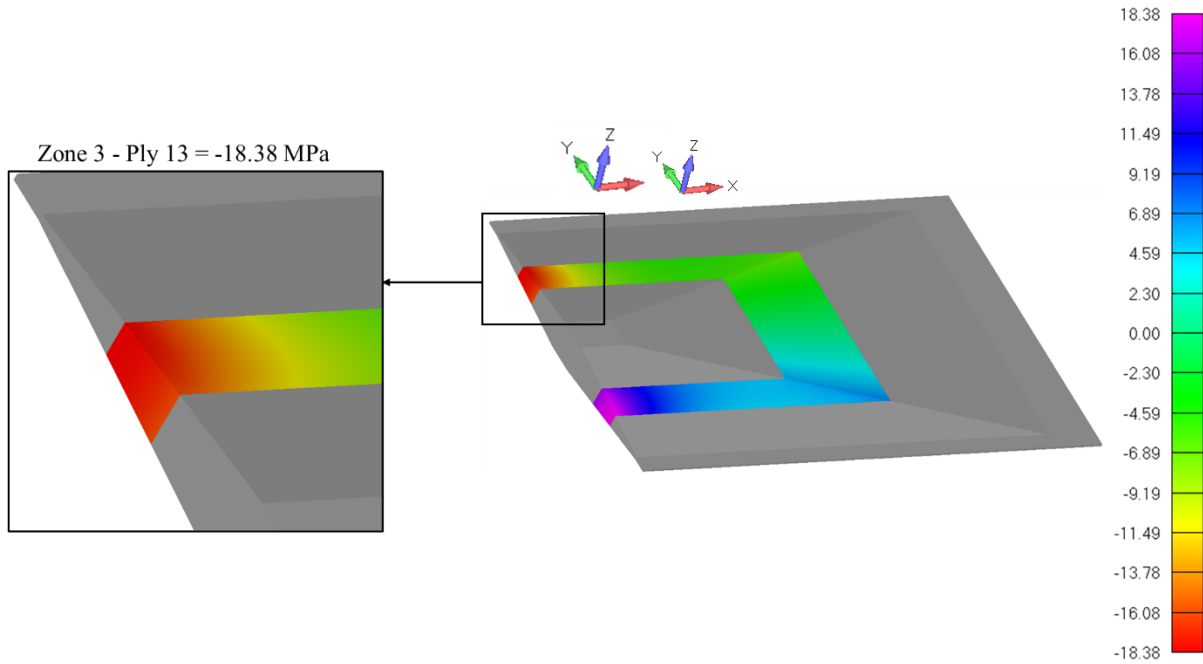
Figure 34 - Stress σ_{11} contour in Solid laminate model - Load Case – Torque
All values are in "MPa"

Neglecting the concentrated stress areas of the blade shown in Figure 32, the maximum values of stress σ_{11} occur in ply number 2 and 13 in zone 3 of the blade and this is validated by all three models, although with some differences in the peak value. The results are shown in Figure 33 and Figure 34 and are tabulated below in Table 7 for linear elements and Table 8 for quadratic elements.

Table 7 - Torque results – Linear elements

Elements Type	Maximum Deflection T₃		Maximum Stress σ₁₁			Zone & Ply #
	mm	*% Difference*	*MPa*		*% Difference*	
Plate Laminate	5.48	10.04	Compression	-19.95	8.5	Zone 3 Ply 2 and 13
			Tension	19.95		
Solid	8.87	78.11	Compression	-21.35	16.15	
			Tension	21.35		
Solid Laminate	4.98	-	Compression	-18.38	-	
			Tension	18.38		

Table 8 - Torque results - Quadratic elements

Elements Type	Maximum Deflection T$_3$		Maximum Stress σ$_{11}$			Zone &
	mm	% Difference	MPa		% Difference	Ply #
Plate Laminate	5.49	10.2	Compression	-20.00	9.2	Zone 3 Ply 2 and 13
			Tension	20.00		
Solid	8.97	80.1	Compression	-21.11	15.2	
			Tension	21.11		
Solid Laminate	4.98	-	Compression	-18.31	-	
			Tension	18.31		

4.2.4. In-Plane Distributed Load (Centrifugal Force)

A distributed load of 10 kN was applied along the longitudinal axis of the blade (+X-axis). The three models give similar results with a max difference of 8% in terms of tip deformation T$_1$. The solid element model gives the greater value of maximum tip deformation T$_1$ while the solid laminate element model gives the lesser value of maximum tip deformation T$_1$ out of the three models. The results for the plate laminate models are intermediary and close to solid element model.
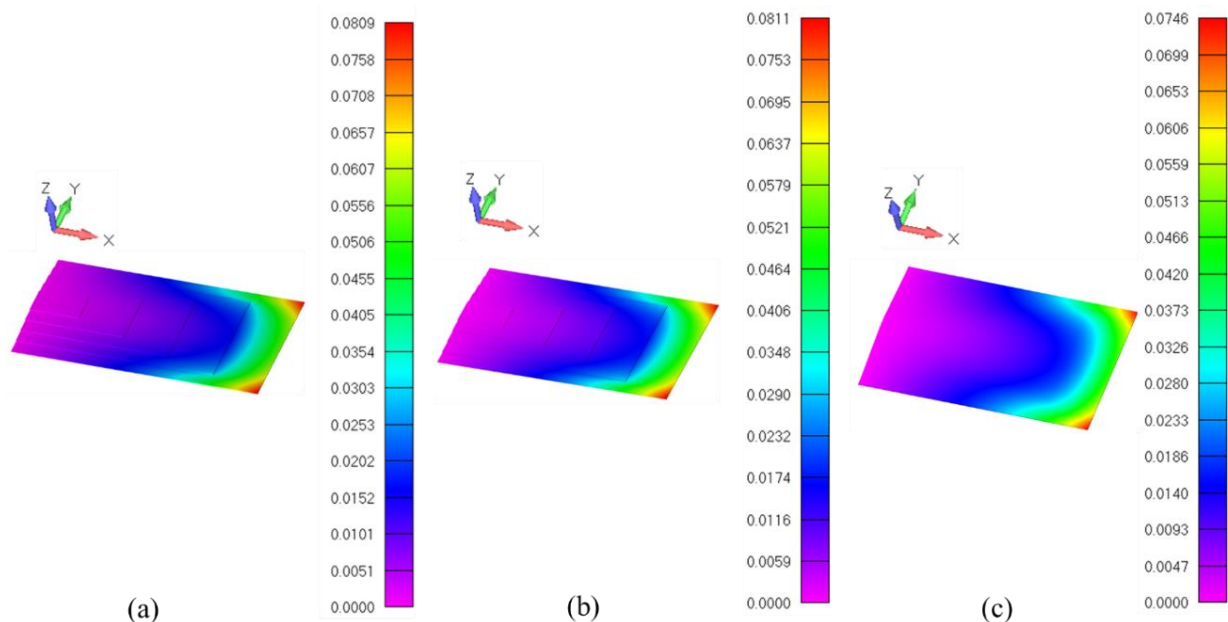
Figure 35 - Max deformation T$_1$ for models - (a) Plate Laminate, (b) Solid, (c) Solid Laminate
Load Case – Centrifugal Force, All values are in "mm"

The three models give significant difference in values of stress σ_{11}. The stepped geometries for the laminate and the solid element models again create regions of abrupt thickness drop with stress concentration areas, where the maximum stresses occur in zone 5 as shown in Figure 36. These maximum σ_{11} values are geometry dependent, as the solid laminate model with a tapered thickness drop gives smooth distribution of stress σ_{11} over the blade without any hotspots due to abrupt thickness change.
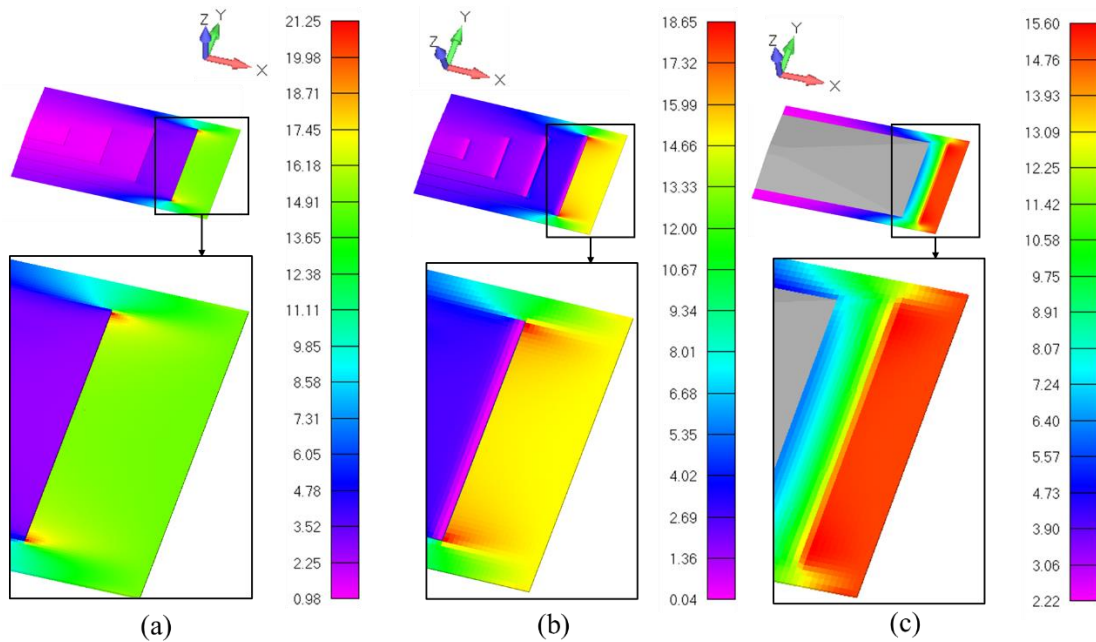
Figure 36 - Stress σ_{11} contour in models - (a) Plate Laminate, (b) Solid, (c) Solid Laminate
Load Case – Centrifugal Force, All values are in "MPa"

Table 9 - Centrifugal force results – Linear elements

Elements Type	Maximum Deflection T_1		Maximum Stress σ_{11}			Zone and Ply #
	mm	*% Difference*	*MPa*		*% Difference*	
Plate Laminate	0.0809	8.4	Tension	21.25	36.2	Zone 5 Ply 1 and 2
Solid	0.0811	8.7	Tension	18.65	19.55	
Solid Laminate	0.0746	-	Tension	15.60	-	

Table 10 - Centrifugal force results - Quadratic elements

Elements Type	Maximum Deflection T_1		Maximum Stress σ_{11}			Zone and Ply #
	mm	*% Difference*	*MPa*		*% Difference*	
Plate Laminate	0.0816	7.8	Tension	20.63	32.2	Zone 5 Ply 1 and 2
Solid	0.0887	17.1	Tension	19.16	22.8	
Solid Laminate	0.0757	-	Tension	15.60	-	

4.3. Conclusions

The FE model created using solid laminate elements gives non-conservative results in terms of maximum tip deformations and stresses compared to plate laminate and solid FE models. The higher deformations shown by plate laminate and solid FE models are due to the significant thickness drop between consecutive zones, particularly zones 4 and 5, which reduces the stiffness of the FE model. Since maximum deformations occur at the tip of the plate in zone 5, the pressure load causes consecutive zones to act like a clamped beam in bending for plate laminate and solid FE models, as shown in Figure 37. This occurs because of the stepped geometry inherent in FE models created using these two element types. The solid laminate elements FE model lacks this stepped geometry and, therefore, does not suffer from this thickness and stiffness drop. Additionally, the solid laminate FE model maintains a higher thickness in zone 5 compared to the other two models, as shown in Figure 38. These factors combined result in the solid laminate FE model showing lower tip deformations compared to the plate laminate and solid FE models under pressure load.
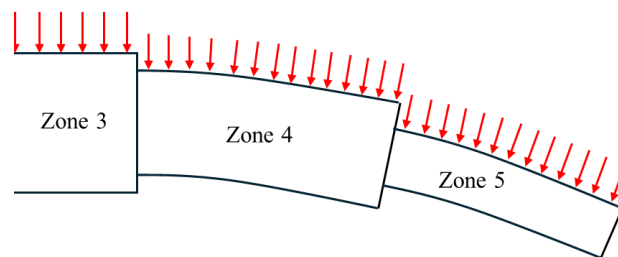
Figure 37. Each zone of the plate acting as stepped clamped beam under pressure load
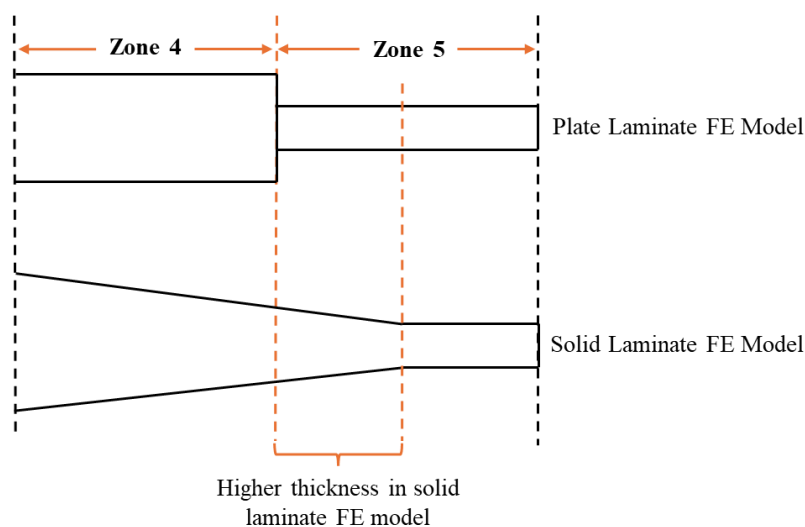
Figure 38. Thickness difference in zone 5 between plate laminate and solid laminate FE models

This is further proven by the study of the deformation results obtained in the case of concentrated load. Since no load is applied on zone 4 and zone 5, the maximum deformations for all the FE models are very close to each other with a maximum of 5% difference in the peak values. On the other hand, FE model creation using plate laminate elements is a fairly easier task as compared to solid laminate elements. Creating a mid-surface shell model is sufficient to use plate laminate elements as opposed to the requirement of creating a detailed geometrical model for using solid laminate elements. The main conclusions of this benchmark study are tabulated below in Table 11.

Table 11. Finite elements comparison

Model type	Plate Laminate	Solid	Solid Laminate
Reliability of the results (FE formulation)	- -	-	+
Time to develop model and meshing	+ +	+	-
Load application — data transfer with CFD	-	+	+
Simulation time	+ +	+	- -
Ease of allocating material directions	+	-	-
Modification of the stacking sequence	+ +	-	-
Failure criterion, type of outputs	+	- -	+
Visual validation of results	+ +	-	+

5. MODELLING & SCANTLING

In this chapter, the detailed process of modelling the propeller blade is explained starting from raw data of propeller geometry to the final model ready for FSI analysis. The FSI analysis was performed for three cases: two cases of one-way coupling and one case of two-way coupling. The initial agenda of the thesis work was to perform two cases of two-way coupling as well (explicit two-way BEM-FEM and CFD-FEM coupled FSI analysis), but explicit two-way BEM-FEM coupled FSI analysis using ComPropApp couldn't be performed due to technical issues with ComPropApp while assigning composite layup to the propeller blade. Instead, the structural mesh and the pressure loads created using ComPropApp are imported into FEMAP where the material layup is correctly assigned to the FE mesh and only one-way BEM-FEM coupled FSI analysis is performed in FEMAP using NX NASTRAN solver. The three FSI analysis performed are shown in the flow chart below in Figure 39.
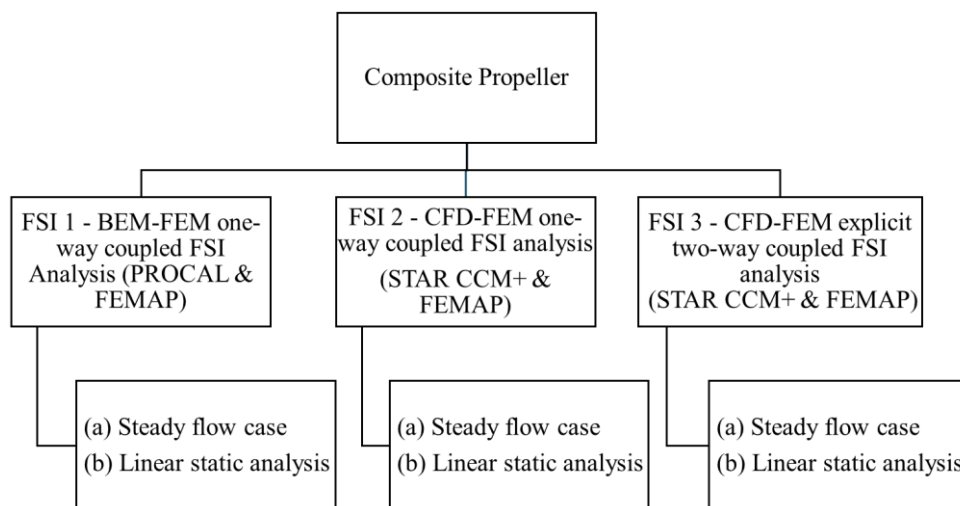
Figure 39. FSI analysis flowchart

5.1. FSI 1 – One way BEM – FEM coupled FSI analysis

As the name itself suggests, it is only a one-way coupling analysis where the loads from the fluid solver are imported into the structural solver only once.

- PROCAL performs steady state flow analysis to generate pressure loads. This is accomplished using ComPropApp

- The structural model (FE model) is created by FEM software TRIDENT using the ComPropApp

- Both the fluid loads and the structural model are imported into FEMAP simultaneously

- New material coordinate systems are created in FEMAP for each element to replace the old material coordinate systems created by TRIDENT and then the layups based on zones (A1 to A16) are assigned to the FE model

- Layup and properties are assigned to the FE mesh in FEMAP based on the existing material coordinate systems which were imported from TRIDENT and linear static analysis is performed using NX NASTRAN

The reason for using TRIDENT for creating the structural model is that it is fairly simple to create the model in TRIDENT as opposed to the time consuming modelling and meshing required in FEMAP.

5.2. FSI 2 – One way CFD – FEM coupled FSI analysis

This FSI analysis is achieved by transferring the loads generated from RANSE simulations into FEMAP. Salient features of this coupling analysis are listed below

- STAR CCM+ performs steady state flow analysis using RANSE to generate the pressure loads

- The structural model (FE mesh) is created by FEM software TRIDENT using ComPropApp

- The pressure loads from STAR CCM+ and the structural model including the material coordinate systems from TRIDENT are imported into FEMAP

- New material coordinate systems are created in FEMAP for each element to replace the old material coordinate systems created by TRIDENT and then the layups based on zones (A1 to A16) are assigned to the FE model

- Layup and properties are assigned to the FE mesh in FEMAP based on the existing material coordinate systems which were imported from TRIDENT and linear static analysis is performed using NX NASTRAN

5.3. FSI 3 – Two way CFD – FEM coupled FSI analysis

In this FSI, a two-way coupling analysis using both the RANSE (STAR CCM+) and FEM (FEMAP) solvers is conducted for Fluid-Structure Interaction (FSI). This type of analysis is used when the structural deformations due to fluid forces are significant enough to influence the hydrodynamic loads. FSI 2 and FSI 3 both are carried out in collaboration with Bureau Veritas Solutions Marine and Offshore (BVS M&O) where BVS has performed the CFD

simulations, and the author of this report has carried out the FEM simulations. The exchange of information between CFD and FEM softwares is a manual process carried out using the exchange of .DAT files between the two softwares. The steps involved in this analysis are as follows:

- Initially, a Computational Fluid Dynamics (CFD) analysis is carried out in STAR-CCM+ (based on RANSE method), where pressure forces are calculated
- These pressure forces are then imported into FEMAP and mapped onto the structural mesh, where the structural mesh is created by TRIDENT using ComPropApp
- New material coordinate systems are created in FEMAP for each element to replace the old material coordinate systems created by TRIDENT and then the layups based on zones (A1 to A16) are assigned to the FE model in FEMAP and then NX NASTRAN solver is used to carry out linear static analysis
- Subsequently, the deformations obtained from the static analysis from FEMAP are imported into STAR CCM+ where the fluid mesh is morphed around the deformed geometry of the propeller blade. Then the CFD simulations are performed again using the deformed geometry and new pressure forces are generated
- These new pressure forces are imported back into FEMAP and new deformed geometry of the propeller blade is obtained after performing again the linear static analysis using NX NASTRAN
- This cycle is carried on until we have reached convergence of deformations which is given in the results section

The flowchart of explicit two-way CFD-FEM coupled FSI analysis is given below in Figure 40
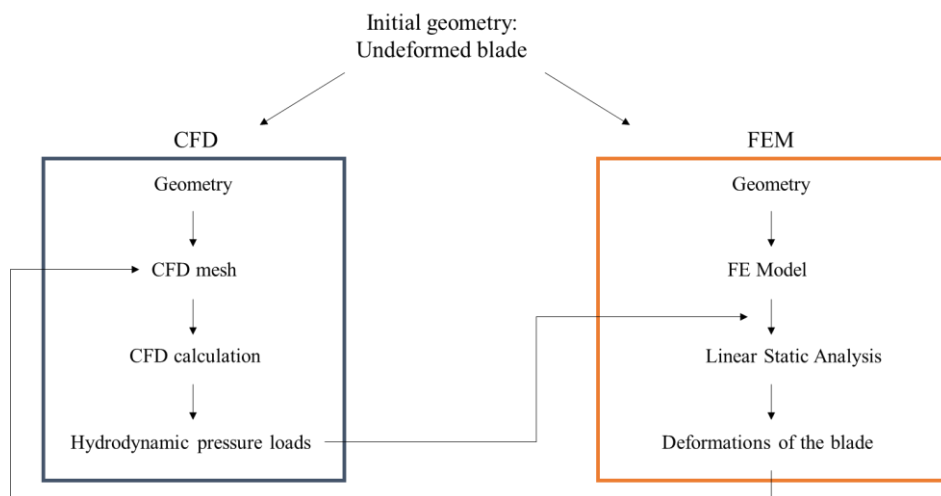
Figure 40. FSI 3 flowchart

The three FSI analysis are summarized below in Table 12

Table 12. FSI analysis and their summary

	FSI 1	**FSI 2**	**FSI 3**
Type of Coupling	One way BEM - FEM	One Way CFD - FEM	Explicit Two Way CFD - FEM
Fluid Solver	PROCAL	STAR CCM+	STAR CCM+
Fluid Analysis Type	Steady	Steady	Steady
Structural Solver	FEMAP / NASTRAN	FEMAP / NASTRAN	FEMAP / NASTRAN
Structural Analysis Type	Linear Static	Linear Static	Linear Static

5.4. Geometry

The geometrical data for creating the geometry of the propeller blade is provided by MECA in three forms

- A 2D mid-surface model of the propeller blade shown in Figure 42
- A 3D surface model of the propeller blade shown in Figure 42
- An excel file containing raw data for r/R = [0.2, 0.25, 0.3, 0.35, 0.4, 0.45, 0.5, 0.55, 0.6, 0.65, 0.7, 0.75, 0.8, 0.85, 0.9, 0.95, 0.975, 0.99]. For each r/R ratio, the data provided in the excel file includes
    - Chord Length
    - C_LE
    - Skew
    - Pitch
    - Rake
    - Section Profile in terms of 2D (x, y and r/R) and 3D (x, y and z) coordinates

A sample of this data is shown in Figure 41 where the section profile is defined using 2D x and y coordinates at r/R = 0.2

r/R		0.2
Radius	*mm*	109.50
Chord Length	*mm*	227.22
Skew	*mm*	31.51
Pitch Angle	*deg*	54.61
Rake	*mm*	411.61
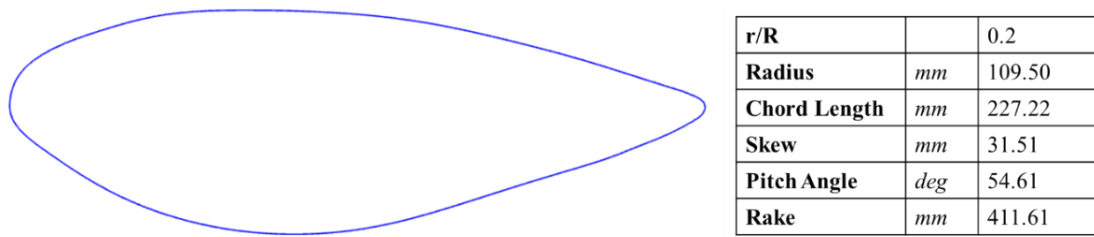
Figure 41 Geometrical data at r/R = 0.2
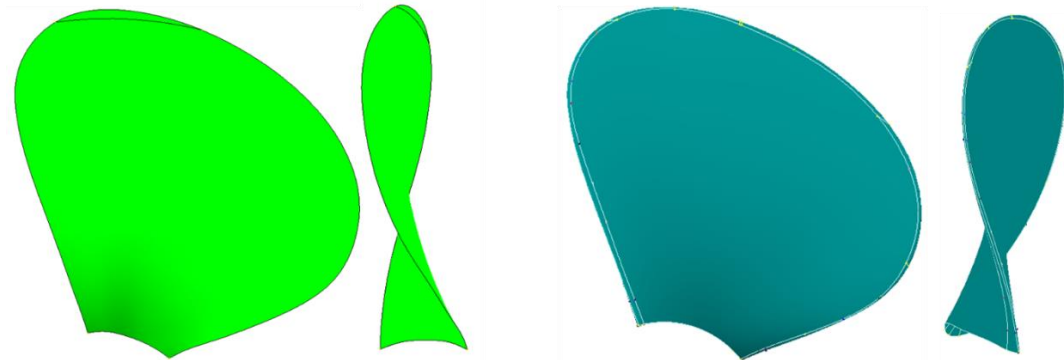
Figure 42 Geometrical models by MECA - 2D mid-surface model (left) and 3D surface model (right)

The initial step involved transforming raw data into a usable format suitable for input into the ComPropApp. This process was both meticulous and iterative, demanding refinement of the data for each r/R value. A MATLAB script (see Appendix 1) was developed for this purpose. The script accepts either excel or text files as input and gives output of normalized coordinates in the local axis of the profile section. In the local axis which is illustrated in Figure 43 (Tirandaz and Rezaeiha 2021), x-values are normalized relative to the chord length of the profile section, while y-values represent the thickness of the profile at each normalized x-coordinate. This refined data is essential for generating the .PRP file, which ComPropApp utilizes to construct both the blade geometry and the structural model.
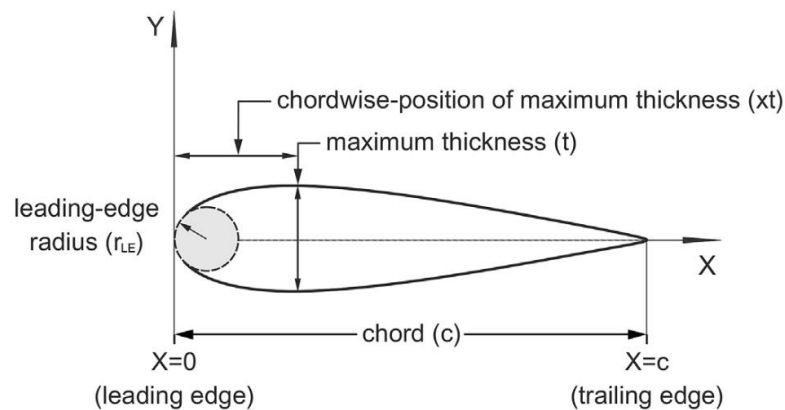
Figure 43. Local axis of profile section (Tirandaz and Rezaeiha 2021)

Initially, the geometrical model created using the data from the provided excel file was not exactly similar to the 2D and 3D surface models provided by MECA. There were discrepancies observed in rake, skew and pitch values of the propeller blade. This difference is shown on the left in Figure 44 where the black lines represent the target geometry from the 3D surface model and the white lines represent the blade model generated by ComPropApp using the refined data from excel file. A manual iterative process of changing the values of rake, skew and pitch was carried out until both the white and the black curves coincided coherently throughout the model. The final output is shown on the right in Figure 44.
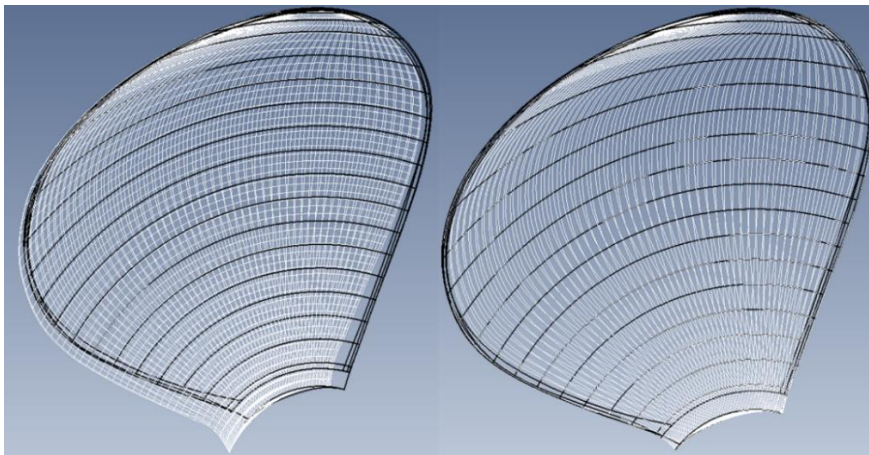
Figure 44. Discrepancy in the geometric models (left) and rectified model (right)

5.5. FE Modelling

In the scope of this thesis, only solid laminate elements were used to carry out FSI analysis. The structural mesh (FE model) for both BEM-FEM coupling and CFD-FEM coupling is created through ComPropApp (using TRIDENT). Unfortunately, due to technical errors, ComPropApp is unable to correctly apply composite material properties to the FE model as already explained at the start of section 5. Hence, no explicit two-way BEM-FEM coupled FSI analysis is performed using ComPropApp, only the mesh created by ComPropApp is imported into FEMAP and the linear static analysis for all coupling cases (BEM-FEM and CFD-FEM) is performed in FEMAP using NASTRAN solver. The FE model created by ComPropApp has a mesh of 50 x 50 elements (50 elements in radial direction and 50 elements in chordwise direction) and has one element in the thickness direction as shown in Figure 45. A mesh convergence study is carried out on a different small scale propeller blade to study the effect of the number of elements on the maximum blade deformations. The results are tabulated below in Table 13. Although the maximum difference in deformations is less than 3 %, the

computational time for all the models is almost similar and hence a mesh of 50 x 50 is created for the actual propeller blade.

Table 13. Mesh convergence study of a small scale propeller blade

# of Radial Elements	# of Chordwise Elements	# of Total Elements	Relative Difference in Maximum Deformations
-	-	-	%
20	20	400	2.36
25	25	625	2.36
50	25	1250	0.01
50	50	2500	-

The FE model of the actual propeller blade created by ComPropApp is not an exact representation of the real geometry of the propeller blade, rather it is an approximation. Indeed, the FE model has coarse leading edge, trailing edge and blade tip. The chord length is reduced by 0.4% and the blade radius is reduced by 0.8% while creating the input files for ComPropApp to avoid having skewed elements at the edges and the tip that would cause the ComPropApp to abort the creation of structural model. This limitation is demonstrated in Figure 46 where 0.992R implies that the radius of the structural model is equal 99.2 % of the actual radius.
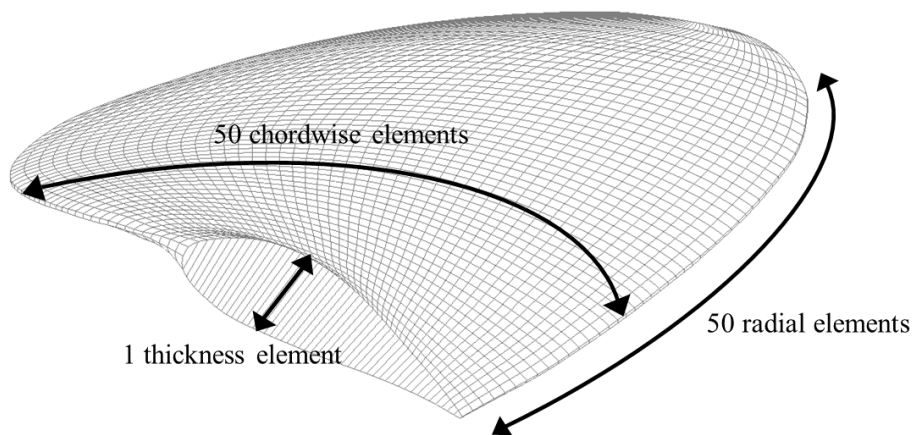
Figure 45. FE model created by ComPropApp using the geometry from MECA

Coarse tip due to meshing limitations

0.992R

Coarse leading and trailing edges
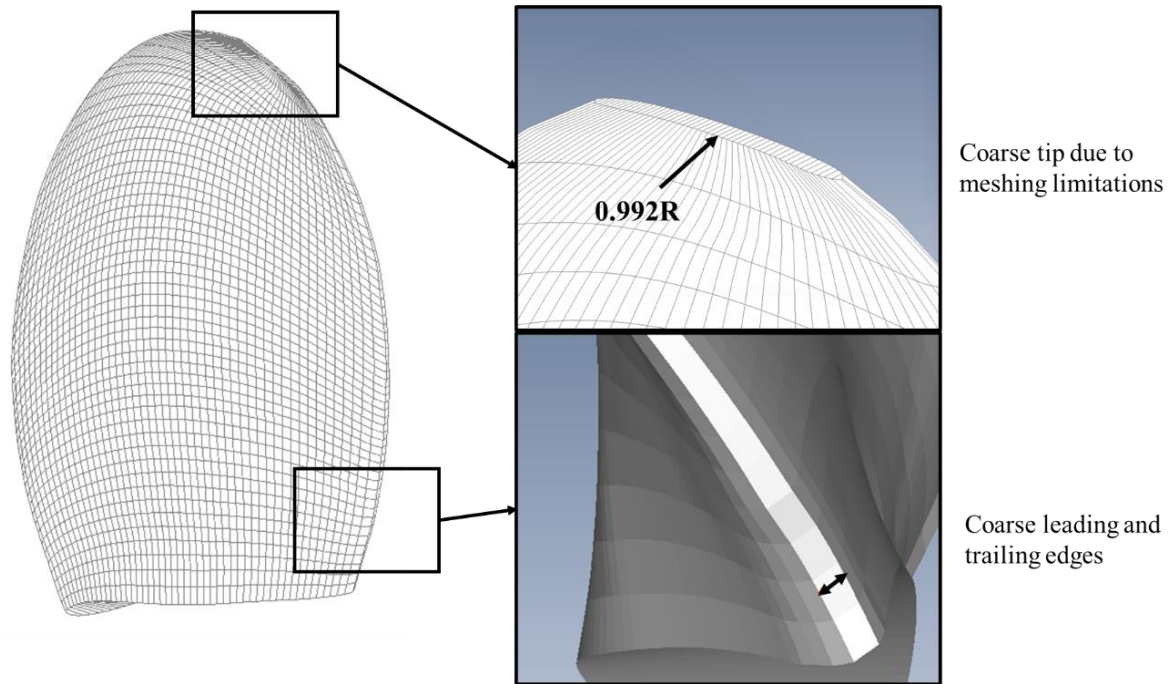
Figure 46. Modelling limitations using ComPropApp

5.6. Boundary Conditions

When importing the structural model from Trident (ComPropApp) into FEMAP, the boundary conditions are also imported as part of the model. Alternatively, these conditions can be created after importing the model in FEMAP if they are not imported from ComPropApp. The blade's hub connection is modeled as a clamped support by restricting the six degrees of freedom of all the nodes in the hub area. However, this boundary condition does not accurately represent the actual connection between the blade and the hub. Consequently, stress hotspots near the hub area will be disregarded during result comparisons. It is acceptable to ignore stress results upto second row of elements.

Clamped Nodes
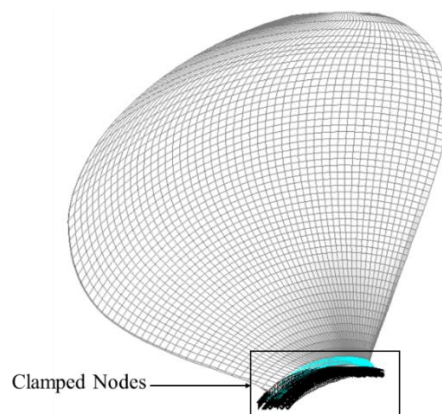
Figure 47. Boundary Conditions

5.7. Loadings

Since two types of FSI coupling analysis are performed in the thesis work as explained in chapter 3, the loads are imported either from the BEM solver PROCAL using ComPropApp or from RANSE solver STAR-CCM+. In either of the cases, the loads are imported into FEMAP and they act as pressure forces on elemental faces as shown in Figure 48. The operational conditions to generate these loads are tabulated below in Table 14. The simulations are performed at two different operating conditions with advance ratios of 0.69 and 0.88 while keeping the propeller speed constant.

Table 14 - Operating Conditions

Advance Ratio		0.69	0.88
Ship Speed	m/s	9.20	11.74
Propeller Speed	rps	12.19	
Fluid Density	kg/m^3	1026.021	
Dynamic Viscosity	$Pa.s$	0.00122	
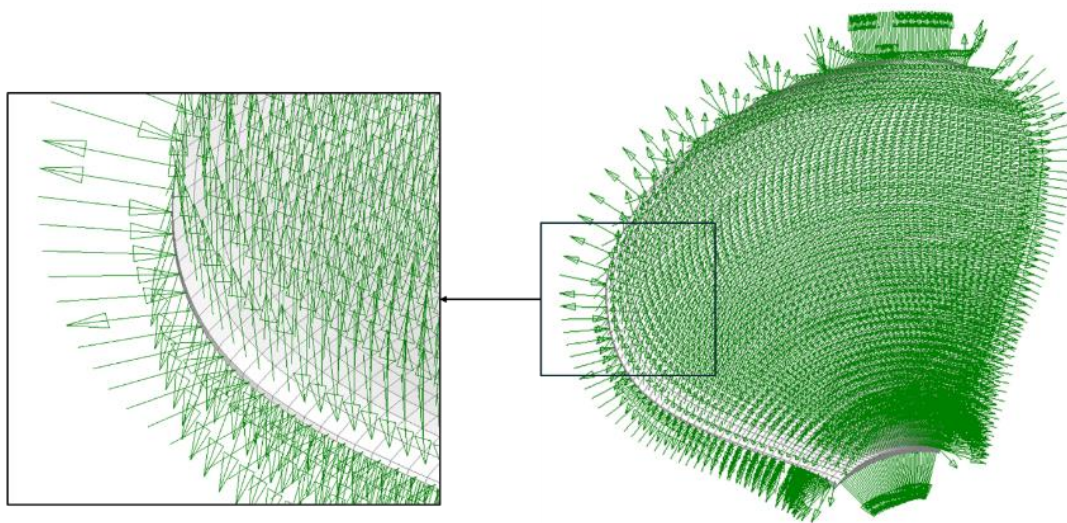
Figure 48. Loads acting as surface pressure on elemental faces

5.8. Materials

The composite propeller is made of unidirectional and twill layers of carbon fiber and epoxy resin with a repeating pattern of stacking as shown in Figure 49. The properties for these raw materials (fibers and resin) are taken from Bureau Veritas rule BV NR546 and are given below

in Table 15. The core of the blade uses a new confidential material termed as "blade core" for the scope of this thesis.

Table 15 - Material Properties

		HS Carbon	**Epoxy**
Density	kg/m^3	1790	1250
Glass Transition Temperature	°C	-	80-150
Tensile modulus	MPa	238000	3100
Axial Poisson ratio	-	0.3	0.39
Transverse Young modulus	MPa	15000	-
Transverse Poisson ratio	-	0.02	-
Shear modulus	MPa	50000	1500
Tensile strength	MPa	3600	75
Compressive strength	MPa	2140	75
Shear strength	MPa	1200	80

The blade has a total of 16 zones, with ply drop off between two consecutive zones as we move from the hub of the blade to the tip of the blade. The division of zones and the corresponding layup properties for each zone including the ply drop off sequence are provided by MECA as shown in Figure 49 and Figure 50. A brief info on the layup is as follows

- X implies that it is a twill sheet
- U implies that it is a unidirectional sheet
- Y implies that it is blade core
- There is a total of 16 zones with different thicknesses marked as A1 to A16 with zone A16 close to the blade root and zone A1 close to the blade tip as shown in Figure 50.
- The thickness of the blade core is variable and it is limited upto zone A8 only
- The 0˚ line in Figure 50 indicates the direction of material axis. More details on this are presented in section 5.10.

Ply #	A1	A2	A3	A4	A5	A6	A7	A8	A9	A10	A11	A12	A13	A14	A15	A16	Region
Ply # 33	X	X	X	X	X	X	X	X	X	X	X	X	X	X	X	X	INTRADOS
Ply # 32	U	U	U	U	U	U	U	U	U	U	U	U	U	U	U	U	
Ply # 31		U	U	U	U	U	U	U	U	U	U	U	U	U	U	U	
Ply # 30			U	U	U	U	U	U	U	U	U	U	U	U	U	U	
Ply # 29				X	X	X	X	X	X	X	X	X	X	X	X	X	
Ply # 28					U	U	U	U	U	U	U	U	U	U	U	U	
Ply # 27						U	U	U	U	U	U	U	U	U	U	U	
Ply # 26							U	U	U	U	U	U	U	U	U	U	
Ply # 25									X	X	X	X	X	X	X	X	
Ply # 24										U	U	U	U	U	U	U	
Ply # 23											U	U	U	U	U	U	
Ply # 22												U	U	U	U	U	
Ply # 21													X	X	X	X	
Ply # 20														U	U	U	
Ply # 19															U	U	
Ply # 18																U	
Ply # 17								Y	Y	Y	Y	Y	Y	Y	Y	Y	
Ply # 16																U	EXTRADOS
Ply # 15															U	U	
Ply # 14														U	U	U	
Ply # 13													X	X	X	X	
Ply # 12												U	U	U	U	U	
Ply # 11											U	U	U	U	U	U	
Ply # 10										U	U	U	U	U	U	U	
Ply # 9									X	X	X	X	X	X	X	X	
Ply # 8							U	U	U	U	U	U	U	U	U	U	
Ply # 7						U	U	U	U	U	U	U	U	U	U	U	
Ply # 6					U	U	U	U	U	U	U	U	U	U	U	U	
Ply # 5				X	X	X	X	X	X	X	X	X	X	X	X	X	
Ply # 4			U	U	U	U	U	U	U	U	U	U	U	U	U	U	
Ply # 3		U	U	U	U	U	U	U	U	U	U	U	U	U	U	U	
Ply # 2	U	U	U	U	U	U	U	U	U	U	U	U	U	U	U	U	
Ply # 1	X	X	X	X	X	X	X	X	X	X	X	X	X	X	X	X	
Zone Number	A1	A2	A3	A4	A5	A6	A7	A8	A9	A10	A11	A12	A13	A14	A15	A16	
Number of Plies	4	6	8	10	12	14	16	17	19	21	23	25	27	29	31	33	

Figure 49. Layup details of each zone
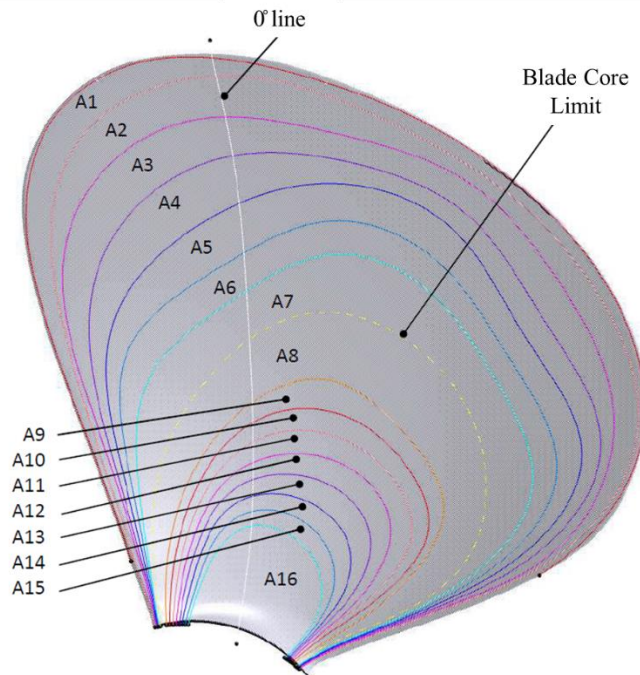
Figure 50. Material zones

5.9.Material Mapping

As the FE model is imported from ComPropApp into FEMAP, the next step is to assign the right material properties to each of the individual 2500 elements. As ComPropApp is unable to correctly assign composite material properties to the mesh itself and as such this task has to be carried out manually in FEMAP which is a very tedious and laborious process. The steps involved in this process are elaborated here.

Step 1 – A 2D model with curves defining the boundaries of each of the 16 zones is provided by MECA. This 2D model is imported into FEMAP and superimposed onto the 3D FE model as shown in Figure 51.
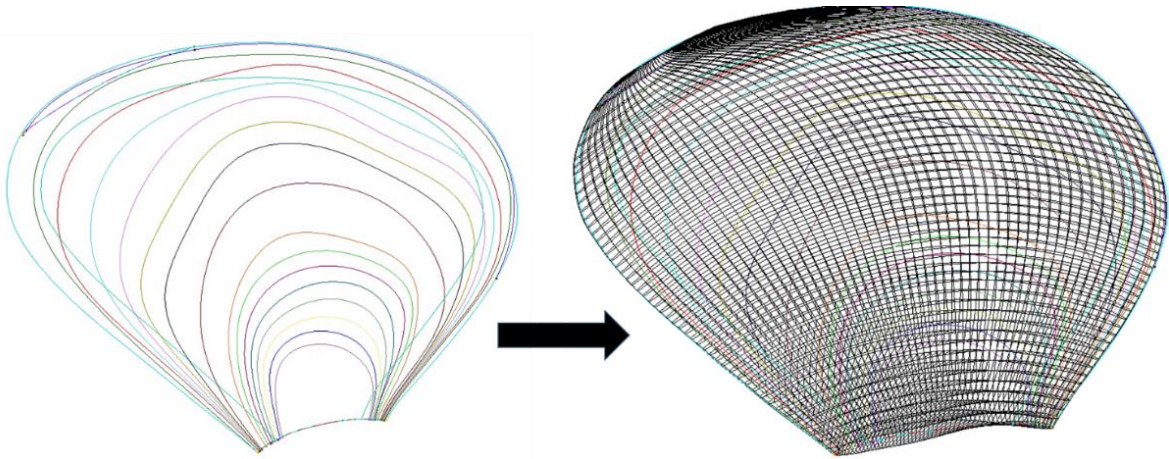
Figure 51 Superimposition of 3D model on 2D curves

Step 2 – In this step, the superimposed model is utilized to create a 50x50 grid in a text file that specifies the number of zones, ranging from 1 to 16, associated with each element. This task is inherently manual and time-consuming, as it requires each element to be visually inspected within the superimposed model to accurately assign a zone number based on its location. The output of this meticulous process is shown in Figure 53. The superimposed model in Figure 51 reveals that a significant number of elements in the FE mesh are positioned at the boundaries of two distinct zones as shown in Figure 52. Additionally, some elements near the root of the blade span more than two zones. In these instances, a judgment call must be made to determine the most appropriate zone assignment for these elements.

- For elements located at the intersection of two zones, the zone with the smaller thickness is assigned. Assigning the zone with smaller thickness to these elements means that these elements will have a modeled stiffness that is intentionally lower than the true stiffness. This is a conservative approach which avoids any potential overestimation of stiffness of the blade.

- For elements that encompass more than two zones, a different strategy is employed. In these cases, the zone that represents the average characteristics of all included zones is selected. Typically, this results in choosing the middle zone, as it provides a balanced representation of the varying material properties. This approach ensures that the overall stiffness is neither underestimated nor overestimated, providing closer results to the actual material behavior of these elements.

The middle zone chosen for these kinds of elements – Stiffness is average of the actual layup

The zone with the smaller thickness chosen for these type of elements – Stiffness is less than the actual layup
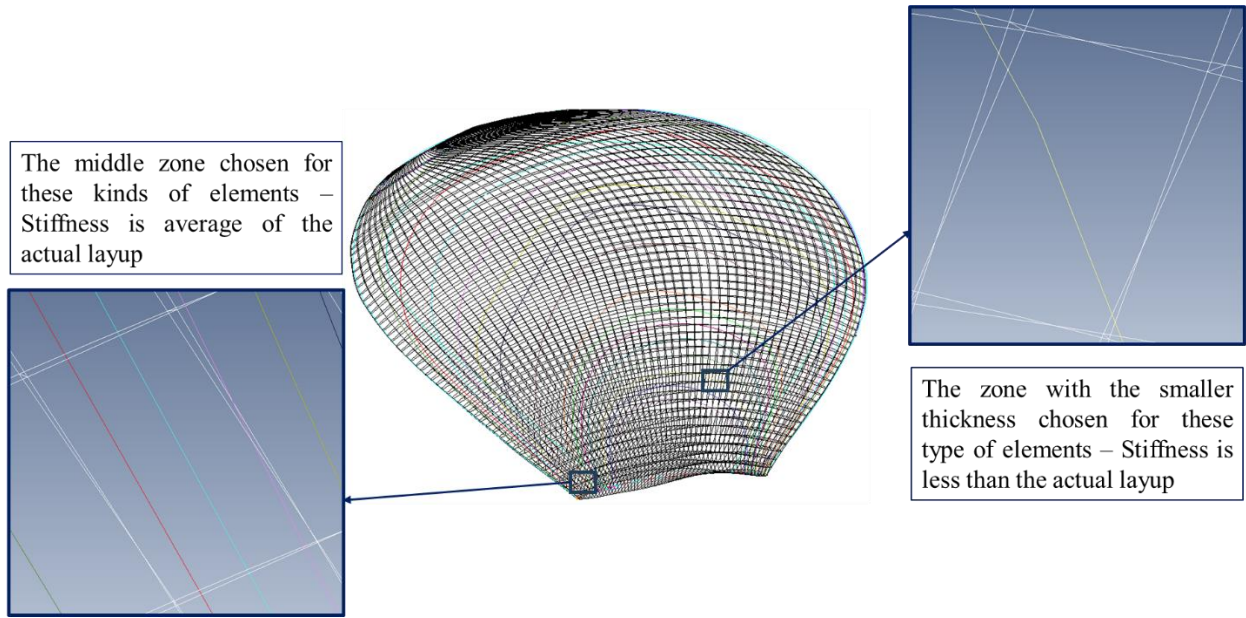
Figure 52. Elements encompassing two or more zones
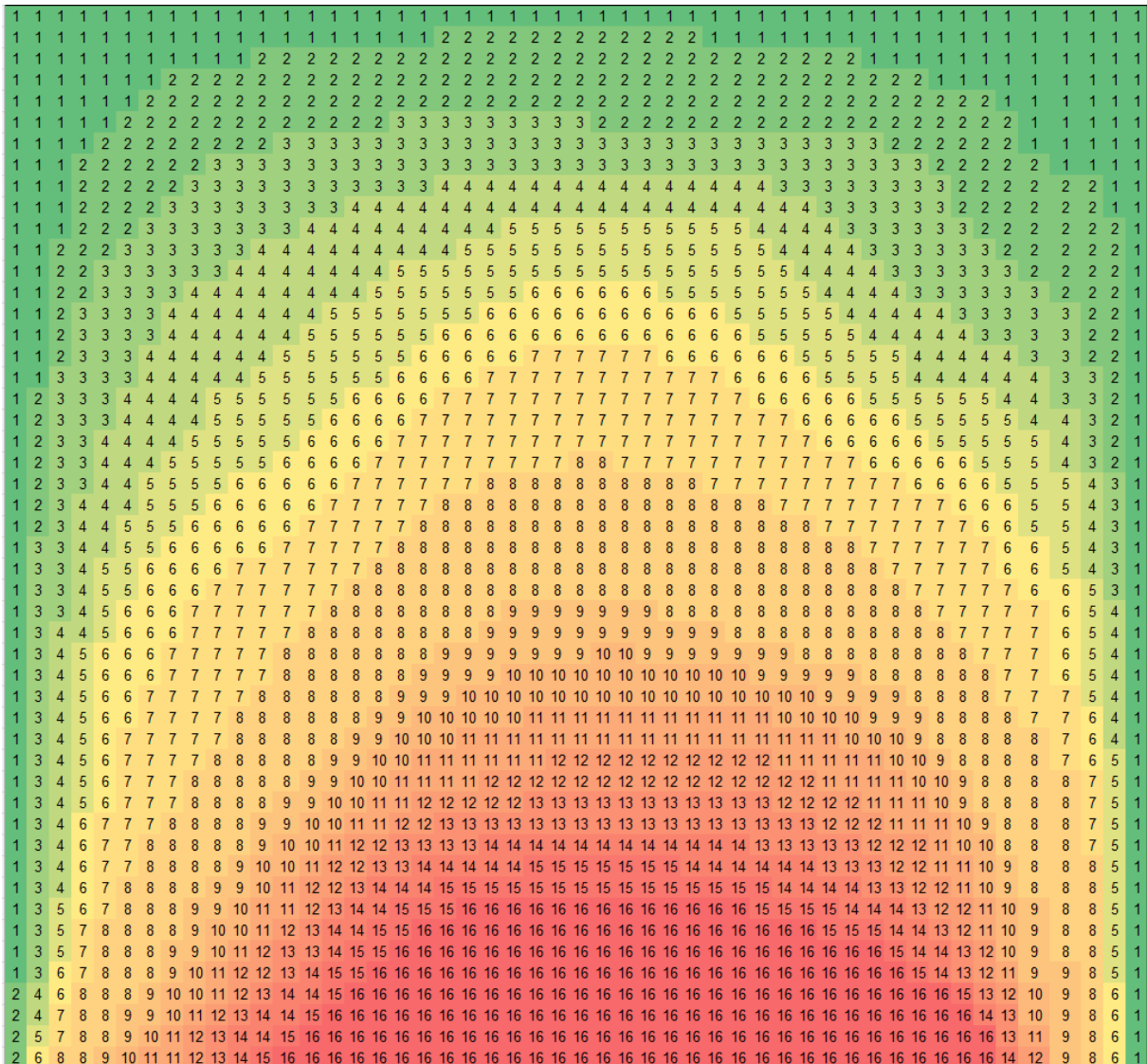
Figure 53. Zone mapping chart

Step 3 – The material mapping from step 2 is used to assign the properties to each of the 2500 elements in FEMAP. It is not possible to do this process manually for each element, hence an API script using VBA for FEMAP (Appendix 2) is written that reads the text file containing the material mapping and assigns the respective zone number 1 to 16 to each of the 2500 elements.

As the structural model is created using blade geometry, the thickness of each solid laminate element is equal to the thickness of the propeller geometry. On the other hand, the thickness of the layup assigned to each of the elements in Step 3 is based on the thickness of the layups provided by MECA. Hence, there is always a discrepancy between the mean thickness of each element and the thickness of the layup assigned to that element. These discrepancies for a few random elements in the blade model are tabulated below

Table 16. Difference in elemental and layup thickness values

Element ID	Difference in thickness
#	*%*
50	-40.4
70	-37.4
99	-18.2
806	24.3
913	15.0
1331	37.6
1912	-28.5

To study the effect of this discrepancy between element and layup thicknesses, an API script was written (see Appendix 3) which calculates the percentage difference between the layup thickness and the geometrical thickness of each element and assigns a specific color to the elements based on the value of percentage difference as shown in Figure 54. Figure 55 shows the color-coded elements where the elemental thickness is greater than the associated layup thickness while Figure 56 shows the elements where the elemental thickness is smaller than the layup thickness.

1194 – Element Thickness > Layup Thickness

1306 – Element Thickness < Layup Thickness
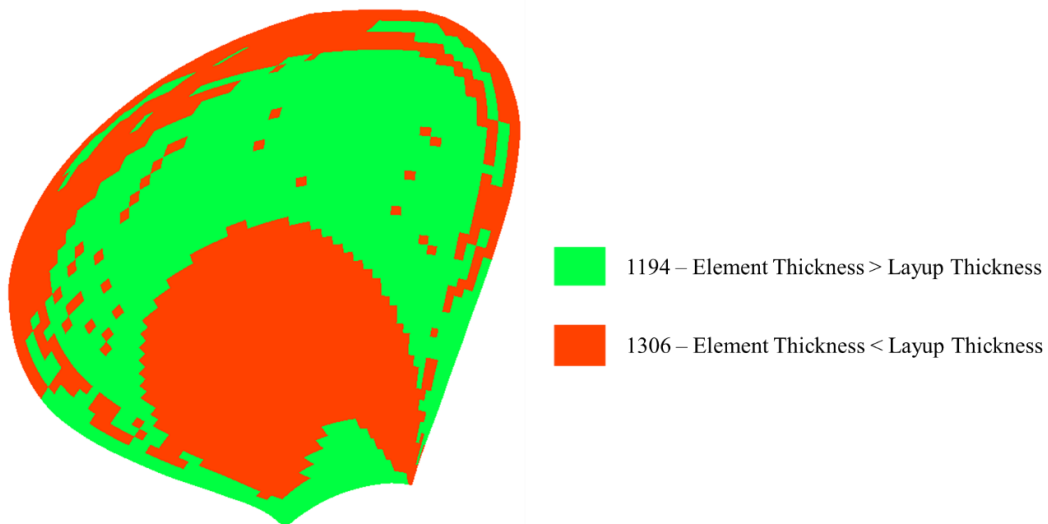
Figure 54. Difference between elemental and layup thickness
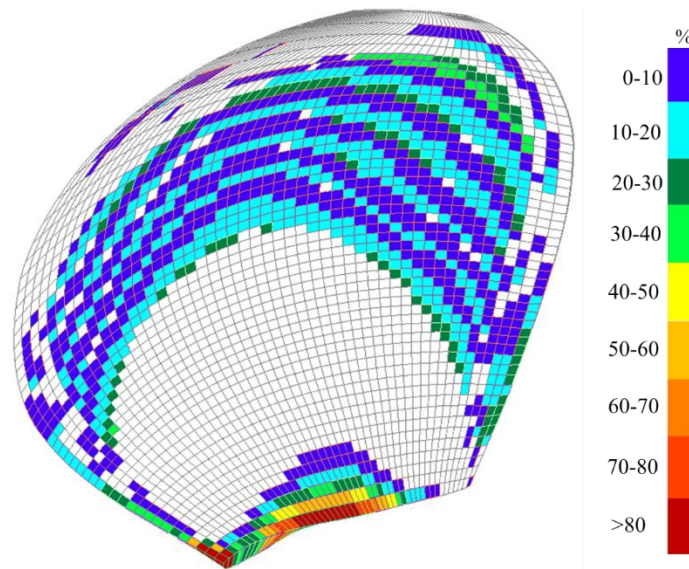
Figure 55. Elements having thickness greater than layup thickness
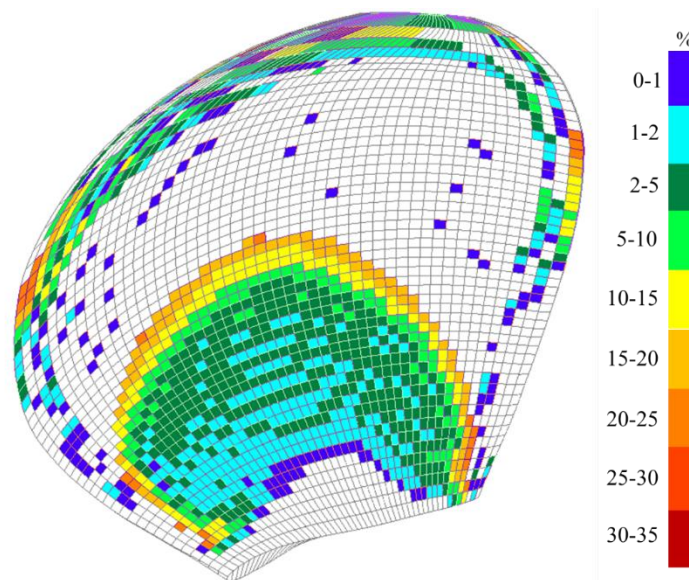
Figure 56. Elements having thickness smaller than layup thickness

The study of this discrepancy is important as it significantly affects the stiffness of the blade during simulations. While performing static linear analysis using FEMAP, which uses NX NASTRAN solver, two things happen

- For all the elements where the thickness of the elements is greater than the thickness of the associated layup, NASTRAN scales up the layup to match it with the thickness of the element. In this case, we gain additional stiffness in these elements since each ply of the layup has been scaled up and has more thickness now than originally assigned.

- For all the elements where the thickness of the elements is smaller than the thickness of the associated layup, NASTRAN scales down the layup to match it with the thickness

of the element. In this case, we lose stiffness in these elements since each ply of the layup has been scaled down and has less thickness now than originally assigned.

5.10.   Material Orientation

Creating isotropic material models for FE models is a straightforward process even for complicated geometries. However, developing orthotropic material models is a relatively complex process due to the care and attention required in creating the material coordinate system and material directions. For orthotropic materials, as is the case with propeller blade, material coordinate systems must be defined which are based on elemental coordinate systems. These material coordinate systems are used as the reference to assign direction angles to the fibers within the layups.

5.10.1. Material Coordinate System created by ComPropApp

In the scope of this thesis work, when the FE model of the blade is imported from ComPropApp into FEMAP, the material coordinate systems are also imported as part of the element properties for each of the 2500 elements. These material coordinate systems are created by ComPropApp using TRIDENT. The logic for creating these coordinate systems was established during the development of ComPropApp, and consequently, there is no option for users to define their own material coordinate systems while working with ComPropApp.

This limitation has significant adverse effects on the hydrodynamic and structural results because the orientation of the default material coordinate systems created by ComPropApp is impractical to be used for defining actual material orientations of the propeller blade.

The material directions created by ComPropApp for the propeller blade are given in Figure 57. In this figure, it is evident that the main direction of the material axis is oriented to follow the chordwise curvature of the propeller blade.
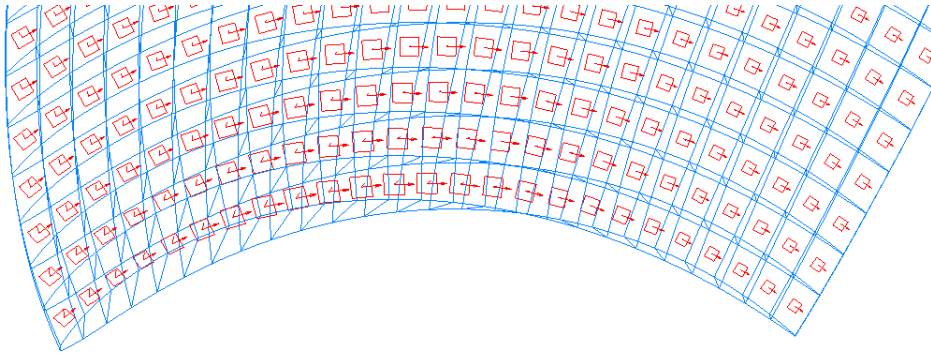
Figure 57. Material directions created by ComPropApp

5.10.2. Material Coordinate System in FEMAP

To overcome this limitation, a new material coordinate system must be created in FEMAP for each element which more accurately represents the main direction of material axis used by MECA. For this purpose, a 2D model with curves representing the main direction of material axis is provided by MECA. An API (see Appendix 4) is written here which picks the coordinates of these curves, makes direction vectors and creates material coordinate system based on these direction vectors. The newly created main material axis is very closely aligned with the material axis direction curves provided by MECA for a major part of the propeller blade. Only close to the tip of the propeller blade, there is discrepancy between the new material directions created by the API and the material direction curves provided by MECA. Although further refinement could be performed to rectify this error, it would be a very time-consuming process and the effect of this rectification on the results is expected to be insignificant. As such, these newly created material coordinate systems are accepted for carrying out the FSI analysis of the propeller.

In Figure 58, the red arrows represent the main material direction created using the API while the yellow curve represents the material direction curve provided by MECA.
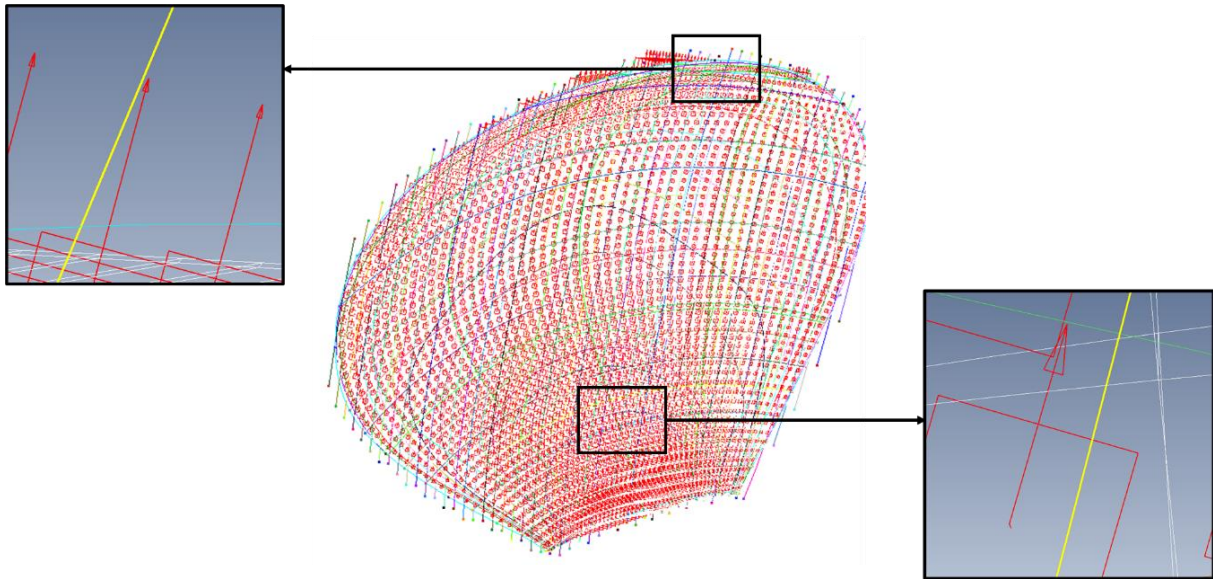
Figure 58. Material directions created in FEMAP using curves from MECA

5.11.   Safety Factors, Safety Margins and Failure Theories

The failure criteria for the stress analysis presented in section 6.4.2 is based on the safety factors provided in "BV NI663 – Propellers in Composite Materials". BV NI663 specifies safety factors based on

- The type of stress (parallel to fiber, perpendicular to fiber, shear)
- Fatigue analysis – if fatigue analysis is not included in the design, then the safety factors are multiplied by a partial factor (C_i) of 2.2. For cases where fatigue analysis is considered in the overall design, this partial safety factor is not included.
- The type of ply (Unidirectional or Woven Roving)

The following tables present the safety factors for each type of stress

Table 17. Safety factors for main stress parallel to fiber direction

Safety factor for		**UD**	**Woven Roving**
Accuracy of calculation	α	1.1	1.1
Aging effect	C_v	1.2	1.2
Fabrication process	C_F	1.15	1.15
Type and direction of stress	C_R	2.1	2.4
Fatigue analysis	C_i	2.2	2.2
Total Safety Factor			
With fatigue analysis		3.19	3.64
Without fatigue analysis		7.01	8.02

Table 18. Safety factors for main stress perpendicular to fiber direction

Safety factor for		UD	Woven Roving
Accuracy of calculation	α	1.1	1.1
Aging effect	C_v	1.2	1.2
Fabrication process	C_F	1.15	1.15
Type and direction of stress	C_R	1.25	2.4
Fatigue analysis	C_i	2.2	2.2
Total Safety Factor			
With fatigue analysis		1.90	3.64
Without fatigue analysis		4.17	8.02

Table 19. Safety factors for shear stress

Safety factor for		UD	Woven Roving
Accuracy of calculation	α	1.1	1.1
Aging effect	C_v	1.2	1.2
Fabrication process	C_F	1.15	1.15
Type and direction of stress	C_R	1.6	1.8
Fatigue analysis	C_i	2.2	2.2
Total Safety Factor			
With fatigue analysis		2.43	2.73
Without fatigue analysis		5.34	6.01

Table 20. Safety factors for combined stress

Safety factor for		UD	Woven Roving
Accuracy of calculation	α	1.1	1.1
Aging effect	C_v	1.2	1.2
Fabrication process	C_F	1.15	1.15
Type and direction of stress	C_R	1.7	2.1
Fatigue analysis	C_i	2.2	2.2
Total Safety Factor			
With fatigue analysis		2.58	3.19
Without fatigue analysis		5.68	7.01

Two types of stress analysis are carried out in the scope of this thesis work

- Main stress analysis
- Combined stress analysis

For the main stress analysis, the minimum safety margin of each ply is obtained by dividing the maximum stress occurring in the ply by the theoretical breaking stress of the ply as

$$Minmum\ Safety\ Margin\ = \frac{Maximum\ Stress\ in\ the\ Ply}{Breaking\ Stress\ of\ the\ Ply} \tag{23}$$

The minimum safety margin obtained from equation 23 should be smaller than the required safety factors presented above in Table 17,

Table 18 and Table 19 for main stress parallel to fiber direction, main stress perpendicular to fiber direction and shear stress respectively.

For the combined stress analysis, the failure indices for each individual ply are obtained using Hoffman Failure criteria. According to Hoffman criteria, the ply will not fail as long as

$$T_1\sigma_{11} + T_2\sigma_{22} + T_{11}\sigma_{11}^2 + T_{22}\sigma_{22}^2 + T_{66}\tau_{12}^2 + 2T_{12}\sigma_{11}\sigma_{22} < 1 \tag{24}$$

Where all the parameters are taken in MPa and are defined in local ply axis and are given as follows

σ_{ii}, τ_{ij} : Primary stresses occurred because of application of the load case

σ_{brcii} : Strength in compression

σ_{brtii} : Strength in tension

τ_{brij} : Shear strength

with

$$T_1 = \frac{|\sigma_{brc11}| - |\sigma_{brt11}|}{|\sigma_{brt11}\ \sigma_{brc11}|}$$

$$T_2 = \frac{|\sigma_{brc22}| - |\sigma_{brt22}|}{|\sigma_{brt22}\ \sigma_{brc22}|}$$

$$T_{11} = \frac{1}{|\sigma_{brt11}\sigma_{brc11}|}$$

$$T_{22} = \frac{1}{|\sigma_{brt22}\sigma_{brc22}|} \tag{25}$$

$$T_{66} = \frac{1}{\tau_{br12}^2}$$

$$T_{12} = \frac{1}{|\sigma_{brc11}\sigma_{brt11}|}$$

Note:

MECA has computed safety margins for both cases i.e. main stress analysis and combined stress analysis and has compared these safety margins with safety factors provided in Tables 17 to 20 to analyze the failure behavior of the propeller blade. In this thesis work, same approach is carried out for main stress analysis, but for combined stress analysis, only failure indices have been calculated using equation 24 instead of safety margins. Failure indices and safety margins can be understood as inverse of each other, having high safety margins means having low failure indices. Having a safety margin equal to the required safety factor means that the failure indices should be equal to 1.

6. RESULTS

The hydrodynamical and structural results are presented here which are obtained by performing the three FSI analysis and these results are compared with MECA results where possible.

6.1. Normalization of Results

The results obtained in the scope of this thesis work are confidential as this thesis is part of the CoPropel Project. A normalization approach has been taken here to share the results without breaching the confidentiality requirements. For this purpose, all the results are normalized with respect to the results of FSI 3 - explicit two-way CFD-FEM coupled FSI analysis. The FSI 3 results which are taken as reference are given below in Table 21.

Table 21. Reference parameters used for normalization of results

Advance Ratio	0.69	0.88
Reference Deformation	$d_{0.69}$	$d_{0.88}$
Reference Stress	$\sigma_{0.69}$	$\sigma_{0.88}$
Reference Strain	$\varepsilon_{0.69}$	$\varepsilon_{0.88}$
Reference Thrust	$T_{0.69}$	$T_{0.88}$
Reference Torque	$Q_{0.69}$	$Q_{0.88}$

The results obtained during the thesis work are titled as "**BV results**" to make the comparison easy with **MECA results**.

6.2. Preliminary Study of Material Coordinate Systems

For the first study, the one-way CFD-FEM coupled FSI analysis was performed using the FE model and the material coordinate systems imported directly from TRIDENT into FEMAP. The objective of this study is to understand the practicality of the material coordinate systems created by TRIDENT using ComPropApp and to conclude if these coordinate systems can be used in the FE model used for carrying out the three FSI analysis. The structural and hydrodynamics results were compared with the MECA results and useful conclusions were drawn from this comparison.

The deformations obtained from one-way CFD-FEM coupled FSI analysis were compared with the deformations provided by MECA. There is quite a big difference in the maximum deformations observed in both results. The deformation contours are shown in Figure 59 for

advance ratio 0.69 and Figure 60 for advance ratio 0.88. The percentage differences in the maximum deformation values are tabulated below in Table 22. Two observations are made here

- There is significant difference in the maximum deformation between the results from one-way CFD-FEM coupling and MECA's results, which cannot be justified by using only modelling differences as the reason
- The contour plot of deformations is also significantly different, which puts a question mark on the material orientations in the FE model of one-way CFD-FEM coupling

Even if the maximum deformations showed acceptable percentage differences, the difference in the contour plots of the deformations would still be reason enough to question the material directions in the FE model.
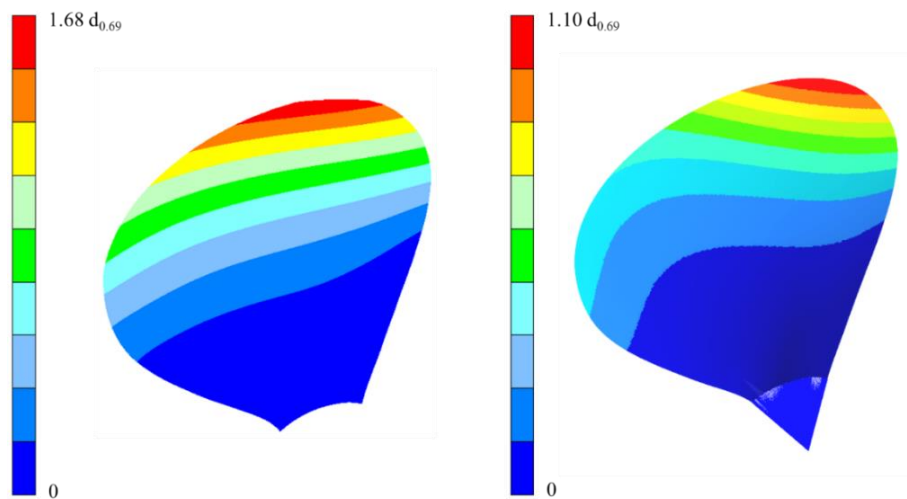
Figure 59. Deformation contour for advance ratio 0.69 – BV (left) and MECA (right)
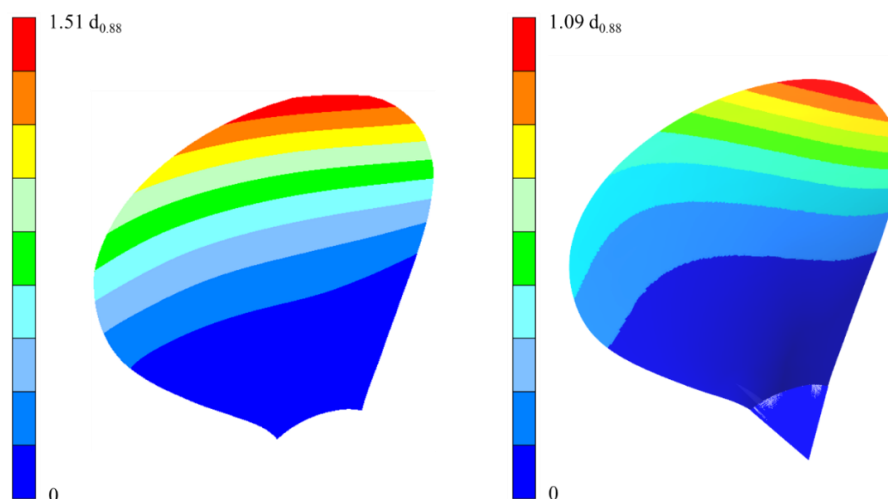
Figure 60. Deformation contour for advance ratio 0.88 – BV (left) and MECA (right)

Table 22. Comparison of maximum deformations between BV and MECA

Advance Ratio	One way CFD – FEM	MECA	Difference
	-	-	%
0.69	1.68 $d_{0.69}$	1.10 $d_{0.69}$	52.72
0.88	1.51 $d_{0.88}$	1.09 $d_{0.88}$	38.53

Comparing the resultant strains for ply number 1 for both advance ratios (0.69 and 0.88) also shows significant differences in the maximum strain values and the contour plots for strain. The percentage differences in maximum strain in ply number 1 for 0.69 and 0.88 advance ratios are tabulated below in Table 23 and the contours are shown in Figure 61 and Figure 62 for advance ratios 0.69 and 0.88 respectively. It only serves to prove the initial assumption that the modelling approach needs to be reevaluated in terms of material directions assigned to the FE model.
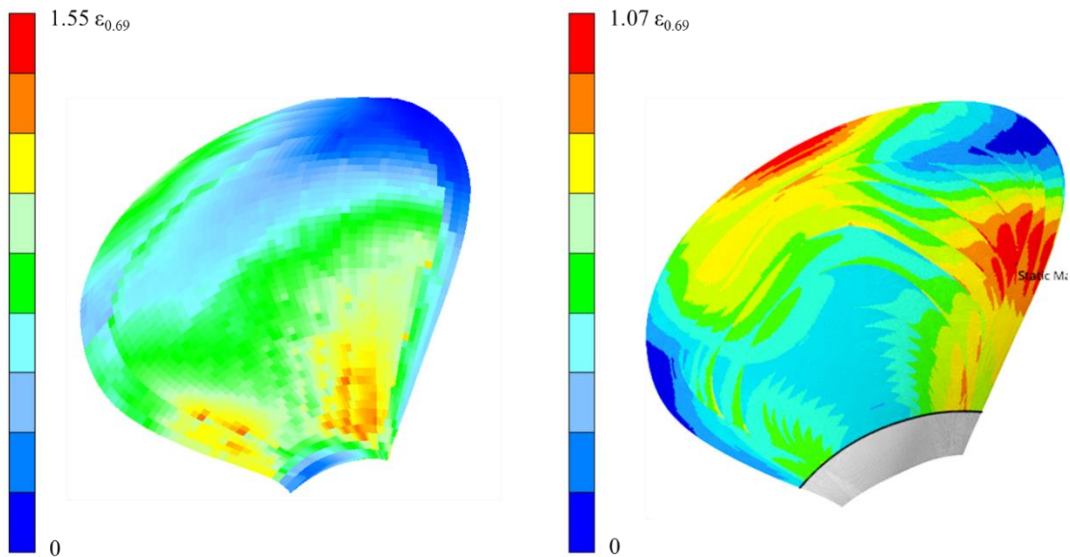
Figure 61. Strain contour for advance ratio 0.69 – BV (left) and MECA (right)
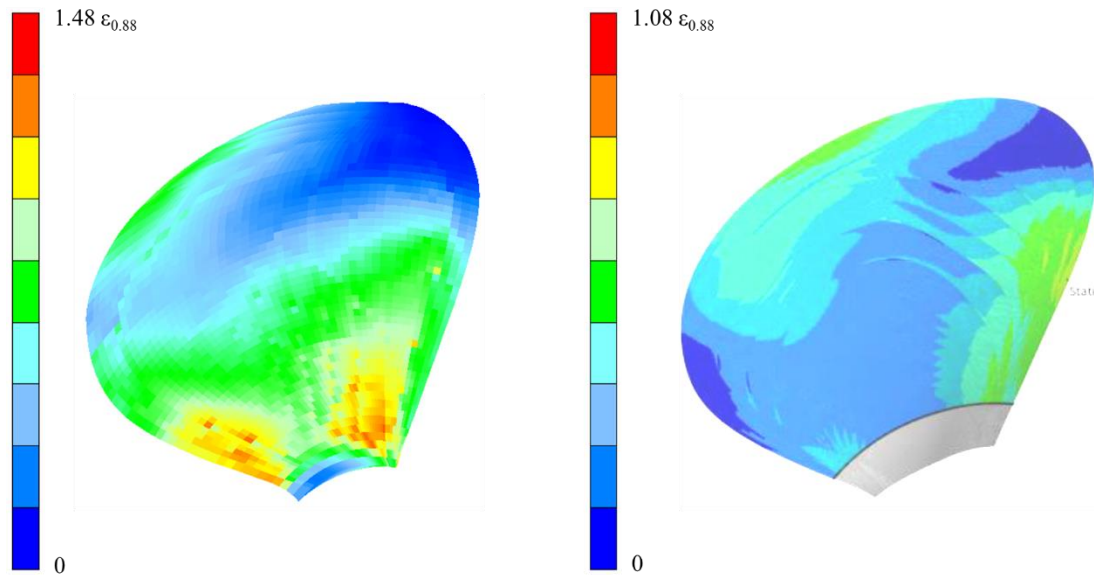
Figure 62. Strain contour for advance ratio 0.88 – BV (left) and MECA (right)

Table 23. Comparison of maximum strains between BV and MECA

Advance Ratio	One way CFD – FEM	MECA	Difference
	-	-	%
0.69	1.55 $\varepsilon_{0.69}$	1.07 $\varepsilon_{0.69}$	44.85
0.88	1.48 $\varepsilon_{0.88}$	1.08 $\varepsilon_{0.88}$	37.03

Based on these results, a decision was made to discard the material coordinate systems created by TRIDENT (using ComPropApp) and create new material coordinate systems using FEMAP that resemble closely to the material coordinate system of MECA. The approach taken to establish new material coordinate systems is already described in section 5.10.2. The three FSI analysis explained in section 5 are carried out using the new material coordinate systems.

6.3. Material Model Selection

As already explained in detail in section 5.9 that the drawback of using solid laminate elements for composite modelling is the difference of thickness between the element and the associated layup. The thickness of the element is based on the geometry of the propeller while the thickness of the layup is based on the associated zone assigned to each element (zones A1 to A16 in Figure 49). Three different modelling approaches were considered here based on how the thickness of the layup is changed to make it equal to the thickness of the associated elements.

The influence of these three approaches on deformations and stresses is studied and finally one model is chosen based on the results.

6.3.1. Model – 1

In this model, one-way CFD-FEM coupled FSI analysis is carried out without manually changing the layup thickness. This is the same case that is already described in section 5.9 and repeated here for understanding. While performing static linear analysis using FEMAP, which uses NX NASTRAN solver, two things happen

- For all the elements where the thickness of the elements is greater than the thickness of the associated layup, NASTRAN scales up the layup to match it with the thickness of the element. In this case, we gain additional stiffness in these elements since each ply of the layup has been scaled up and has more thickness now than originally assigned. Referring back to Figure 54, the total number of these elements is 1194 which turns out to be 47.8% of the total 2500 elements

- For all the elements where the thickness of the elements is smaller than the thickness of the associated layup, NASTRAN scales down the layup to match it with the thickness of the element. In this case, we lose stiffness in these elements since each ply of the layup has been scaled down and has less thickness now than originally assigned. The total number of these elements is 1306 which turns out to be 52.2% of the total 2500 elements.

In conclusion, we are gaining additional stiffness in 47.8% of our FE model while we are loosing stiffness in 52.2% of our FE model. The net effect here is expected to be averaged and the overall stiffness of the FE model is expected to be close to the actual stiffness of the blade.

6.3.2. Model – 2

An additional material with the properties of foam is added in the model here. The idea here is to scale up or scale down the layup thickness so that the overall thickness of the layup and elements is the same. This scale up operation is performed by adding foam while the scale down operation is performed by subtracting the blade core. The properties of foam are given in Table 24

Table 24. Material properties of foam

Tensile Strength	*MPa*	44
Shear Strength	*MPa*	18
Poisson Ratio	-	0.25
Density	*kg/m³*	8

An API using VBA is written for FEMAP (see Appendix 5) which serves the following purpose

- For zones A8 to A16 (these zones have blade core), the API reads the difference of thickness between the elements and the associated layups and
    - Reduces the thickness of the blade core to match the overall thickness if the layup thickness is greater than the element thickness
    - Adds foam on top and bottom of the layup to match the overall thickness if the layup thickness is smaller than the element thickness
- For zones A1 to A7 (these zones don't have blade core), the API again reads the differences of thickness between the elements and the associated layups and
    - Adds foam on top and bottom of the layup to match the overall thickness if the layup thickness is smaller than the element thickness
    - Leaves the layup as it is if the layup thickness is greater than the element thickness since in this case, nothing can be done except to carry out the linear static analysis and let NX NASTRAN scale down the layup thickness to match it with the element thickness

Compared to Model 1, Model 2 is expected to have lower overall stiffness since we have incorporated the use of foam material to make up the discrepancies in the thicknesses before carrying out the linear static analysis and as such, no scaling operation is performed by NX NASTRAN except for the elements in zones A1 to A7 having smaller thicknesses than the associated layups.

6.3.3. Model – 3

For this model, the API from model – 2 is modified so that the following output is achieved

- For zones A8 to A16 (these zones have blade core), the API reads the difference of thickness between the elements and the associated layups and
    - Reduces the thickness of the blade core to match the overall thickness if the layup thickness is greater than the element thickness same as model – 2

   o Increases the thickness of the blade core to match the overall thickness if the layup thickness is smaller than the element thickness. This is the main difference compared to model – 2 where foam was added on the top and bottom of the layups in model – 2 to make up the discrepancy in the thickness

- For zones A1 to A7 (these zones don't have blade core), the API again reads the differences of thickness between the elements and the associated layups and
  - o Adds foam on top and bottom of the layup to match the overall thickness if the layup thickness is smaller than the element thickness same as model – 2
  - o Leaves the layup as it is if the layup thickness is greater than the element thickness since in this case, nothing can be done except to carry out the linear static analysis and let NX NASTRAN scale down the layup thickness to match it with the element thickness same as model – 2

6.3.4. Choice of Model

The deformations and the strains are studied for the three models and compared with the MECA results to come to a conclusion. The comparison of maximum deformations between the three models and the MECA results are tabulated below in Table 25 while the comparison of ply # 1 maximum strains with MECA results for all three models are tabulated below in Table 26. Looking at the results, it is quite evident that model – 1 presents the most accurate modelling approach out of the three models. This was also the intuition from the start since model – 1 achieves almost a balance between gaining additional stiffness and losing stiffness based on the difference of thickness between the elements and the layup. Hence, model – 1 is selected for further FSI analysis using one-way and two-way CFD-FEM and only one-way BEM-FEM couplings.

Table 25. Comparison of deformations obtained from the three models with MECA results

Advance Ratio	Model 1		Model 2		Model 3	
	Deformation	Diff from MECA	Deformation	Diff from MECA	Deformation	Diff from MECA
	mm	*%*	*mm*	*%*	*mm*	*%*
0.69	$1.12\ d_{0.69}$	1.8	$1.54\ d_{0.69}$	40	$1.46\ d_{0.69}$	24.7
0.88	$1.08\ d_{0.88}$	-0.9	$1.43\ d_{0.88}$	31.2	$1.39\ d_{0.88}$	27.5

Table 26. Comparison of max strains in ply # 1 obtained from the three models with MECA results

Advance Ratio	Model – 1		Model – 2		Model – 3	
	Strain	Diff from MECA	Strain	Diff from MECA	Strain	Diff from MECA
	-	*%*	-	*%*	-	*%*
0.69	$1.24\ \varepsilon_{0.69}$	15.9	$1.52\ \varepsilon_{0.69}$	42	$1.41\ \varepsilon_{0.69}$	31.8
0.88	$1.12\ \varepsilon_{0.88}$	3.7	$1.40\ \varepsilon_{0.88}$	29.6	$1.31\ \varepsilon_{0.88}$	21.3

After creating new material coordinate systems for each individual element in model-1, the FSI analysis was performed for the three cases mentioned in Table 12. Here, the results will be compared with the MECA results by referring to each of the FSI analysis by its number (i.e. FSI 1, FSI 2, FSI 3) as allocated in Table 12.

6.4. Results Comparison and Discussions

6.4.1. Hydrodynamic Results

The hydrodynamic results from the three FSI analysis are compared with the MECA results based on thrust and torque produced in each case. The presentation of the results is as follows

Table 27. Hydrodynamics results comparison for advance ratio 0.69

	FSI 1	**FSI 2**	**FSI 3**	**MECA**	**Relative Difference with MECA**		
					%		
					FSI 1	FSI 2	FSI 3
Thrust	$0.977\ T_{0.69}$	$1.005\ T_{0.69}$	$T_{0.69}$	$0.971\ T_{0.69}$	0.66	3.61	3.02
Torque	$0.883\ Q_{0.69}$	$1.001\ Q_{0.69}$	$Q_{0.69}$	$0.975\ Q_{0.69}$	-9.41	2.622	2.53

Table 28. Hydrodynamics results comparison for advance ratio 0.88

	FSI 1	**FSI 2**	**FSI 3**	**MECA**	**Relative Difference with MECA**		
					%		
					FSI 1	FSI 2	FSI 3
Thrust	$1.082\ T_{0.88}$	$0.992\ T_{0.88}$	$T_{0.88}$	$0.959\ T_{0.88}$	12.76	3.40	4.21
Torque	$0.956\ Q_{0.88}$	$0.992\ Q_{0.88}$	$Q_{0.88}$	$0.959\ Q_{0.88}$	-0.34	3.38	4.20

- FSI 2 and FSI 3 both yield less than a 5% relative difference compared to the MECA results. Notably, FSI 2 shows an even smaller relative difference to the MECA results than FSI 3. This can be justified by considering that MECA also utilized a one-way CFD-FEM coupling approach, although the solver used for performing the fluid simulations is different than STAR CCM+.

- FSI 1 shows significant deviation form MECA results as compared to FSI 2 and FSI 3. This can be justified based on the assumptions and simplifications that go into the setup of Boundary Element Method (BEM).

  o Viscous Effects - BEM theory neglects viscous effects, assuming an ideal, inviscid fluid flow, which often leads to error in the values of computed thrust and torque. This simplification ignores the drag forces and boundary layer effects that are present in actual flow around a propeller, resulting in erroneous predicted performance.

  o Tip Pressures - BEM does not account for tip pressure corrections, which are essential in accurately modelling the complex flow interactions at the blade tips. These interactions include tip vortices and pressure changes at the tip, which significantly affect the propeller's efficiency and load distribution.

CFD models provide a more comprehensive analysis by solving the Reynold Average Navier-Stokes equations, capturing the detailed viscous effects and pressure variations, including those at the blade tips. This results in more accurate thrust and torque predictions, reflecting the real operating conditions of the propeller more accurately as compared to BEM.

6.4.2. Structural Results

To validate the MECA results, three different comparisons have been carried out

- Deformation comparisons
- Strain comparisons
- Stress and safety margin comparisons

6.4.2.1. Deformations and Strains

The following Figures 63 to 68 represent the deformations and strain comparison between BV results and MECA results. The distribution of deformations and strains is very similar for each case of FSI and MECA results, although with certain differences in the maximum values. The results of the maximum deformations obtained using the three FSI validate the MECA results,

although with some differences. Since MECA is using plate laminate elements as opposed to the solid laminate elements used for the three FSI analysis, the discrepancies between BV and MECA results is justified. Also, the approximations used during the creation of FE model in terms of geometry and material mapping described in section 5 further contribute to the difference in results between BV and MECA.
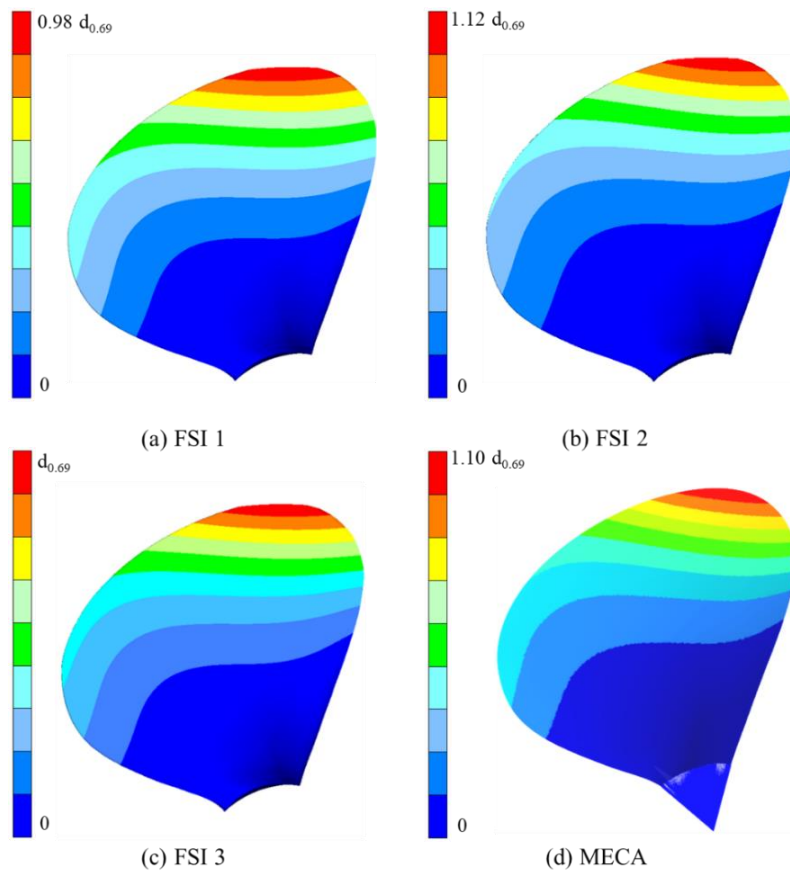
Figure 63. Deformations for advance ratio 0.69
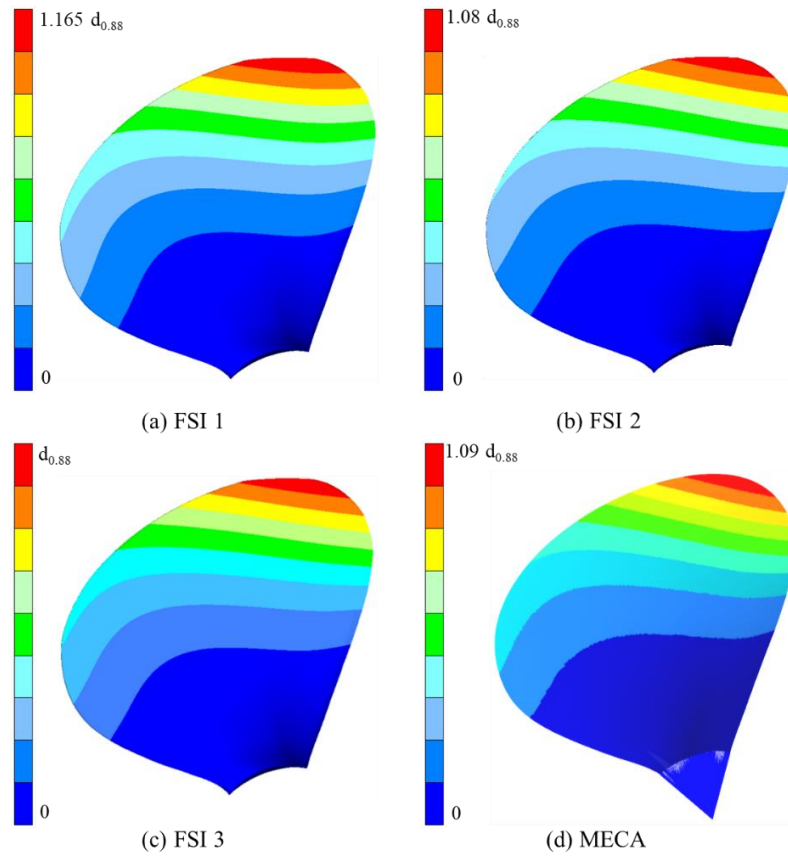
Figure 64. Deformations for advance ratio 0.88

Table 29. Comparison of maximum deformations

	FSI 1	FSI 2	FSI 3	MECA	Relative Difference with MECA		
					%		
					FSI 1	FSI 2	FSI 3
0.69	$0.98\ d_{0.69}$	$1.12\ d_{0.69}$	$d_{0.69}$	$1.10\ d_{0.69}$	-10.9	1.8	-9.1
0.88	$1.165\ d_{0.88}$	$1.08\ d_{0.88}$	$d_{0.88}$	$1.09\ d_{0.88}$	6.9	-0.9	-8.2
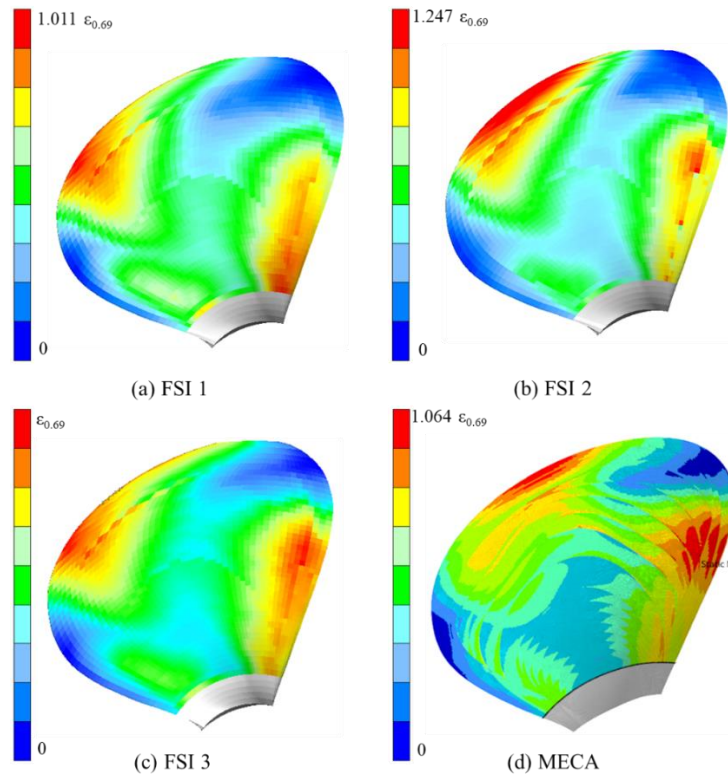
Figure 65. Ply # 1 strain for advance ratio 0.69
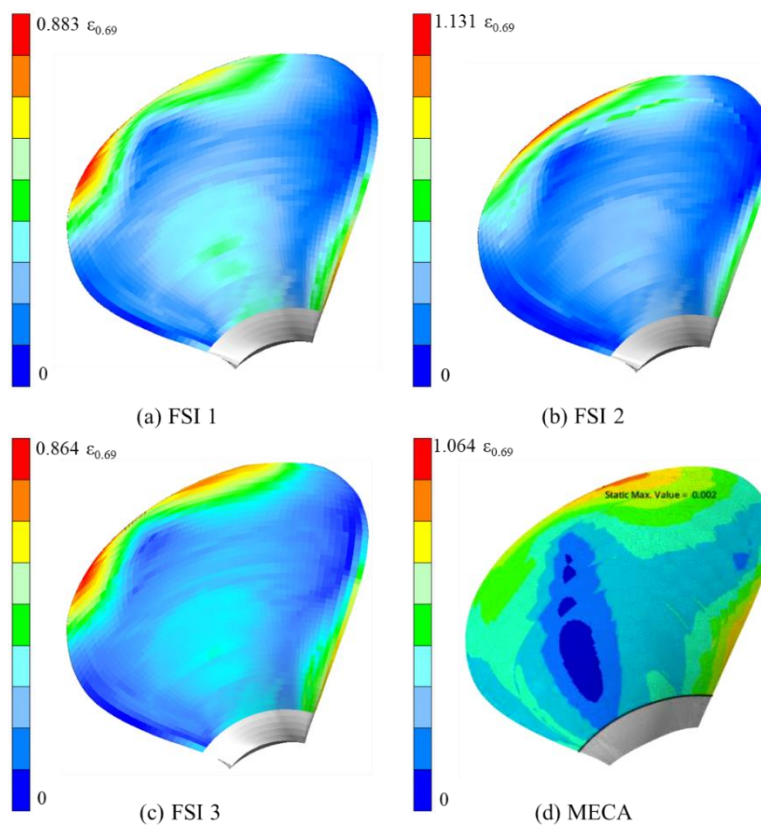
Figure 66. Ply # 33 strain for advance ratio 0.69

Table 30. Comparison of maximum strain for advance ratio 0.69

	FSI 1	FSI 2	FSI 3	MECA	Relative Difference with MECA		
					%		
					FSI 1	FSI 2	FSI 3
Ply # 1	1.011 $\varepsilon_{0.69}$	1.247 $\varepsilon_{0.69}$	$\varepsilon_{0.69}$	1.064 $\varepsilon_{0.69}$	-5.0	17.2	-6
Ply # 33	0.883 $\varepsilon_{0.69}$	1.131 $\varepsilon_{0.69}$	0.864 $\varepsilon_{0.69}$	1.064 $\varepsilon_{0.69}$	-17.0	6.35	-18.75

(a) FSI 1 (b) FSI 2

(c) FSI 3 (d) MECA
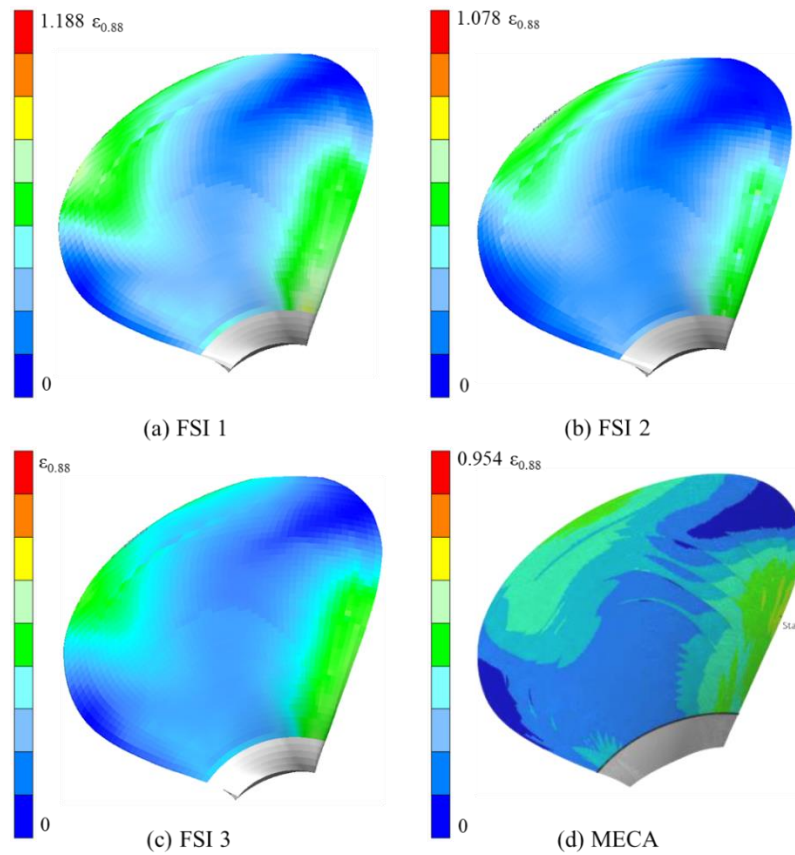
Figure 67. Ply # 1 strain for advance ratio 0.88
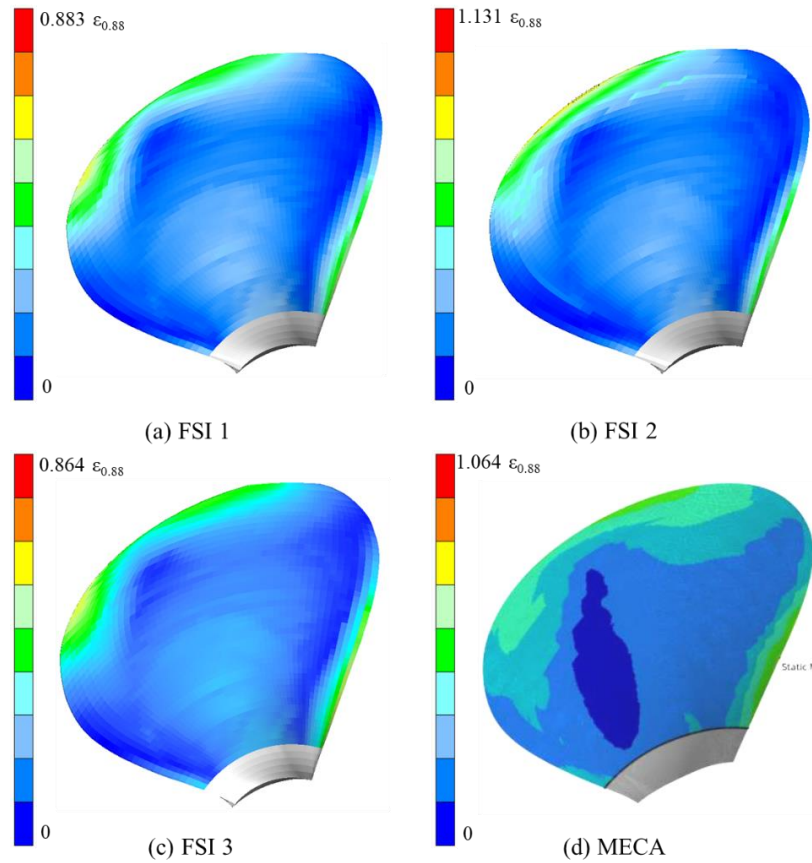
Figure 68. Ply # 33 strain for advance ratio 0.88

Table 31. Comparison of maximum strain for advance ratio 0.88

	FSI 1	FSI 2	FSI 3	MECA	Relative Difference with MECA		
					%		
					FSI 1	FSI 2	FSI 3
Ply # 1	1.188 $\varepsilon_{0.88}$	1.078 $\varepsilon_{0.88}$	$\varepsilon_{0.88}$	0.954 $\varepsilon_{0.88}$	24.5	13.0	4.8
Ply # 33	1.023 $\varepsilon_{0.88}$	0.965 $\varepsilon_{0.88}$	0.864 $\varepsilon_{0.88}$	0.954 $\varepsilon_{0.88}$	7.3	1.2	-9.5

The convergence behavior of the deformations obtained through FSI 3 is shown below in Figure 69. Five complete iterations were performed to analyze the convergence behavior. Based on the results, just two iterations prove sufficient to have final deformations that present less than 5 % error compared to the deformations after five complete iterations.
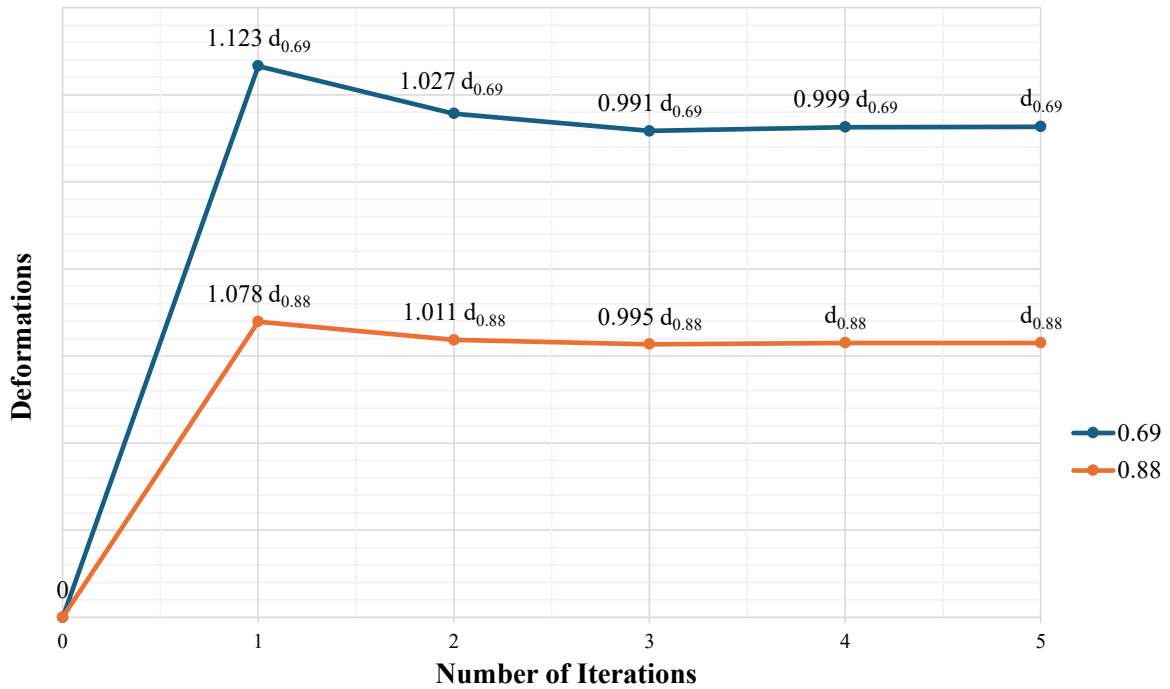
Figure 69. Convergence of deformations of propeller blade

Table 32. Relative difference of each iteration with iteration 5

	Percentage Difference	
Advance Ratio	**0.69**	**0.88**
Iteration # 1	12.3	7.8
Iteration # 2	2.7	1.1
Iteration # 3	-0.09	0.005
Iteration # 4	-0.001	0
Iteration # 5	-	-

6.4.2.2.   Stresses and Safety Margins

The analysis of maximum stress values across all plies has shown a correlation with the MECA results. For combined stress analysis, the plies that exhibit the lowest safety margins in MECA results show highest failure indices in BV results and this is verified by reduction of strength of the material using appropriate safety factor as detailed in section 5.11.

Using the Hoffman Failure criteria for combined stress given in equation 24, the failure indices were calculated for both UD and twill plies, after reduction of the material strength through the application of appropriate safety factors given in section 5.11. The failure indices were calculated for all the individual plies and the results are in line with MECA results for the plies having the minimum values of safety margins. The results are separately discussed here for UD and twill plies.

UD Plies

There is a total of 24 UD plies in the layup. Failure Indices were calculated for each of these plies based on the Hoffman criteria for combined stress. Any direct numerical comparison with MECA results isn't possible in this case because

- MECA calculated safety margins for combined stress for all the plies instead of failure indices and then compared these safety margins with the safety factors provided in section 5.11.

- Hoffman criteria uses quadratic formulation for calculating failure indices as shown in equation 24 and as such, linear comparison between failure indices obtained during thesis work and safety margins provided by MECA isn't possible

The failure indices obtained during this thesis work using a safety factor of 5.68 and the safety margins by MECA are provided in Table 33. According to MECA results, only ply # 2 gives a minimum safety margin which is below the required value of safety factor (5.68 without fatigue justification). On the contrary, the failure indices for ply numbers 2,3 31 and 32 exceed a value of 1. The reason for this discrepancy is given in the next section. Following conclusion can be drawn from the comparison

- The top and bottom UD plies demonstrate the highest values of failure indices and lowest values of safety margins

- FSI 2 gives an overall conservative approach to stress analysis as compared to FSI 1 and FSI 3, except the top and bottom plies.

- FSI 2 gives abnormally higher values of failure indices for top and bottom plies when compared to FSI 1 and FSI 3. Looking at the hydrodynamic results, FSI 2 has the highest values of thrust and torque, but this sole reason is not sufficient for justifying such an abnormal discrepancy in the results for top and bottom plies. To get the cause of this anomaly, further detailed stress analysis of ply # 2 and ply # 32 has been carried out

Table 33. Failure indices and safety margins based on combined stress analysis for UD plies

Ply Number	Failure Indices			Safety Margins by MECA
	FSI 1	FSI 2	FSI 3	
2	**1.245**	**1.492**	**1.195**	**5.051**
3	**1.136**	**1.336**	**1.090**	5.863
4	**1.062**	**1.105**	0.818	6.324
6	0.961	**1.011**	0.743	7.221
7	0.912	0.966	0.708	7.657
8	0.866	0.922	0.675	8.144
10	0.543	0.546	0.444	12.086
11	0.437	0.431	0.353	14.874
12	0.343	0.336	0.281	19.355
14	0.143	0.136	0.122	30.724
15	0.119	0.102	0.091	29.478
16	0.104	0.084	0.079	30.361
18	0.209	0.188	0.160	17.904
19	0.235	0.212	0.180	17.267
20	0.265	0.238	0.202	16.669
22	0.331	0.295	0.252	15.383
23	0.368	0.326	0.279	14.585
24	0.407	0.360	0.308	13.796
26	0.616	0.695	0.507	12.439
27	0.628	0.766	0.543	10.1
28	0.674	0.799	0.556	9.403
30	0.809	0.973	0.769	7.701
31	**1.074**	**1.280**	**1.031**	6.882
32	**1.153**	**1.352**	**1.106**	5.841

In case of main stress analysis for plies # 2 and 32, a direct numerical comparison of safety margins with MECA results is possible as opposed to combined stress analysis. This is because safety margins for all the main stress values can be calculated directly by dividing the stress value with the relative strength of the ply as shown in equation 23 which is not the case for combined stress. The resultant safety margins for main stresses are given in Table 34

Table 34. Safety margins based on main stress analysis for UD ply # 2 and 32

Main Stress	Ply #	FSI 1	FSI 2	FSI 3	MECA	Relative Difference with MECA		
						%		
						FSI 1	FSI 2	FSI 3
Max Tension Parallel to Fiber	2	12.36	14.25	14.07	13.59	-9.02	4.86	3.52
Max Compression Parallel to Fiber	32	8.27	9.24	9.32	10.22	-19.04	-9.64	-8.77
Max Tension Perpendicular to Fiber	2	6.79	5.89	6.85	6.19	9.70	-4.84	10.64
Max Compression - Perpendicular to Fiber	32	16.40	13.48	16.32	11.5	42.57	17.21	41.90
Max positive Inplane Shear	32	7.42	5.62	7.40	5.46	35.87	2.92	35.47
Max negative Inplane Shear	2	5.98	5.44	6.70	5.74	4.24	-5.15	16.67

Ply # 2 and 32 show high values of shear stress for FSI 2 (and hence lower safety margins in Table 34) as compared to FSI 1 and FSI 3. Safety margins obtained through FSI 2 are closer to the ones provided by MECA as compared to FSI 1 and FSI 3. Since MECA used one-way CFD -FEM coupled FSI analysis to obtain the safety margins, this conclusion was anticipated from the start.

For ply # 2, the contours for main stress parallel and perpendicular to the fiber direction are given in Figure 70 and Figure 71 respectively. Figure 72 shows the contours for in plane shear stress for ply # 2. To provide better readability and comparison, all the stress values given are normalized using only one reference value i.e. maximum stress value perpendicular to fiber direction (σ-$Y_{0.69}$) for FSI 3 (two-way CFD-FEM coupled FSI analysis) in ply # 2.

(a) FSI 1   (b) FSI 2

(c) FSI 3
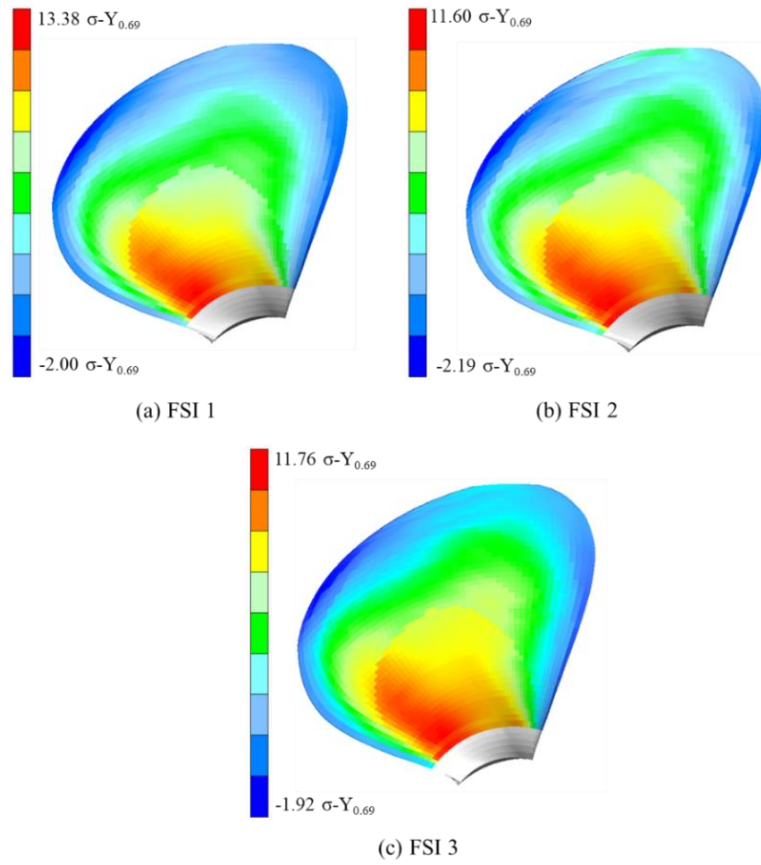
Figure 70. Ply # 2 main stress parallel to fiber direction

(a) FSI 1   (b) FSI 2

(c) FSI 3
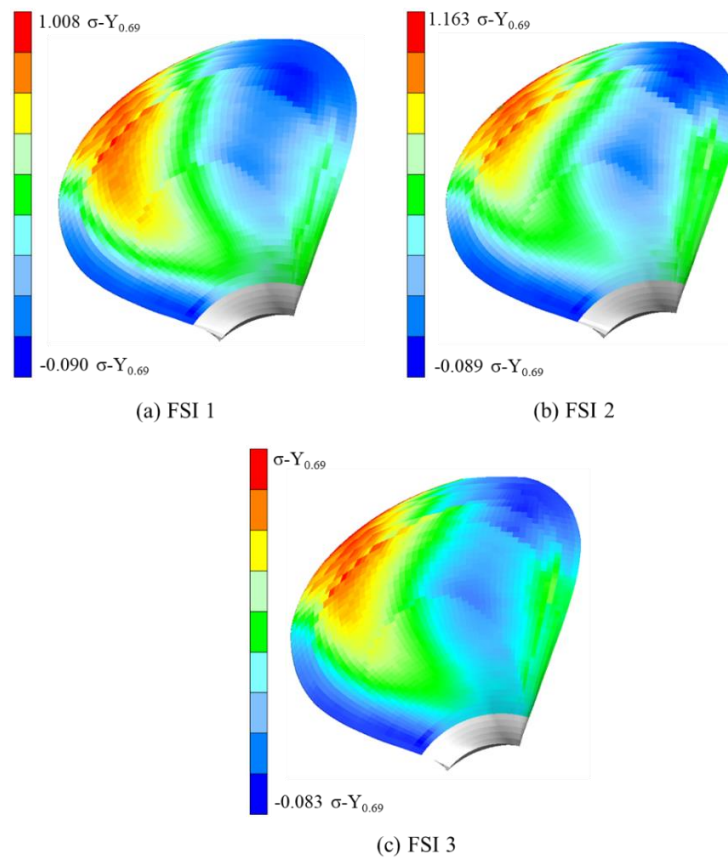
Figure 71. Ply # 2 main stress perpendicular to fiber direction

(a) FSI 1

(b) FSI 2

(c) FSI 3
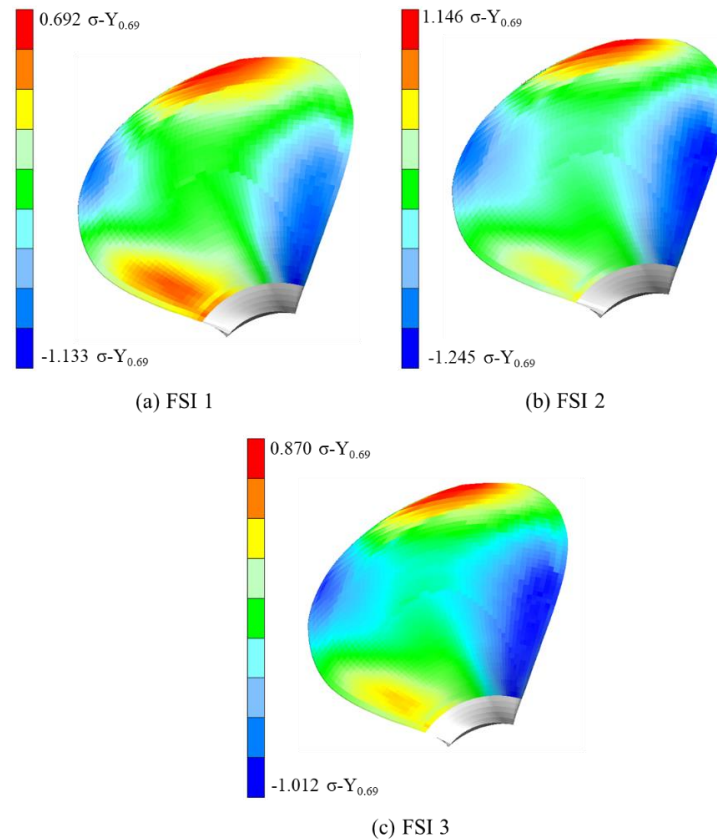
Figure 72. Ply # 2 shear stress

Justification of discrepancies between BV and MECA results for UD plies

For the UD plies, there is discrepancy between the two results in terms of the number of plies that do not fulfill the required safety criteria of BV NI663. This discrepancy can be justified using following reasons

- The modelling approach implemented by MECA and BV is different as MECA is using plate laminate elements while BV is using solid laminate elements. Based on the differences in the types of elements used and how the layup and material properties are assigned to the FE model, some discrepancies in the results were expected from the start

- The three FSI analysis in this thesis work are carried out using the layup defined in section 5.8 and shown in Figure 49 which has a total of 33 plies. Towards the end of the thesis work, MECA modified the layup by adding two additional woven roving plies in the middle of the layup, increasing the total number of plies from 33 to 35. These new plies have not been included in the FE models used to carry out the three FSI analysis. Although the effect of these additional plies is not significant on the hydrodynamical and structural results, it is also not negligible. The effect of adding two

additional plies on the maximum failure indices for the UD plies # 2, 3, 4, 6, 31 and 32 was studied only for the case of FSI 2 and the results are tabulated below.

Table 35. Effect of two additional plies on failure indices for UD plies

| Ply # | Failure Indices | | Safety Margins by MECA |
	Original FE model	New FE model with two additional plies	
2	**1.492**	**1.328**	**5.051**
3	**1.336**	0.991	5.863
4	**1.105**	0.910	6.324
6	**1.011**	0.778	7.221
31	**1.28**	0.763	6.882
32	**1.352**	**1.262**	5.841

It becomes clear by looking at Table 35 that the use of new FE model with two additional plies removes the discrepancy in the results between BV and MECA. By addition of two new woven roving plies, the overall stress values in all of the plies go down and hence we get acceptable maximum failure indices values for plies # 3, 4, 6 and 31 which initially seemed to have maximum failure indices values greater than 1. The BV and MECA results are now in line.

Woven Roving

There is a total of eight woven roving plies in the layup as shown in Figure 50. The safety factors used for the calculations of main stresses and combined stress are different for woven roving plies as compared to UD plies as already detailed in section 5.11. The failure indices obtained for woven roving plies using a safety factor of 7.01 are given in Table 36. Failure indices and safety margins based on combined stress analysis for woven rovingagainst the safety margins obtained by MECA.

The analysis of the results is as follows

- Plies # 1, 5, 29 and 33 have safety margins lower than the required value of 7.01 (safety factor without fatigue analysis) in MECA results. These same plies give maximum failure indices greater than 1 in BV results.

- As the safety margins in MECA results are greater than the safety factor of 3.19 (safety factor with fatigue analysis included) for all woven roving plies, same trend was observed in BV results where the maximum failure indices using a safety factor of 3.19 for all the woven roving plies is smaller than 1. Hence failure indices obtained using

safety factor of 3.19 are not shared in the report. Only the failure indices using safety factor 7.01 are given in Table 36.

- Since the results for all the plies are justified between BV and MECA, failure indices using new layup with two additional plies need not to be calculated, as was done for UD plies. This is because we already have conservative results obtained from FSI analysis based on original FE model as compared to the results from MECA based on new FE model. Using the new FE model with two additional plies for FSI analysis would only decrease the value of maximum failure indices, which would serve no further purpose.

Table 36. Failure indices and safety margins based on combined stress analysis for woven roving

Ply Number	Failure Indices			Safety Margins by MECA
	FSI 1	FSI 2	FSI 3	
1	**2.154**	**2.717**	**1.883**	**4.677**
5	**1.369**	**1.396**	**1.106**	**6.962**
9	0.849	0.833	0.6711	9.982
13	0.334	0.23	0.237	21.525
21	0.619	0.591	0.483	10.779
25	0.954	0.882	0.738	8.817
29	**1.452**	**1.325**	**1.105**	**6.268**
33	**2.089**	**2.392**	**1.856**	**3.698**

7. CONCLUSIONS

- The objectives stated at the start of the thesis were achieved based on the results obtained from the three FSI analysis performed in the thesis work. The hydrodynamical and structural results obtained by MECA are validated although with some differences and discrepancies, which are justified where possible.

- Composite modelling using 3D solid laminate elements as opposed to using typical 2D laminate elements produces similar results between 3D and 2D models with acceptable differences. The use of 3D solid laminate elements to create the FE model gives more freedom to capture the tapered or curved geometric details of the propeller blades as compared to 2D plate laminate elements. On the other hand, the FE models using 2D plate laminate elements capture stress hotspots due to ply drop off better than 3D solid laminate elements, sometimes overestimating the stress values in the hotspot areas. Creating FE models using 2D laminate elements is a fairly easier and quick process as compared to creating FE models using solid laminate elements.

- The design of the composite propeller blade is satisfactory provided that fatigue analysis of the propeller blade is also included as part of the complete design process. If fatigue analysis is not included in the complete design process, the design needs to be reevaluated to achieve an outcome where all the plies fulfill the safety requirements of BV NI663 without considering the fatigue analysis.

- The use of BEM-FEM coupled FSI analysis using ComPropApp for design validation is an attractive avenue based on the accuracy of the results and the time taken to obtain these results. A comparison of the total time taken between BEM-FEM coupled FSI analysis using ComPropApp and CFD-FEM coupled FSI analysis is given in Table 37. Time comparison between BEM-FEM and CFD-FEM coupled FSI analysis

Table 37. Time comparison between BEM-FEM and CFD-FEM coupled FSI analysis

	BEM – FEM		CFD – FEM	
	BEM	**FEM**	**CFD**	**FEM**
Modelling and Preprocessing	2 hours	5 hours	3 days	5 hours
Computation upto deformation convergence	2 mins	30 mins	3 days	30 mins
Post processing	5 hours		5 hours	
Total Time	1.5 days		6 – 7 days	

BEM-FEM coupled FSI gives results with a maximum difference of less than 10 % compared to the results obtained using CFD-FEM coupled FSI analysis. Thus, ComPropApp offers tremendous potential to be used as a quick design validation tool by BV in the future to validate the design of composite propellers. Thus, the interest of BV in CoPROPEL project is to validate the ComPropApp and develop trust in its functionalities and its produced results.

- For future studies, ComPropApp still needs significant improvement before it is ready to be used as a complete tool for quick design validation by BV. Currently, the material coordinate systems created by ComPropApp are impractical to be used as the basis to assign required material directions of the fibers. Also, ComPropApp is unable to assign correctly the layup and material properties to the FE model which is a developer's bug and needs to be rectified. Once these issues have been taken care of, two-way BEM-FEM coupled FSI analysis can be carried out using ComPropApp which would eliminate the need to import the FE model into FEMAP. This will further reduce the total time taken by BEM-FEM coupled FSI analysis in Table 37 from 1.5 days to perhaps less than 1 day.

- Further work is needed to improve/automate the process of both BEM-FEM and CFD-FEM couplings. For BEM-FEM coupling, Abaqus or FEMAP present a better option to be used as FE software in ComPropApp in place of TRIDENT since TRIDENT is an outdated software with a very difficult-to-use user interface. Additionally, the results obtained from TRIDENT are subject to scrutiny since TRIDENT is unable to display the stress output results, rather it only displays deformation results.

- For the Le Palais propeller, further investigation is needed to study the underwater cavitation behavior of the propeller. This requires the use of numerical modelling supported by open water tests. Sea trails for the propeller are also planned in the near future to validate the theoretical results presented in this thesis report.

DECLARATION OF AUTHORSHIP

I declare that this thesis and the work presented in it are my own and have been generated by me as the result of my own original research.

Where I have consulted the published work of others, this is always clearly attributed.

Where I have quoted from the work of others, the source is always given. With the exception of such quotations, this thesis is entirely my own work.

I have acknowledged all main sources of help.

Where the thesis is based on work done by myself jointly with others, I have made clear exactly what was done by others and what I have contributed myself.

This thesis contains no material that has been submitted previously, in whole or in part, for the award of any other academic degree or diploma.

I cede copyright of the thesis in favour of the University of Rostock, Germany

Date: 25/07/2024   Signature

ACKNOWLEDGEMENTS

I am deeply grateful to **GOD Almighty** for guiding me through the struggles of life and throughout this thesis work. I extend my heartfelt thanks to my **Mother** and my **Wife**, who have been a constant source of support and motivation in my life, particularly during the tenure of this thesis.

I would like to express my sincere gratitude to **Professor Philippe RIGO** for providing me with the exceptional opportunity through the Erasmus Mundus double degree program, EMSHIP+. It is because of the opportunity provided by him that I was able to start my thesis internship at Bureau Veritas Marine and Offshore (BV M&O).

I am eternally grateful to **Stéphane PABOEUF** for giving me the opportunity to carry out my master's thesis and internship under his supervision at Bureau Veritas Marine and Offshore Composite Materials Section. I am also profoundly thankful to my thesis supervisor, **Maxime DEYDIER**, for his expert guidance and unwavering support throughout my thesis work. His contributions have been invaluable to the successful completion of this thesis.

I would like to extend my gratitude to **Sébastien LOUBEYRE** and **Pauline REGNIER** from Bureau Veritas Solutions M&O for their constant support in carrying out the CFD simulations using STAR-CCM+. A significant portion of the thesis work was carried out in collaboration with BV Solutions, thanks to the help of the aforementioned individuals.

Lastly, I would like to thank **Gabriel HEGUY**, **Valentin JEANNEAU** and **Pierre BERTHELOT** from MECA for their consistent support and valuable input.

REFERENCES

A.P. Mouritz , E. Gellert , P. Burchill and K. Challis, 2001. Review of advance composite structures for naval ships and submarines. *Composite Structures*, 53(1), 21-42

M.R. Motley, Z. Liu and Y.L. Young, 2009. Utilizing fluid–structure interactions to improve energy efficiency of composite marine propellers in spatially varying wake. *Composite Structures*, 90(3), 304-313

Y.L. Young, 2008. Fluid-structure interaction analysis of flexible composite marine propellers. *Journal of Fluids and Structures*, 24(6), 799-818

Pieter Maljaars, Nicola Grasso, Mirek Kaminski and Wim Lafeber, 2017. Validation of a steady BEM-FEM coupled simulation with experiments on flexible small scale propellers. *Proceedings of the 5th International Symposium on Marine Propulsion (SMP 2017)*, 795-802

Jiasheng Li, Yegao Qu and Hongxing Hua, 2017. Hydroelastic analysis of underwater rotating elastic marine propellers by using a coupled BEM-FEM algorithm. *Ocean Engineering*, 146, 178-191

Lex Mulcahy, Gangadhara B Prusty and C.P. Gardiner, 2010. Hydroelastic tailoring of flexible composite propellers. *Ships and Offshore Structures*, 5(4), 359-370

Justin E. Kerwin and Jacques B. Hadler, 2010. *Principles of Naval Architecture Series: Propulsion*. Society of Naval Architects and Marine Engineers

Tadashi Taketani, Koyu Kimura, Satoko Ando and Koutaku Yamamoto, 2013. Study on performance of a ship propeller using a composite material. *Third International Symposium on Marine Propulsors smp'13*

Rickard E. Bensow and Göran Bark, 2010. Implicit LES predictions of the cavitating flow on a propeller. *Journal of Fluids Engineering*, 132

Stefano Gaggero, Giuliano Vernengo, Diego Villa and Luca Bonfiglio, 2019. A reduced order approach for optimal design of efficient marine propellers. *Ships and offshore structures*, 15(4), 1-15

H.J. Lin, W.M. Lai and Y.M. Kuo, 2016. Effects of stacking sequence on nonlinear hydroelastic behavior of composite propeller blade. *Journal of Mechanics*, 26(3), 293-298

Pankaj Kumar Singh, Rishabh Chaturvedi and Aman Sharma, 2021. Implementation of finite element model in compound propeller blades for using in aircraft. *Material Today: Proceedings*, 45(2), 2747-2750

Benjamin Y.H. Chen, Stephen K. Neely, Thad J. Michael, Scott Gowing, Richard P. Szwerc, Dirk Buchler and Reinert Schult, 2006. Design, fabrication and testing of pitch-adapting (flex) propellers. *SNAME 11th Propellers and Shafting Symposium*

Stephen R. Turnock and Alexander Mitchell Wright, 2000. Directly coupled fluid structural model of a ship rudder behind a propeller. *Marine Structures*, 13(1), 53-72

COPROPEL PROJECT. https://www.copropel.com. Accessed: 2024-05-18

John Carlton, 2018. *Marine propellers and propulsion*. Butterworth-Heinemann

Volker Bertram, 2011. *Practical ship hydrodynamics*. Elsevier

Friedrich-Karl Benra, Hans Josef Dohmen, Ji Pei, Sebastian Schuster, and Bo Wan. 2011. A comparison of one-way and two-way coupling methods for numerical analysis of fluid-structure interactions. *Journal of applied mathematics*

Matthias Heil, 2004. An Efficient Solver for the Fully Coupled Solution of Large-Displacement Fluid-Structure Interaction Problems. *Computer Methods in Applied Mechanics and Engineering*, 193(1-2), 1-23

Serge Piperno and Charbel Farhat, 2001. Partitioned Procedures for the Transient Solution of Coupled Aeroelastic Problems Part II: Energy Transfer and Three-Dimensional Applications. *Computer Methods in Applied Mechanics and Engineering*, 190(24–25), 3147-3170

Yuri Bazilevs, Kenji Takizawa and Tayfun Tezduyar (2013). *Computational fluid-structure interaction: methods and applications*. John Wiley & Sons.

Gene Hou, Jin Wang and Anita Layton (2012). Numerical methods for fluid-structure interaction—a review. *Communications in Computational Physics*, 12(2), 337-377.

Pieter Maljaars, 2019, *Hydro-elastic analysis of flexible marine propellers,* Ph.D. Thesis, Delft University of Technology

F. M. White, 2006. *Fluid Mechanics*. McGraw Hill Higher Education

David C Wilcox et al., 1998. *Turbulence modeling for CFD*, volume 2. DCW industries LaCanada, CA,

Katz, J. and Plotkin, A., 2001. *Low-speed aerodynamics: From wing theory to panel methods*. Cambridge University Press, 2nd Edition.

Morino, L., Chen, L-T. and Suciu, E.O. , 1975. *Steady and oscillatory subsonic andsupersonic aerodynamics around complex configurations*, AIAA Journal Vol 13, No. 3.

Bureau Veritas. *NR546 Hull, Composite, Plywood, and High-Density Polyethylene Materials*. https://marine-offshore.bureauveritas.com/nr546-hull-composite-plywood-and-high-density-polyethylene-materials. Accessed: 2024-06-13

M. Rasoul Tirandaz and Abdolrahim Rezaeiha (2021). Effect of airfoil shape on power performance of vertical axis wind turbines in dynamic stall: Symmetric Airfoils. *Renewable Energy*, 173, 422-441

APPENDIXES

Appendix 1

MATLAB script for propeller geometry data processing

```matlab
clear all
clc
close all

%% Info
% This script covertas the raw cordinates of the profile section into 29
% points alongs the localized x cordinate of the blade

%% SCRIPT START
% Load the CSV file containing the global coordinates
data = readtable('.csv file input here');

%% Finding the cordinates for the Leading Edge (LE) and the Trailing Edge (TE)

% Extract X and Y coordinates
X = data.X;
Y = data.Y;

% Calculate the pairwise Euclidean distances between points
distances = pdist([X Y]);          % Calculate pairwise distances in vector form
distanceMatrix = squareform(distances); % Convert to a square matrix

% Find the indices of the maximum distance
[maxDist, linearIndex] = max(distanceMatrix(:));
[i, j] = ind2sub(size(distanceMatrix), linearIndex); % Convert linear index to matrix indices

% Select the points with the maximum distance
point1 = [X(i), Y(i)];
point2 = [X(j), Y(j)];

% Assign LE and TE based on the coordinates' signs
if point1(1) > 0 && point1(2) > 0
    LE = point1;
    TE = point2;
else
    LE = point2;
    TE = point1;
end

% Checking if both points need to be reassigned
if point2(1) > 0 && point2(2) > 0 && (point1(1) <= 0 || point1(2) <= 0)
    LE = point2;
    TE = point1;
end

% Display the results
fprintf('LE: (%f, %f)\n', LE(1), LE(2));
fprintf('TE: (%f, %f)\n', TE(1), TE(2));
fprintf('The two points with the maximum distance are: (%f, %f) and (%f, %f)\n', X(i), Y(i), X(j), Y(j));

figure(1);
```

```matlab
hold on;
plot(X, Y, 'b-');
plot(LE(1),LE(2),"r.",TE(1),TE(2),"r.",'MarkerSize',15);
axis equal
grid on;
hold off

clear distances distanceMatrix maxDist linearIndex
clear point1 point2 i j
```

%% Rotation of profile to align with the horizontal axis

```matlab
% Calculate the angle theta
theta = atan2(TE(2) - LE(2), TE(1) - LE(1));

% Calculate the chord length
chord_length = sqrt((TE(1) - LE(1))^2 + (TE(2) - LE(2))^2);

% Display the chord length and angle
disp(['Chord Length: ', num2str(chord_length)]);
disp(['Angle (in degrees): ', num2str(rad2deg(theta))]);

% Define the rotation matrix
R = [cos(-theta) -sin(-theta); sin(-theta) cos(-theta)];

% Subtract LE coordinates to set LE as origin, then apply rotation
translated_points = [X - LE(1), Y - LE(2)]';  % Transpose for matrix multiplication

rotated_points = R * translated_points;

% Extract x and y coordinates from rotated points
rotated_x = rotated_points(1, :)';
rotated_y = rotated_points(2, :)';

figure(2);
plot(rotated_x, rotated_y, 'b-');
axis equal
grid off;
axis off

% Set values smaller than 0.0001 in magnitude to zero in both x and y columns
rotated_x(abs(rotated_x) < 0.0001) = 0;
rotated_y(abs(rotated_y) < 0.0001) = 0;

% Create a new table with the rotated coordinates
rotated_data = table(rotated_x, rotated_y, 'VariableNames', {'Rotated_X', 'Rotated_Y'});

% Since the rotation aligns the chord line to the x-axis, and LE is at origin,
% any point with y <= 0 after rotation is on the suction side, and y > 0 is on the pressure side
suction_indices = rotated_y <= 0;
pressure_indices = rotated_y > 0;

% Create tables for suction and pressure sides
suction_data = table(rotated_x(suction_indices), rotated_y(suction_indices), 'VariableNames', {'X', 'YS'});
pressure_data = table(rotated_x(pressure_indices), rotated_y(pressure_indices), 'VariableNames', {'X', 'YP'});
```

%% Interpolation to find the pressure side points at the suction side

```matlab
% Sort data to aid in interpolation
suction_data = sortrows(suction_data, 'X');
pressure_data = sortrows(pressure_data, 'X');
```

```matlab
% Interpolate YP values at the X locations of the YS values
interpolated_YP = interp1(pressure_data.X, pressure_data.YP, suction_data.X, 'linear', 'extrap');

interpolated_YP(1) = 0;
interpolated_YP(end) = 0;

% Create a final table with X, YS, and the interpolated YP
final_data = table(suction_data.X, suction_data.YS, interpolated_YP, 'VariableNames', {'X', 'YS', 'YP'});

% Display some of the final data
disp(head(final_data));

% Plotting the suction and pressure sides for verification
figure(3);
hold on;
plot(suction_data.X, suction_data.YS, 'r-', 'DisplayName', 'Suction Side');
plot(pressure_data.X, pressure_data.YP, 'b-', 'DisplayName', 'Pressure Side');
plot(final_data.X, final_data.YP, 'g--', 'DisplayName', 'Interpolated Pressure Side');
legend show;
axis equal;
title('Blade Profile with Suction and Pressure Sides');
xlabel('X Coordinate');
ylabel('Y Coordinate');
grid on;


clear X Y LE R TE filename interpolated_YP pressure_data pressure_indices
clear rotated_points rotated_x rotated_y suction_data suction_indices x y
clear translated_points


%% Reduction of DATA POINTS

% Creating new data variable for suction and pressure data for simplification process
full_data = [final_data.X final_data.YS]';

% Simplify the curve while maintaining the shape using the Douglas-Peucker algorithm

target_length = 29;
increment = 0.0001;
tolerance = 0.10;
while true
    simplified_data = DouglasPeucker(full_data, tolerance);
    data_length = length(simplified_data);

    if data_length == target_length
        break; % Exit the loop if the length is exactly 25
    elseif data_length > target_length
        tolerance = tolerance + increment; % Increase tolerance if too many points
    else
        tolerance = tolerance - increment; % Decrease tolerance if too few points
    end
end

clear increment tolerance target_length data_length

simplified_x = simplified_data(1, :)';
simplified_ys = simplified_data(2, :)';

% Fetch the YP values from the final_data table for the simplified X values
[~, idx] = ismember(simplified_x, final_data.X);
```

```matlab
simplified_yp = final_data.YP(idx);

camber = (simplified_yp + simplified_ys)/2;

% Create a final table with the simplified data
simplified_final_data = table(simplified_x, simplified_ys, simplified_yp, 'VariableNames', {'X', 'YS', 'YP'});

% Display some of the simplified data
disp(head(simplified_final_data));

% Plotting the simplified suction and pressure sides for verification

plot(simplified_x, simplified_ys, 'ko--', 'DisplayName', 'Simplified Suction Side');
plot(simplified_x, simplified_yp, 'k*--', 'DisplayName', 'Simplified Pressure Side');
plot(simplified_x, camber, 'k.--', 'DisplayName', 'Camber');
legend show;

%simplified_final_data = abs(simplified_final_data);

% Display some of the simplified data
disp(head(simplified_final_data));

% Save the simplified data table to a new CSV file
writetable(simplified_final_data, 'reduced.csv');


% Display final checks for simplified data
disp('Simplified blade profile data has been saved and displayed.');
```

Appendix 2

API to apply zone numbers based on material mapping to 2500 elements in the FE model

```
Sub Main
    Dim App As femap.model
    Set App = feFemap()

    ' Preserve old layups by moving them to new IDs 2501-2516
    Dim oldLayupID As Long, newLayupID As Long
    Dim layup As femap.Layup
    For oldLayupID = 1 To 16
        newLayupID = 2500 + oldLayupID  ' Move old layup ID to new range 2501-2516
        Set layup = App.feLayup

        If layup.Get(oldLayupID) = FE_OK Then
            layup.id = newLayupID  ' Set new layup ID
            layup.Put(newLayupID)  ' Save the new layup
        Else
            App.feAppMessage(FCM_ERROR, "Failed to retrieve old layup ID " & CStr(oldLayupID))
        End If
    Next oldLayupID

    ' Read the material mapping from the file
    Dim filePath As String
    filePath = "C:\Users\kaali\Downloads\Internship\Task2-Comprop Work\MECA Data Full scale
propeller\APIs for Full Scale\Material_Mapping_50x50.txt"

    Dim fileNum As Integer
    fileNum = FreeFile()
    Open filePath For Input As #fileNum

    Dim zonePattern(1 To 50, 1 To 50) As Integer
    Dim lineData As String
    Dim dataPoints() As String
    Dim row As Integer, col As Integer
    row = 1

    Do While Not EOF(fileNum)
        Line Input #fileNum, lineData
        dataPoints = Split(lineData, vbTab)

        For col = 1 To 50
            zonePattern(row, col) = Val(dataPoints(col - 1))
        Next col
        row = row + 1
    Loop

    Close #fileNum

    ' Assign new layup IDs to properties based on the zonePattern
    Dim prop As femap.Prop
    Set prop = App.feProp
    Dim propID As Long
    Dim baseLayupID As Long

    For row = 50 To 1 Step -1
```

```vbnet
    For col = 50 To 1 Step -1
        propID = ((50 - row) * 50) + (50 - col + 1)  ' Corrected calculation for property ID
        baseLayupID = 2500 + zonePattern(row, col)  ' Corrected retrieval of layup ID from zonePattern

        If prop.Get(propID) = FE_OK Then
            prop.layupID = propID  ' Assign a new unique layup ID equal to the property ID
            layup.id = propID  ' Create a new layup ID for each property

            If layup.Get(baseLayupID) = FE_OK Then
                ' Copy properties from base layup to new layup if necessary
                layup.Put(propID)  ' Save the new layup with modified properties
                ' Print the output to the Immediate Window
                Debug.Print "New layup ID #" & propID & " created using old layup ID #" & baseLayupID
            End If

            prop.Put(propID)  ' Save the property with the new layup ID
        Else
            App.feAppMessage(FCM_ERROR, "Failed to get property ID " & CStr(propID))
        End If
    Next col
Next row

    App.feAppMessage(FCM_NORMAL, "Layup properties have been successfully reassigned based on new
mappings.")
    App.feFileSave(False)  ' Save the changes
End Sub
```

Appendix 3

API to assign color scheme to FE model based on the difference of thickness between the layup and elements

```vb
Sub Main()
    Dim App As femap.model
    Set App = feFemap()

    ' Initialize the node set
    Dim nodeSet As femap.Set
    Set nodeSet = App.feSet
    nodeSet.AddAll(FT_NODE)

    ' Initialize array to store thicknesses for 2500 elements
    Dim thicknesses(1 To 2500) As Double

    ' Variables for node indexing and element counting
    Dim totalElements As Long
    Dim nodeID_Start As Long
    nodeID_Start = 254  ' Because node indices usually start at 1 and we skip 253 nodes

    While totalElements < 2500
        If nodeID_Start + 101 > nodeSet.Count Then Exit While ' Ensure there are enough nodes left

        ' Perform thickness calculations for the next 102 nodes
        Dim i As Long
        For i = 1 To 50
            If totalElements + i > 2500 Or nodeID_Start + 3 > nodeSet.Count Then Exit For ' Check boundaries

            ' Calculate and record thickness
            Dim thickness As Double
            thickness = CalculateMeanThickness(App, nodeID_Start, nodeID_Start + 1, nodeID_Start + 2,
nodeID_Start + 3)
            thicknesses(totalElements + i) = thickness  ' Store thickness in the array

            nodeID_Start = nodeID_Start + 2 ' Move to the next pair
        Next i

        ' Update total elements processed
        totalElements = totalElements + i - 1

        ' Correctly update nodeID_Start for the next batch
        nodeID_Start = nodeID_Start + 253 + 2 ' Correct adjustment to skip nodes for the next set
    Wend

    ' Check the total thickness of layups from 1 to 2500
    Dim LayUp As femap.Layup
    Set LayUp = App.feLayup
    Dim layups As femap.Set
    Set layups = App.feSet
    layups.AddAll(FT_LAYUP)

    Dim layup_id As Long
    Dim numplys As Long
    Dim matids As Variant
```

```vba
    Dim thicknessesLayup As Variant
    Dim angles As Variant
    Dim globalPlys As Variant
    Dim totalThicknessLayup As Double

    ' Initialize counters for summary
    Dim countLarger As Long
    Dim countSmaller As Long

  layup_id = layups.First

  While layup_id > 0 And layup_id <= 2500
     Set LayUp = App.feLayup
     LayUp.Get(layup_id)
     LayUp.GetAllPly(numplys, matids, thicknessesLayup, angles, globalPlys)

     ' Calculate total thickness of the layup
     totalThicknessLayup = 0
     Dim j As Long
     For j = 0 To numplys - 1
        totalThicknessLayup = totalThicknessLayup + thicknessesLayup(j)
     Next j

     ' Compare the element thickness with the layup thickness
     Dim elementThickness As Double
     elementThickness = thicknesses(layup_id)

     ' Determine the palette ID based on the thickness comparison
     Dim paletteID As Long
     If elementThickness > totalThicknessLayup Then
        paletteID = 45 ' Element thickness is greater than layup thickness
        countLarger = countLarger + 1
     Else
        paletteID = 9  ' Element thickness is less than layup thickness
        countSmaller = countSmaller + 1
     End If

     ' Apply palette ID to the element
     Dim elem As femap.Elem
     Set elem = App.feElem
     elem.Get(layup_id)
     elem.color = paletteID
     elem.Put(layup_id)

     layup_id = layups.Next
  Wend

  ' Output the summary information
  App.feAppMessage(FE_MSG_INFO, "Layup and element thickness comparison and coloring completed.")
  App.feAppMessage(FE_MSG_INFO, "Number of elements where element thickness is larger than layup: " &
countLarger)
  App.feAppMessage(FE_MSG_INFO, "Number of elements where element thickness is smaller than layup: "
& countSmaller)

  ' Regenerate the view to reflect changes
  rc = App.feViewRegenerate(0)
End Sub

Function CalculateMeanThickness(App As femap.model, nodeID1 As Long, nodeID2 As Long, _
                 nodeID3 As Long, nodeID4 As Long) As Double
  Dim feNode1 As femap.Node
```

```vb
    Dim feNode2 As femap.Node
    Dim feNode3 As femap.Node
    Dim feNode4 As femap.Node
    Set feNode1 = App.feNode
    Set feNode2 = App.feNode
    Set feNode3 = App.feNode
    Set feNode4 = App.feNode

    feNode1.Get(nodeID1)
    feNode2.Get(nodeID2)
    feNode3.Get(nodeID3)
    feNode4.Get(nodeID4)

    Dim dist1 As Double
    Dim dist2 As Double
    dist1 = Sqr((feNode2.x - feNode1.x)^2 + (feNode2.y - feNode1.y)^2 + (feNode2.z - feNode1.z)^2)
    dist2 = Sqr((feNode4.x - feNode3.x)^2 + (feNode4.y - feNode3.y)^2 + (feNode4.z - feNode3.z)^2)

    CalculateMeanThickness = (dist1 + dist2) / 2
End Function
```

Appendix 4

API to create new material coordinate systems in FEMAP

```vb
Sub Main()
    Dim App As femap.model
    Set App = feFemap()

    Dim propSET As femap.Set
    Set propSET = App.feSet

    ' Attempt to select all properties
    Dim rc As Integer
    rc = propSET.Select(FT_PROP, True, "Select Properties to Update CSys")
    If rc <> FE_OK Then Exit Sub

    Dim feCSys As femap.CSys
    Set feCSys = App.feCSys

    ' Define the origin, direction vector, and a point on the XY plane
    Dim origin(2) As Double
    Dim x_axis(2) As Double
    Dim y_plane(2) As Double

    ' Origin at the start of the vector
    origin(0) = 37.91441: origin(1) = -318.2464: origin(2) = 85.78855

    ' X-axis ending at the end of the vector
    x_axis(0) = 24.80249: x_axis(1) = -460.8742: x_axis(2) = 548.8117

    ' A point in the XY plane provided
    y_plane(0) = 49.1811: y_plane(1) = -299.1544: y_plane(2) = 82.5404

    Dim propID As Long
    propID = propSET.First()

    While propID > 0
        ' Create/Update the coordinate system for the property
        rc = feCSys.XYPoints(origin, x_axis, y_plane)
        If rc = FE_OK Then
            rc = feCSys.Put(feCSys.NextEmptyID)
            If rc = FE_OK Then
                ' Update the property to reference the new CSys
                Dim feProp As femap.Prop
                Set feProp = App.feProp
                If feProp.Get(propID) = FE_OK Then
                    feProp.refCS = feCSys.ID
                    feProp.Put(propID)
                End If
            End If
        End If

        propID = propSET.Next()
    Wend
End Sub
```

Appendix 5

API to create Model – 2 in section 6.3.2

```
Sub Main
    Dim App As femap.model
    Set App = feFemap()

    ' Calculate thicknesses of elements from 1 to 2500
    Dim nodeSet As femap.Set
    Set nodeSet = App.feSet
    nodeSet.AddAll(FT_NODE)

    Dim totalElements As Long
    Dim nodeID_Start As Long

    ' Initialize array to store thicknesses
    Dim thicknesses(1 To 2500) As Double

    ' Calculate starting index after initial skip of 253 nodes
    nodeID_Start = 254  ' Because node indices usually start at 1 and we skip 253 nodes
    While totalElements < 2500
        If nodeID_Start + 101 > nodeSet.Count Then Exit While ' Ensure there are enough nodes left

        ' Perform thickness calculations for the next 102 nodes
        Dim i As Long
        For i = 1 To 50
            If totalElements + i > 2500 Or nodeID_Start + 3 > nodeSet.Count Then Exit For ' Check boundaries

            ' Calculate and record thickness
            Dim thickness As Double
            thickness = CalculateMeanThickness(App, nodeID_Start, nodeID_Start + 1, nodeID_Start + 2, nodeID_Start + 3)
            thicknesses(totalElements + i) = thickness  ' Store thickness in the array

            nodeID_Start = nodeID_Start + 2 ' Move to the next pair
        Next i

        ' Update total elements processed
        totalElements = totalElements + i - 1

        ' Correctly update nodeID_Start for the next batch
        nodeID_Start = nodeID_Start + 253 + 2 ' Correct adjustment to skip nodes for the next set
    Wend

    ' Check the total thickness of layups from 1 to 2500
    Dim LayUp As femap.Layup
    Set LayUp = App.feLayup
    Dim layups As femap.Set
    Set layups = App.feSet
    layups.AddAll(FT_LAYUP)

    Dim layup_id As Long
    Dim numplys As Long
    Dim matids As Variant
    Dim thicknessesLayup As Variant
    Dim angles As Variant
```

```vb
Dim globalPlys As Variant
Dim totalThicknessLayup As Double
Dim found As Boolean

layup_id = layups.First

While layup_id > 0 And layup_id <= 2500
    Set LayUp = App.feLayup
    LayUp.Get(layup_id)
    LayUp.GetAllPly(numplys, matids, thicknessesLayup, angles, globalPlys)

    ' Calculate total thickness of the layup
    totalThicknessLayup = 0
    Dim j As Long
    For j = 0 To numplys - 1
        totalThicknessLayup = totalThicknessLayup + thicknessesLayup(j)
    Next j

    ' If layup thickness is less than element thickness, add material ID 6 on top and bottom
    If totalThicknessLayup < thicknesses(layup_id) Then
        ' Create a new layup above 2500
        Dim newLayUp As femap.Layup
        Set newLayUp = App.feLayup
        Dim newLayupID As Long
        newLayupID = 2500 + layup_id

        newLayUp.title = "Temp Layup"
        newLayUp.NumberOfPlys = numplys + 2

        Dim additionalThickness As Double
        additionalThickness = (thicknesses(layup_id) - totalThicknessLayup) / 2

        Dim newMatIDs() As Long
        Dim newThicknessesLayup() As Double
        Dim newAngles() As Double

        ReDim newMatIDs(newLayUp.NumberOfPlys - 1)
        ReDim newThicknessesLayup(newLayUp.NumberOfPlys - 1)
        ReDim newAngles(newLayUp.NumberOfPlys - 1)

        newMatIDs(0) = 6
        newThicknessesLayup(0) = additionalThickness
        newAngles(0) = 0

        For j = 0 To numplys - 1
            newMatIDs(j + 1) = matids(j)
            newThicknessesLayup(j + 1) = thicknessesLayup(j)
            newAngles(j + 1) = angles(j)
        Next j

        newMatIDs(newLayUp.NumberOfPlys - 1) = 6
        newThicknessesLayup(newLayUp.NumberOfPlys - 1) = additionalThickness
        newAngles(newLayUp.NumberOfPlys - 1) = 0

        newLayUp.vmatlID = newMatIDs
        newLayUp.vthickness = newThicknessesLayup
        newLayUp.vangle = newAngles
        newLayUp.Put(newLayupID)

        ' Replace the original layup with the new layup
        LayUp.Get(newLayupID)
```

```vb
        LayUp.Put(layup_id)

        ' Delete the temporary new layup
        newLayUp.Delete(newLayupID)

      ' If layup thickness is more than element thickness, check for material ID 4 and reduce thickness
      ElseIf totalThicknessLayup > thicknesses(layup_id) Then
        found = False

        For j = 0 To numplys - 1
          If matids(j) = 4 Then
            thicknessesLayup(j) = thicknessesLayup(j) - (totalThicknessLayup - thicknesses(layup_id))
            found = True
            Exit For
          End If
        Next j

        ' If material ID 4 was found and adjusted, update the layup
        If found Then
          totalThicknessLayup = 0
          For j = 0 To numplys - 1
            totalThicknessLayup = totalThicknessLayup + thicknessesLayup(j)
          Next j

          ' Update layup properties with the new thickness
          LayUp.NumberOfPlys = numplys
          LayUp.vmatlID = matids
          LayUp.vthickness = thicknessesLayup
          LayUp.vangle = angles
          LayUp.Put(layup_id)
        End If
      End If

      layup_id = layups.Next
   Wend

   App.feAppMessage(FE_MSG_INFO, "Layup thickness adjustment completed.")
End Sub

Function CalculateMeanThickness(App As femap.model, nodeID1 As Long, nodeID2 As Long, _
                  nodeID3 As Long, nodeID4 As Long) As Double
   Dim feNode1 As femap.Node
   Dim feNode2 As femap.Node
   Dim feNode3 As femap.Node
   Dim feNode4 As femap.Node
   Set feNode1 = App.feNode
   Set feNode2 = App.feNode
   Set feNode3 = App.feNode
   Set feNode4 = App.feNode
   feNode1.Get(nodeID1)
   feNode2.Get(nodeID2)
   feNode3.Get(nodeID3)
   feNode4.Get(nodeID4)

   Dim dist1 As Double
   Dim dist2 As Double
   dist1 = Sqr((feNode2.x - feNode1.x)^2 + (feNode2.y - feNode1.y)^2 + (feNode2.z - feNode1.z)^2)
   dist2 = Sqr((feNode4.x - feNode3.x)^2 + (feNode4.y - feNode3.y)^2 + (feNode4.z - feNode3.z)^2)

   CalculateMeanThickness = (dist1 + dist2) / 2
End Function
```